ISSN 1726-5479

SENSORS & TRANSDUCERS

vol. 261
2/23



Artificial Intelligence & Signal Processing

International Frequency Sensor Association Publishing

IFSA

Sensors & Transducers

International Official Open Access Journal of the International Frequency Sensor Association (IFSA) Devoted to Research and Development of Sensors and Transducers

Volume 261, Issue 2, June 2023

Editor-in-Chief
Prof., Dr. Sergey Y. YURISH

IFSA Publishing: Barcelona • Toronto

Sensors & Transducers is an open access journal which means that all content (article by article) is freely available without charge to the user or his/her institution. Users are allowed to read, download, copy, distribute, print, search, or link to the full texts of the articles, or use them for any other lawful purpose, without asking prior permission from the publisher or the author. This is in accordance with the BOAI definition of open access. Authors who publish articles in *Sensors & Transducers* journal retain the copyrights of their articles. The *Sensors & Transducers* journal operates under the Creative Commons License CC-BY.

Notice: No responsibility is assumed by the Publisher for any injury and/or damage to persons or property as a matter of products liability, negligence or otherwise, or from any use or operation of any methods, products, instructions or ideas contained in the material herein.

Published by International Frequency Sensor Association (IFSA) Publishing. Printed in the USA.



Aims and Scope

Sensors & Transducers is established, international, peer-reviewed, open access journal (print and electronic). It provides the best platform for the researchers and scientist worldwide to exchange their latest findings and results in science and technology of physical, chemical sensors and biosensors. The journal publishes original results of scientific and research works related to strategic and applied studies in all aspects of sensors: reviews, regular research and application specific papers, and short notes. In comparison with other sensors related journals, which are mainly focused on technological aspects and sensing principles, the *Sensors & Transducers* significantly contributes in areas, which are not adequately addressed in other journals, namely: frequency (period), duty-cycle, time-interval, PWM, phase-shift, pulse number output sensors and transducers; sensor systems; digital, smart, intelligent sensors and systems designs; signal processing and ADC in sensor systems; advanced sensor fusion; sensor networks; applications, etc. By this way the journal significantly enriches the appropriate databases of knowledge.

Sensors & Transducers journal has a very high publicity. It is indexed and abstracted very quickly by Chemical Abstracts, EBSCO Publishing, ProQuest Science Journals, CAS Source Index (CASSI), Ulrich's Periodicals Directory, Google Scholar, etc. Since 2011 to 2014 *Sensors & Transducers* journal was covered and indexed by EI Compendex (CPX) index (including a Scopus, Embase, Engineering Village and Reaxys) in Elsevier products. The journal is included in the IFSA List of Recommended Journals (up-dated 9.12.2019), which contains only the best, established sensors related journals.

Topics of Interest

Include, but are not restricted to:

- Physical, chemical sensors and biosensors
- Digital, frequency, period, duty-cycle, time interval, PWM, pulse number output sensors and transducers
- Theory, principles, effects, design, standardization and modelling
- Smart sensors and systems
- Intelligent sensors and systems
- Sensor instrumentation
- Virtual instruments
- Sensors interfaces, buses and networks
- Signal processing, sensor fusion
- Remote sensing
- Frequency (period, duty-cycle)-to-code converters, ADC
- Technologies and materials
- Nanosensors and NEMS
- Microsystems
- Applications

Further information on this journal is available from the Publisher's web site:
http://www.sensorsportal.com/HTML/DIGEST/New_Digest.htm

Free Access and Subscriptions

Sensors & Transducers is the open access journal. All single articles are available for free download (article by article) without any registration and embargo period. For those who want to get the full page journal issue in print and/or pdf format there is an annual subscription. It includes all regular issues and special issues. Annual subscription rates are the following: Electronic version (in printable pdf format): 590.00 EUR; Printed with b/w illustrations: 950.00 EUR; 15 % discount is available for IFSA Members.

Further information about subscription is available on the IFSA Publishing's web site: http://www.sensorsportal.com/HTML/DIGEST/Journal_Subscription.htm

Advertising Information

If you are interested in advertising or other commercial opportunities please contact by e-mail: sales@sensorsportal.com

Instructions for Authors

http://www.sensorsportal.com/HTML/DIGEST/Guides_for_Authors.htm

Sensors & Transducers Journal

Contents

Volume 261
Issue 2
June 2023

www.sensorsportal.com

ISSN 2306-8515
e-ISSN 1726-5479

Research Articles

Vehicle Localization by Optimally Weighted Use of Cross-Correlated MEMS Sensor Data
Takayoshi Yokota 1

Anti-Lock Braking System Control using Backstepping Method Based Fuzzy Logic
Najlae Jennan and El Mehdi Mellouli 10

Multi-Complex Robot Interaction with Homothetic Human Feedback in a Virtual Environment
Taha Houda, Ayman Beghdadi, Lotfi Beji and Ali Amouri 15

Learning from Demonstration and Safe Cobotics Using Digital Twins
A. Rizzotti-Kaddouri, L. Jeanneret, B. Studer, J. Bracamonte, N. Ouerhani and M. Kunze 25

Controlling a Two-Link Robot using Sliding Mode Control Combined with Neural Network
Ayoub Belkheirand El Mehdi Mellouli 33

The Triangular Observer-Based Integral Sliding-Mode Wind System Energy Control
Sanae El Bouassi, Zakaria Chalh and El Mehdi Mellouli 41

Comparison of LMI Solvers for Robust Control of a DC-DC Boost Converter
Jérôme Bosche, David Lara Alabazares and Abdelhamid Rabhi 46

Synergies in the Application of Industry 4.0 and Lean Manufacturing at a Product Label Manufacturer – A Discrete Event Simulation Case Study
Stefan Harrison, Boppana V. Chowdary 55

Digitalization of Aeronautic Painting Shop Floors for Improved Commissioning Activities
J. H. Lugo, A. Abassi, R. Balderas and N. Lassabe 61

The use of Industry 4.0 in Managing the Covid-19 Pandemic: Literature Review
Mephtaha Guennoun and Fatima Bennouna 67

Multimodal Deep Learning Architecture for Hindustani Raga Classification
Stella Paschalidou and Ioanna Miliaresi 77

Authors are encouraged to submit article in MS Word (doc) and Acrobat (pdf) formats
by e-mail: editor@sensorsportal.com. Please visit journal's webpage with preparation instructions:
http://www.sensorsportal.com/HTML/DIGEST/Submition.htm

International Frequency Sensor Association (IFSA).

Sensors & Transducers, Vol. 261, Issue 2, June 2023, pp. 1-9

www.sensorsportal.com

Sensors & Transducers

Published by IFSA Publishing, S. L., 2023
http://www.sensorsportal.com

Vehicle Localization by Optimally Weighted Use of Cross-Correlated MEMS Sensor Data

Takayoshi YOKOTA
Department of Information Design, Tokyo Information Design Professional University,
2-7-1 Komatsugawa, Edogawa-ku, Tokyo, 132–0034, Japan
Tel.: +81-3-6808-3201
E-mail: yokota@tid.ac.jp

Received: 10 April 2023 Accepted: 15 June 2023 Published: 26 June 2023

Abstract: The Global Navigation Satellite System (GNSS) is widely utilized to accurately determine the position of a vehicle, but at present, the accuracy may be degraded depending on the radio wave reception conditions from the satellite. There are also growing concerns about cyber-attacks on GNSS. We have been developing a method for estimating the position of a traveling vehicle using MEMS sensor data obtained from air pressure, acceleration, gyro, and geomagnetic sensors. In the current work, we set up an experimental environment to collect data at 50 Hz and implemented a running test on an actual road. Optimizing the weighting of each item of sensor information enabled us to obtain characteristics of the road that could not be captured in the past. In addition, the application of an extreme data elimination filter confirmed that the position estimation accuracy was improved on the order of sum-meter.

Keywords: Localization, Atmospheric pressure, Acceleration, Geomagnetic, MEMS sensor, Optimum weight.

1. Introduction

The Global Navigation Satellite System (GNSS) is widely utilized for position estimation of vehicles and pedestrians in everyday life, but its accuracy may be degraded depending on the reception status of the radio waves from the satellite. This paper is focused on position estimation of vehicles. Urban areas with high-rise buildings have long been a problem in this regard, and in recent years, radio interference caused by solar flares and intentional jamming, although rare, have occurred in some areas. This has created the need for a new technology that can compensate for the inherent disadvantages of vehicle position estimation technology, which is highly dependent on GNSS and requires huge maintenance costs. In this study, we propose a localization algorithm for a traveling vehicle based on the characteristics of the road obtained from MEMS sensors including acceleration, angular velocity, and magnetization for x, y, and z axes relying only minimally on GNSS. This paper is an extension of an earlier conference paper [1] with new results concerning the effect of the optimum weighting of cross-correlation functions compared with the results obtained by equal weight.

2. Proposed Algorithm

2.1 Literature Review

Terrain-based localization is an interesting research field that has emerged in recent years [1– 6], [8–12]. Most studies in this vein have focused on using the pitch rate of a running vehicle as features of the road surface. Similar to the author's approach [1–6], the

position of a vehicle is estimated by acquiring the properties of the road surface in real time by matching vibration data [8], pitch data [9, 10], or IMU data [11] in time domain. These are position estimation algorithms that attempt to identify a current position by matching reference sensor data prepared in advance. The accuracy of the position estimation obtained by these studies is on the order of several meters, and it remains unclear if sub-meter accuracy is possible. Landmark-based localization is a new technique that deals with suitable objects in a road scene that can be used as features for identifying the location of a vehicle or user. Image processing-based localization including 3D LiDAR depth maps can be effective [12], but the cost of preparing data is not small. Whereas most of the prior studies have used the pitch rate of running vehicles as a feature of the road surface, in the current study, nine types of sensor data comprising acceleration, angular velocity, and geomagnetism for three directions (x, y, and z) are investigated to determine which are useful. Atmospheric pressure data is not included because it does not contain much information in flat road cases.

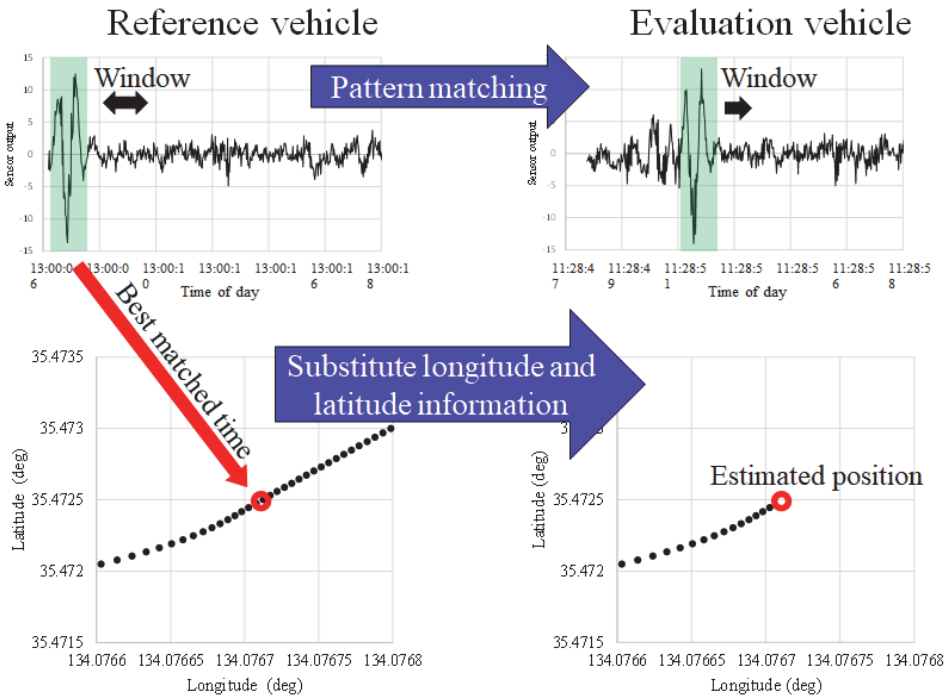


Fig. 1. Outline of proposed algorithm. The reference vehicle stores sensor data together with RTK-GNSS position data for later reference.

2.2. Vehicle Localization Algorithm by MEMS Sensor

We have been working on a vehicle localization algorithm based on MEMS sensors for the past several years [1–6]. In this algorithm, accurate location information obtained by high-precision GNSS including RTK-GNSS (u-blox ZED-F9P) [14] as well as acceleration, angular velocity, and geomagnetism information (Invensense 9250) [15] are collected in advance on an actual road for use as reference data. A test vehicle for evaluating the performance of the localization algorithm is then run to acquire sensor data, which are subsequently compared with the above reference data to obtain an accurate location. The outline of the proposed algorithm is shown in Fig. 1. Pattern matching is performed on the basis of the normalized cross-correlation function defined as

$$R(i,j) = \frac{\sum_{k=0}^{N-1}\left(f_{i+j+k}-\bar{f}_{i+j}\right)\left(g_{i+k}-\bar{g}_i\right)}{\sqrt{\sum_{k=0}^{N-1}\left(f_{i+j+k}-\bar{f}_{i+j}\right)^2}\sqrt{\sum_{k=0}^{N-1}\left(g_{i+k}-\bar{g}_i\right)^2}}, \quad (1)$$

$$\bar{f}_{i+j} = \frac{1}{N}\sum_{k=0}^{N-1} f_{i+j+k}, \quad (2)$$

$$\bar{g}_i = \frac{1}{N}\sum_{k=0}^{N-1} g_{i+k}, \quad (3)$$

where i in Eq. (1) is the index of evaluation for the vehicle's travel time and j is the index of the time lag between two vehicles (reference vehicle and evaluation vehicle). If we can determine this time lag accurately, the location of the evaluation vehicle can be substituted by the location (latitude and longitude)

of the reference vehicle at the matched time. Pattern matching can then be achieved by finding the maximum value of similarity of the sensor data with a mutual correlation function calculated over a specific time region (e.g., one second).

3. Experiments

3.1 Experimental Setup

We evaluated the proposed algorithm on a flat road section (Fig. 2) with very little change in the road attributes, where the localization error was as large as 100 m or more in tests with an earlier version of our method [2], [3]. In the prior tests, even when an accelerometer and gyro sensor were utilized in addition to the barometric sensor, there was no improvement of the position accuracy at the processing interval of 0.1 s. This was due to the influence of aliasing noise caused by the sampling interval being too large. Therefore, the objective in the current study is to reduce the effect of aliasing noise by performing normalized cross-correlation at 0.02 s (50 Hz). The experimental setup is summarized in Table 1. The MEMS sensors (Invensense Mpu9250) and Bosch BME280s were installed in the rear seat of the vehicle, as shown in Fig. 3, and the resultant data were processed with the resolution of 50 Hz for Mpu9250 data. The atmospheric sensor data was utilized simply to identify the flatness of the test course.



Fig. 2. Flat and straight 1.36-km test course alongside a Grade 2 river.

Fig. 4 shows the altitude along the test course, where we can see that the altitude change is very small, especially in the range of 30 to 50 s of the travel time. Since this road is alongside a river, the overall altitude change is 11.0 m/km (15 m / 1.36 km) and is quite smooth. The altitude was measured by averaging 16 atmospheric pressure sensors (Bosch BME280) [13] to reduce random noise and then estimated from the atmospheric pressure.

Table 1 Experimental setup.

Date	Dec.5(Sun),2021 ,Mar.6(Sun),2022
Vehicle	Daihatsu Mira geno (Small car)
MEMS sensors	1. Invensense Mpu-9250, 50Hz data acquisition. Acceleration, angular velocity,geomagnetism 2. Bosche BME280 atmospheric pressure sensor, 20Hz data acquisition
RTK-GNSS	u-blox ZED-F9P,5Hz data acquisition
Test course	1.36km, Shikano-cho, Tottori-shi,Japan

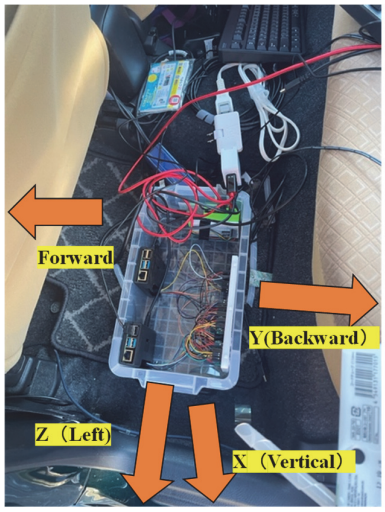


Fig. 3. Sensor axes of Mpu-9250 (indicated by arrows).

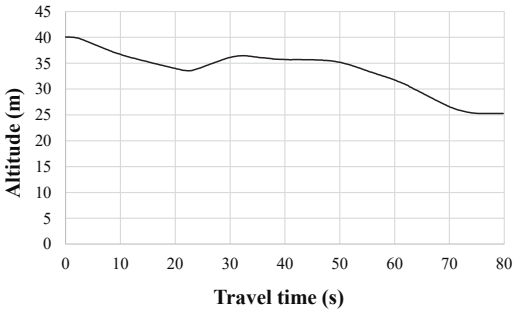


Fig. 4. Altitude profile along test course.

3.2. Pattern Matching by Normalized Cross-correlation Function

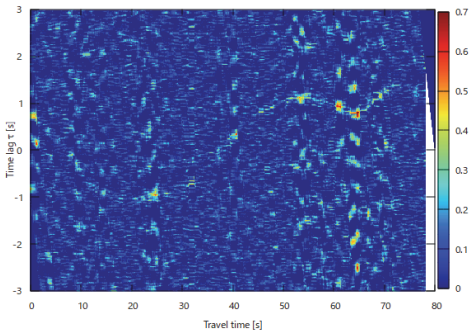
Nine normalized cross-correlation functions were obtained for each sensor data (acceleration, angular

velocity, and magnetization for x, y, and z axes). Each item of sensor data of the evaluation vehicle on Mar. 6, 2022 was correlated with the reference vehicle data of Dec. 5, 2021.

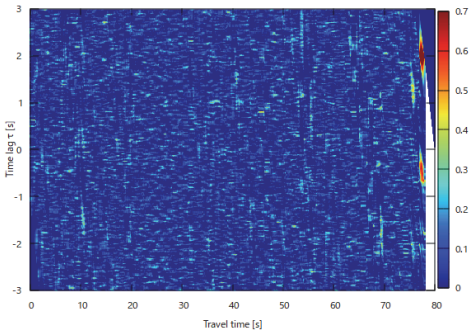
The cross-correlation functions are displayed using the jet colormap in MATLAB.

3.2.1 Normalized Cross-correlation of Acceleration Sensor Data

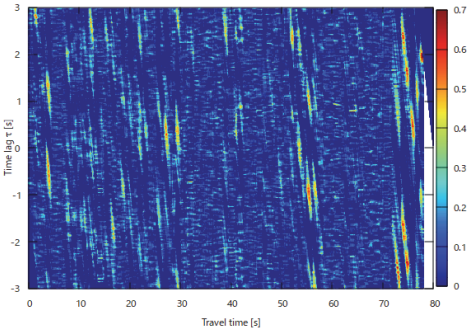
Fig. 5 shows the results of the normalized cross-correlation of the acceleration data. As we can see, there is a slight time lag profile for ax, that is, acceleration in the vertical direction.



(a) ax



(b) ay



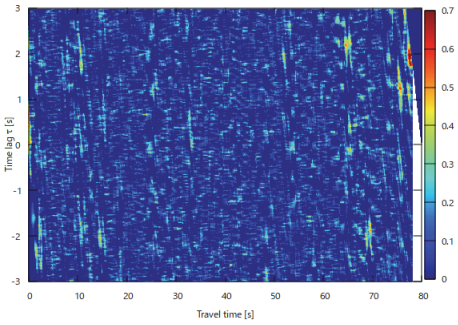
(c) az

Fig. 5. Normalized cross-correlation of acceleration sensor data. Acceleration data toward x, y, and z axes are denoted as ax, ay, and az.

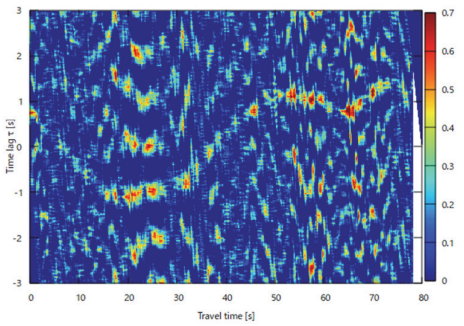
3.2.2. Normalized Cross-correlation of Acceleration Sensor Data for Gyroscope

Fig. 6 shows the results of the normalized cross-correlation of the gyroscope data, where omz clearly shows the time lag profile. Omy shows the time lag profile as well, though its resolution is lower. Gyroscope data around the z axis represents the pitch rate and around the y axis represents the roll rate.

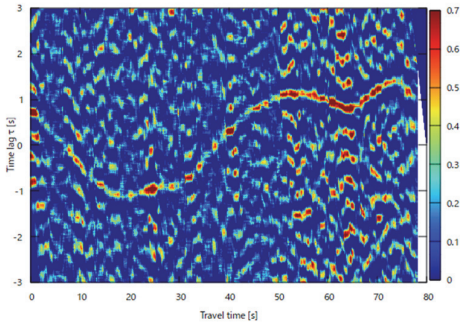
Yaw rate, that is, the rotation rate around the x axis, does not effectively capture the road features and the time lag profile cannot be seen. This is because the test road is mostly straight and so there is very little change in the yaw rate.



(a) omx



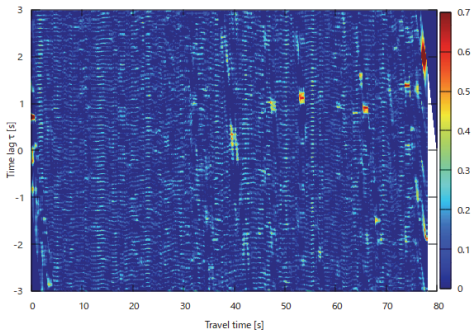
(b) omy



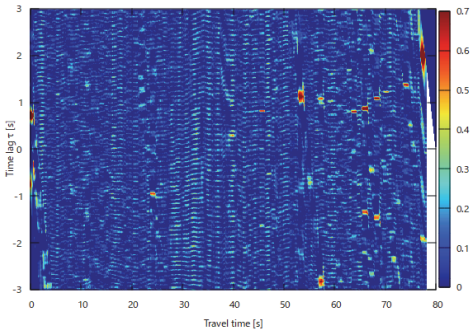
(c) omz

Fig. 6. Normalized cross-correlation of gyroscope data. Gyroscope data around x, y, and z axes are denoted as omx, omy, and omz.

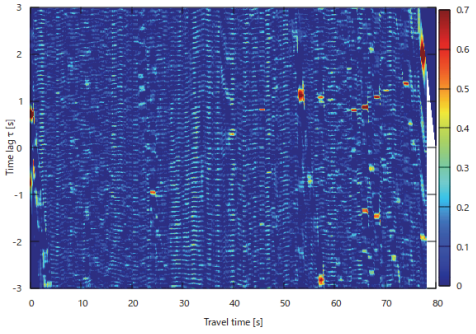
Fig. 7 shows the results of the normalized cross-correlation of the geomagnetism data. Some portions of the time lag profile are visible, especially for the latter part from 40 to 80 s of the evaluation vehicle travel time. The resolution is rather high.



(a) mx



(b) my



(c) mz

Fig. 7. Normalized cross-correlation of geomagnetism data. Geomagnetism data along x, y, and z axes are denoted as mx, my, and mz.

3.3. Optimum Weight of Normalized Cross-correlation Functions

In the previous sections, we demonstrated that nine normalized cross-correlation functions can be obtained, some of which clearly show the time lag profile and others of which do not. In this section, we describe how to optimally weight these functions and average them to form an optimum normalized cross-correlation function. The optimum weights are calculated by a simulated annealing method so that the measure function F (defined in Eq. (7)) is maximized. F measures the signal-to-noise ratio (SNR) of the optimum normalized cross-correlation function of Eq. (4).

$$R_{opt}(i,j) = \sum_{n=0}^{M-1} w_n R_n(i,j) \tag{4}$$

$$w_n \geq 0, n = 0,1,\ldots,8 \tag{5}$$

$$\sum_{n=0}^{8} w_n = 1 \tag{6}$$

$$F = \frac{1}{M}\sum_{i=0}^{M-1} \frac{max_j R_{opt}(i,j)}{\left|min_j R_{opt}(i,j)\right|} \tag{7}$$

Fig. 8 shows the optimum weights we derived. As we can see, the pitch rate, vertical magnetism, roll rate, and backward magnetism all play significant roles (74.7%) in vehicle localization in the proposed algorithm. Fig. 9 shows the optimally weighted cross-correlation functions, where the time lag profile is clearly recognizable.

Fig. 10 shows the equally weighted cross-correlation functions. As we can see, the time lag profile is much more clearly observed in Fig. 9 than in Fig. 10.

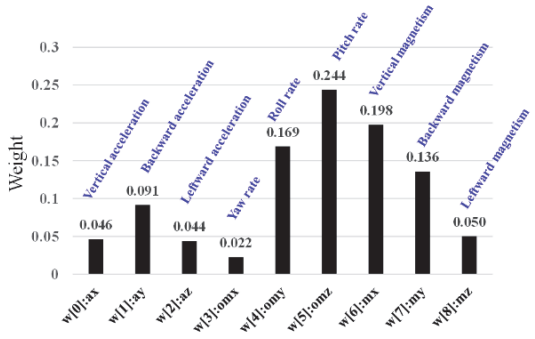


Fig. 8. Optimum weight of cross-correlation functions.

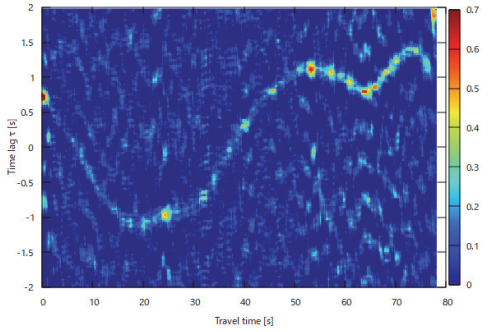


Fig. 9. Optimally weighted cross-correlation functions.

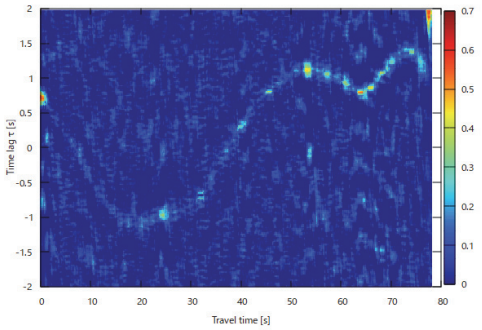


Fig. 10. Equally weighted cross-correlation functions.

3.4. Convergence of Optimum Weight

We applied a simple simulated annealing algorithm to obtain a set of optimum weights. Fig. 11 shows the value profile of the measure defined by Eq. (7) during the simulated annealing. As we can see, it successfully converges to a maximum value of 1.383 starting at its initial value of 1.305, where all weights are set equal to 1/9 = 0.1111.

Fig. 12 shows the values of each weight, all of which have converged almost by iteration 200. The CPU consumption time using an INTEL core-i5 CPU is several minutes. Since these weights only need to be calculated once, high-speed calculation (e.g., within one second) is not required.

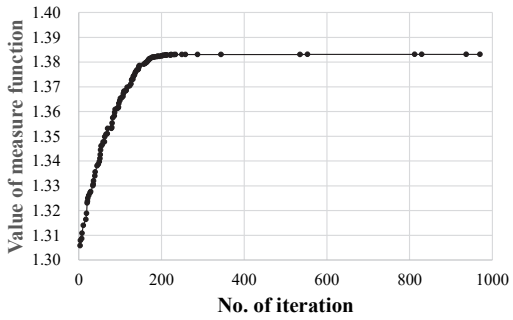


Fig. 11. Convergence of measure function.

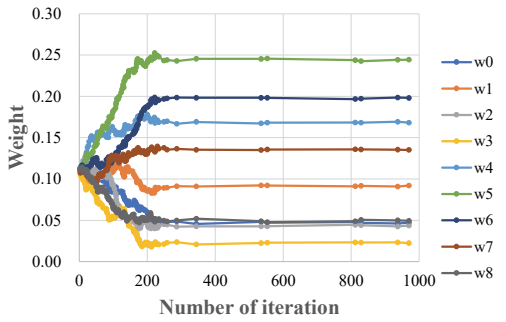


Fig. 12. Convergence of each weight.

3.5. Estimation of Vehicle Time Lag by Noise Reduction

To estimate the vehicle time lag by noise reduction, we first obtained the time lag for each travel time point by searching for a maximum cross-correlation value for each travel time point. Fig. 13 shows the time lag estimates when the weights for each cross-correlation function are equal, and Fig. 14 shows the results when the optimum weights are used. It is clear that a less noisy estimate of the time lag was made possible thanks to using the optimum weight.

The next step is to estimate the time lag profile from the noisy time lag estimates in Fig. 13 (equal weight) or Fig. 14 (optimum weight). Even though noise is eliminated to some extent, especially in the case of Fig. 14, it is still noisy.

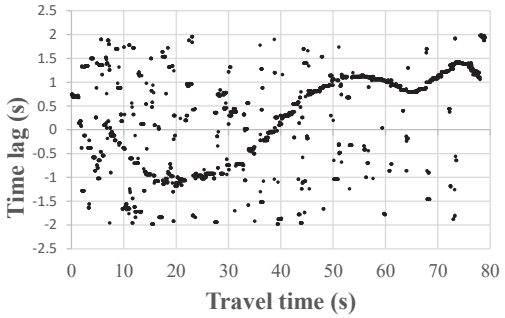


Fig. 13 Time lag estimate with equal weight before applying noise elimination filter.

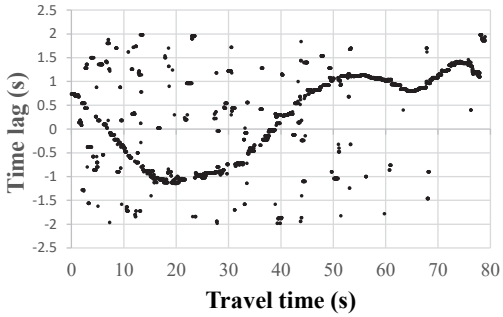


Fig. 14. Time lag estimate with optimum weight before applying noise elimination filter.

We therefore developed a simple but practical noise elimination filter for these noisy time lag data, as described by the pseudocode of Algorithm 1. Parameter θ is a positive threshold value to decide whether the time lag estimate $\hat{\tau}_{i+1}$ should be replaced by the previous estimate $\hat{\tau}_i$ or not. If the next time lag data τ_{i+1} differs from the current estimate $\hat{\tau}_i$ beyond the range limit θ, we keep the current value; otherwise, the time lag τ_{i+1} is accepted.

Algorithm 1. Noise elimination filter.

```
Begin
    for (i=0; 0<IMAX; i=i+1)
        if |τ_{i+1} − τ̂_i| < θ then τ̂_{i+1} = τ_{i+1}
        else τ̂_{i+1} = τ̂_i
        endif
End
```

Here τ_i is the time lag obtained by searching for the maximum value at each travel time, and it may differ significantly from the true value due to sensor noise or other factors. $\hat{\tau}_i$ is the estimated value of the time lag at time index i, and it is hopefully eased somewhat from the effect of noise. i is the time index of the travel time of the evaluation vehicle. IMAX is the quantity of the time series data. In this paper, θ is set to 0.4 s, which is not much strict, and almost the same results are obtained in the range of $0.3\ s < \theta < 0.4\ s$.

Fig. 15 show the time lag profile estimated from the optimally weighted cross-correlation functions after applying the noise elimination filter. The ground truth value of the time lag obtained by RTK-GNSS is also shown.

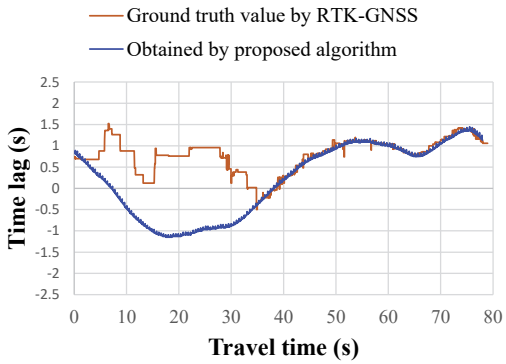


Fig. 15. Time lag estimate with equal weight after applying noise elimination filter.

Fig. 16 show the time lag profile estimated from the equally weighted cross-correlation functions after applying the noise elimination filter. The ground truth value of the time lag obtained by RTK-GNSS is also shown.

It is clear that the time lag profile obtained from the optimally weighted cross-correlation functions (Fig. 16) matches quite well to the ground truth data. In contrast, the time lag estimate from the equally weighted cross-correlation functions (Fig. 15) failed to accurately estimate the time lag in the range of 0 to 35 sec because of insufficient noise elimination. The ground truth of the time lag between the two vehicles was calculated by comparing the RTK-GNSS trace of each vehicle. RTK-GNSS was operating at 5 Hz and the traces were over-sampled at 50 Hz by introducing a linear interpolation of 5-Hz position data. It is reasonable that a vehicles velocity cannot be changed so rapidly within 0.2 seconds, so we consider the obtained 50-Hz resolution ground truth data to be sufficiently reliable. The RMS error of the time lag estimation in the optimum weight case was 0.091 s, which is a far more precise result than what we obtained with our earlier method [2, 3]. At the travel time of 50 s, the time lag estimate reached the maximum error of about 0.3 s.

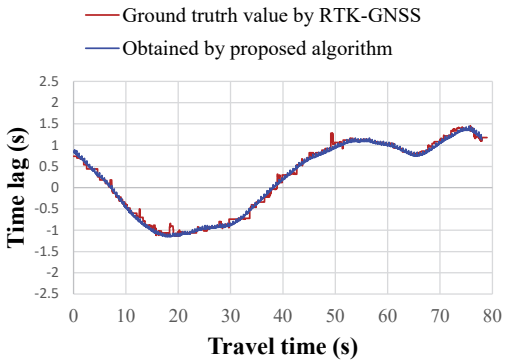


Fig. 16. Time lag estimate with optimum weight after applying noise elimination filter.

3.6. Estimation of Vehicle Position and its Evaluation

We utilized the proposed algorithm to precisely estimate the position error following the data flow in Fig. 17.

The algorithm input is the date and time the evaluation vehicle is running, and its corresponding MEMS sensor data are pattern matched to the reference MEMS sensor data. This pattern matching outputs the time lag between the evaluation vehicle and the reference vehicle. In our study, the reference vehicle was running in December 2021 and the evaluation vehicle was running in March 2022, which is a time lag of roughly three months. For simplicity, we reduced this lag to several seconds (note that this does not limit the generality of the proposed algorithm). The ground truth position of the evaluation vehicle is obtained by the RTK-GNSS and the estimated position is obtained by the position of the reference vehicle obtained by RTK-GNSS at the date and time of the reference vehicle that is obtained by the time lag estimate. The position error can be calculated from longitude and latitude values of the RTK-GNSS data of both vehicles.

Fig. 18 shows the position error along the travel time of the evaluation vehicle when the cross-correlation functions are equally averaged. As we can see, the maximum error is 9.6 m at the travel time of about 22 s. This is due to the failure of the time lag estimate, as shown in Fig. 15.

Fig. 19 shows the position error along the travel time of the evaluation vehicle when the cross-correlation functions are optimally weighted. In this case, the RMS position error is 0.37 m and the spike-like maximum error is 1.75 m. This result is superior

to any result of our previous study. The maximum error occurs at the travel time of 47 s, which is also where the time lag estimate error is apparent in Fig. 16.

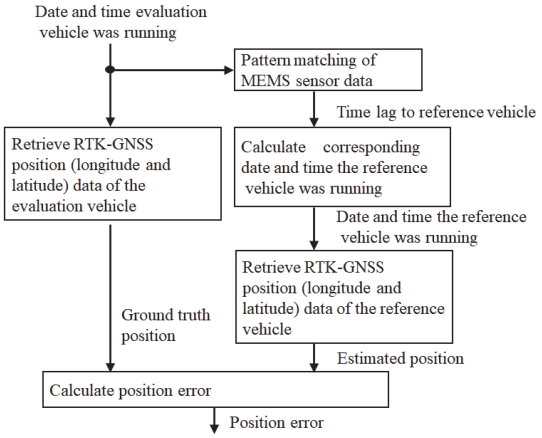


Fig. 17. Flow of position error evaluation.

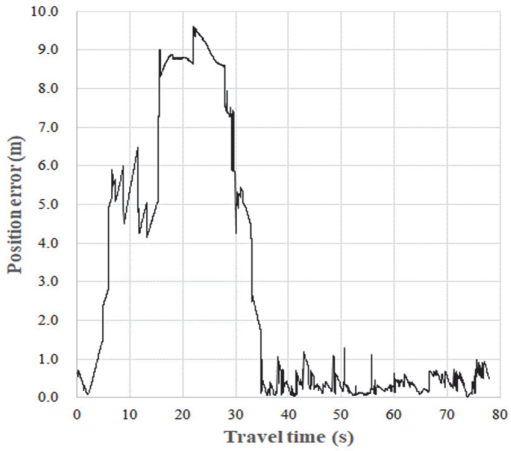


Fig. 18. Position error along evaluation travel time with equally averaged cross-correlation functions. Failure occurs in the range of 0–30 s. The maximum error is 9.6 m at the travel time of about 22 s.

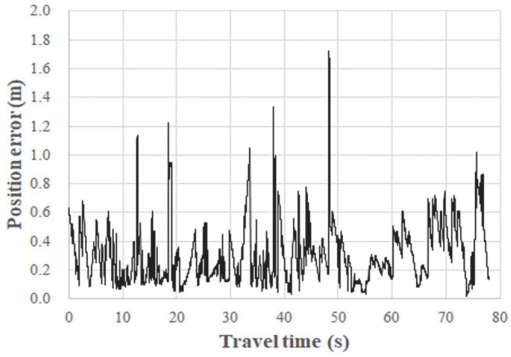


Fig. 19. Position error along evaluation travel time with optimally weighted cross-correlation functions. RMS error is 0.37 m. The maximum error is 1.75 m at the travel time of about 47 s.

Throughout this work, all software is written in C++ and Python for both Windows PC and Raspberry Pi 4B.

4. Conclusions

In this work, we presented a vehicle localization algorithm based on MEMS sensor data and demonstrated through evaluation tests on a real road that it can achieve highly precise position estimation. Our main contributions are summarized as follows.

1. We set up MEMS sensor data acquisition equipment operating at 50 Hz to calculate cross-correlation functions with a sufficient time resolution.
2. Among the nine cross-correlation functions we examined, the pitch rate, vertical magnetism, roll rate, and backward magnetism all played significant roles (74.7 %) in the vehicle localization. Among these types of sensor data, the pitch rate weight makes the largest contribution (24.4 %), which coincides with the fact that most terrain-based localization algorithms utilize pitch rate data as a major feature of roads.
3. After performing optimally weighted averaging of the nine cross-correlation functions using a noise elimination filter, the time lag estimation worked quite well; its estimation RMS error was 0.091 seconds.
4. The accuracy of the vehicle position estimation derived from the optimally weighted cross-correlation function outperformed that obtained from the equally weighted cross-correlation function.
5. Detailed position error analysis revealed that the position RMS error is 0.37 m and its maximum error is 1.75 m, both of which are far lower than our previous results.

Future extensions will involve combining a dead reckoning algorithm to stabilize the position estimation by eliminating the spike-like position errors and extending the algorithm to more general road networks by combining a map-matching algorithm [7]. We will also investigate the performance of the proposed algorithm when different vehicles and drivers are involved.

Acknowledgements

This work was supported by JSPS KAKENHI Grant number JP20K04723.

References

[1]. T. Yokota and T. Yamagiwa, Vehicle Localization by Optimally Weighted Use of MEMS Sensor Data, in *Proceedings of the 3rd IFSA Winter Conference on Automation, Robotics & Communications for Industry 4.0 / 5.0 (ARCI 2023),* Chamonix-Mont-Blanc, France, Feb. 2023, pp. 79–84.

[2]. T. Yamagiwa and T. Yokota, Vehicle Localization Method Based on MEMS Sensor Data Comprising Pressure, Acceleration and Angular Velocity, in *Proceedings of the IEEE International Conference on*

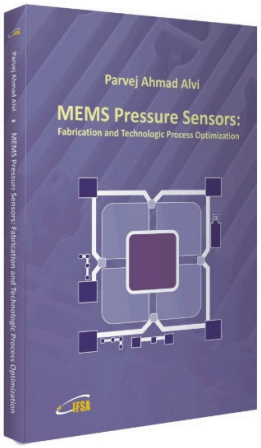
Mechatronics and Automation (ICMA), Guilin, Guangxi, China, 2022, pp. 786-791.
[3]. T. Yokota, Vehicle localisation by altitude data matching in spatial domain and its fusion with dead reckoning, *International Journal of Mechatronics and Automation,* Vol. 8, No. 4, Jan. 2021, pp. 208–216.
[4]. T. Yokota, Vehicle localization by dynamic programming from altitude and yaw rate time series acquired by MEMS sensor, *SICE Journal of Control, Measurement, and System Integration*, Vol. 14, No. 1, April 2021, pp. 78–88.
[5]. T. Yokota, Vehicle Localization Based on MEMS Sensor Data, in *Proceedings of the 60th Annual Conference of the Society of Instrument and Control Engineers of Japan (SICE' 2021)*, Sept. 2021, pp. 1094 - 1100.
[6]. T. Yokota, Localization Algorithm Based on Altitude Time Series in GNSS-Denied Environment, in *Proceedings of the SICE Annual Conference*, September 23–26, 2020, pp. 952–957.
[7]. T. Yokota, M. Okude, T. Sakamoto, and R. Kitahara, Fast and robust map-matching algorithm based on a global measure and dynamic programming for sparse probe data, *IET Intell. Transp. Syst*., Vol. 13, Issue 11, 2019, pp. 1613–1623.
[8]. J. Tsurushiro and T. Nagaosa, Vehicle localization using its vibration caused by road surface roughness, in *Proceedings of the IEEE International Conference on Vehicular Electronics and Safety*, Yokohama, Japan, Nov. 2015, pp. 164–169.
[9]. A. J. Dean, R. D. Martini, and S. N. Brennan, Terrain-based road vehicle localisation using particle filters, *International Journal of Vehicle Mechanics and Mobility*, Vol. 49, Issue 8, 2011, pp. 1209–1223.
[10]. E. I. Laftchiev, C. M. Lagoa, and S. N. Brennan, Vehicle Localization Using In-Vehicle Pitch Data and Dynamical Models, *IEEE Transactions on Intelligent Transportation Systems,* Vol. 16, Issue 1, February 2015, pp. 206–220.
[11]. C. A. Gim, Inertial-Sensor-Based Non-Dead Reckoning Localization for Ground Vehicles, *IEEE Access*, Vol. 9, 2021, pp. 132766–132778.
[12]. X. Qu, B. Soheilian, and N. Paparoditis, Landmark-based localization in urban environment, *ISPRS Journal of Photogrammetry and Remote Sensing*, Vol. 140, June 2019, pp. 90–103.
[13]. https://www.boschsensortec.com/products/environmental-sensors/humidity-sensors-bme280/ (accessed on Jan. 27 2023).
[14]. https://www.u-blox.com/en/product/zed-f9p-module (accessed on April 6 2023).
[15]. https://invensense.tdk.com/products/motion-tracking/9-axis/mpu-9250/ (accessed on April 6 2023).

Published by International Frequency Sensor Association (IFSA) Publishing, S. L., 2023 (http://www.sensorsportal.com).

Parvej Ahmad Alvi

IFSA

MEMS Pressure Sensors:
Fabrication and Technologic Process Optimization



So far, no book has described the step by step fabrication process sequence along with flow chart for fabrication of micro pressure sensors, and therefore, the book has been written taking into account various aspects of fabrication and designing of the pressure sensors as well as fabrication process optimization. A complete experimental detail before and after each step of fabrication of the sensor has also been discussed. This leads to the uniqueness of the book.

Features include:
A complete detail of designing and fabrication of MEMS based pressure sensor.
- Step by step fabrication and process optimization sequence along with flow chart, which is not discussed in other books.
- Description of novel technique (lateral front side etching technique) in terms of chip size reduction and fabrication cost reduction, and comparative study on both the techniques (i.e. Front Side Normal Etching Technology and Front Side Lateral Etching Technology) for the fabrication of thin membrane.
- Discussion on issues of sealing of conical tiny cavity; because the range of pressure applied (i.e. greater or less than atmospheric pressure) can be decided by methodology of sealing of tiny cavity.
- A complete theoretical detail regarding aspects of designing and fabrication, and experimental results before and after each step of fabrication.

MEMS Pressure Sensors: Fabrication and Process Optimization will greatly benefit undergraduate and postgraduate students of MEMS and NEMS courses. Process engineers and technologists in the microelectronics industry including MEMS-based sensors manufacturers.

Hardcover: ISBN 978-84-616-2207-8
e-Book: ISBN 978-84-616-2438-6

Order: http://www.sensorsportal.com/HTML/BOOKSTORE/MEMS_Pressure_Sensors.htm

Sensors & Transducers, Vol. 261, Issue 2, June 2023, pp. 10-14

Sensors & Transducers

Published by IFSA Publishing, S. L., 2023
http://www.sensorsportal.com

Anti-Lock Braking System Control using Backstepping Method Based Fuzzy Logic

*** Najlae Jennan and El Mehdi Mellouli**
Laboratory of Engineering, Systems and Applications, Sidi Mohamed Ben Abdellah University, National School of Applied Sciences, Fez, Morocco
Tel.: 0610035443
E-mail: najlae.sef@gmail.com

Received: 14 April 2023 Accepted: 16 July 2023 Published: 26 June 2023

Abstract: The Anti-Lock Braking system (ABS) is one of most important safety systems of vehicles which must be controlled effectively. In this paper, we are concerned on controlling an Anti-Lock Braking system of an autonomous vehicle using a nonlinear Backstepping control method based on Takagi Sugeno (T-S) Fuzzy Logic method, employing Lyapunov approach to study the system stability. In the first step, we apply the Backstepping control method to the system in order to control it by studying its stability using Lyapunov approach. The second step consists on adding the Fuzzy Logic technique for the aim to optimize the objective function that can provide a desired level of stability to the Anti-Lock Braking system. The simulation of results found shows the accuracy of our proposed control strategy.

Keywords: Anti-lock braking system, Backstepping control, Nonlinear system, T-S fuzzy logic.

1. Introduction

An Anti-Lock Braking System (ABS) is one of important safety systems of vehicles. It prevents the wheels from self-locking during braking, which offers the possibility of maintaining steering control of the vehicle. Driving without the Anti-Lock Bracking System (ABS) is entirely possible, but increases the risk of accidents. Therefore, it is necessary to improve the vehicles safety by using the ABS [1, 2]. For that, the control of this system is very important and must be accurate and efficient for the aim to control the wheel slip at its optimum value [3, 4]. Therefore, the backstepping control method is proposed to control the ABS which is a developed control method that consists in forcing the system to pursue the desired value in a finite time and with certain conditions to respect in order to ensure the system stability, and provides effective results [5-7]. In order to improve the system control, to keep the system in a desired level of stability and to reach better results, the T-S Fuzzy Logic method is proposed to optimize the objective function that is designed to keep the system stable [8-10]. Generalizing the control law requires the study of system stability using Lyapunov approach [11, 12].

The main objective in our works concerns controlling the ABS system using Backstepping Control method, optimizing the objective function of stability using the T-S fuzzy Logic technique and studying the system stability using Lyapunov approach in order to generalize the control law respecting the stability conditions [13-16].

The efficiency of our control strategy proposed is evaluated and shown in the simulations of results achieved.

This paper is organized as follows: Section 2 concerns the ABS system modelling. In Section 3, we present the control strategy proposed. Then in Section 4, the T-S Fuzzy Logic method is presented. After that, we present in Section 5 the simulations of results found. Finally, a conclusion is presented in Section 6.

2. ABS System Modeling

It is necessary to study the mathematical model of the ABS system in order to control it [2]. Fig. 1 represents the wheel model.

The ABS system contains some important units as an electronic control unit, a hydraulic control unit and sensors of speed in each wheel as shown in Fig. 2.

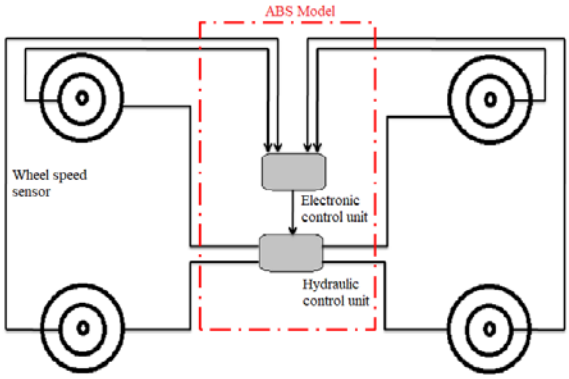


Fig. 1. Wheel model.

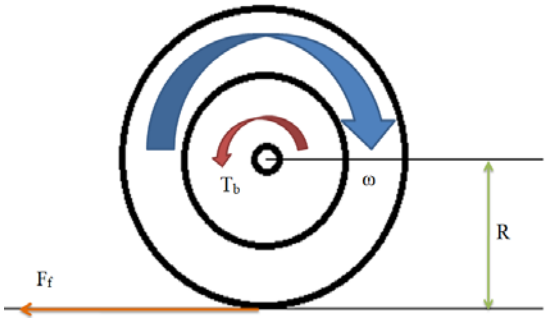


Fig. 2. Anti-Lock Braking model.

Using Newton-Euler formalism, we represent the ABS model by a system of differential equations expressing the velocity v, the angular velocity ω and the slip coefficient λ [1].

$$\begin{cases} \dot{v} = -g.\mu \\ \dot{\omega} = \frac{1}{J}(m.g.\mu.R - T_b) \end{cases} \quad (1)$$

$$\dot{\lambda}(t) = f(\lambda, t) + h(\lambda, t).u(\lambda, t)\,, \quad (2)$$

where f and h are the system dynamics, with:

$$\begin{cases} f(\lambda, t) = \left[\frac{\dot{v}}{v}(1-\lambda) - \frac{m.g.R^2}{v}\mu\right] \\ h(\lambda, t) = \frac{R}{v} \end{cases} \quad (3)$$

$u = T_b$ is the control law that will be studied in the next section which represents the braking torque and $\mu = F(\lambda)$ is the friction coefficient.

With

$$F(\lambda) = c_1\left(1 - e^{-c_2\lambda}\right) - c_3\lambda\,, \quad (4)$$

where c_1, c_2 and c_3 are constant coefficients.

3. Control Strategy

In this work, we are interested in controlling the ABS system using Backstepping control method based on the T-S Fuzzy Logic methodology [5, 7, 17].

To apply this method in the ABS system, we firstly define the tracking error in the following form:

$$\begin{cases} e = \lambda_d - \lambda \\ \dot{e} = \dot{\lambda}_d - \dot{\lambda} \end{cases} \quad (5)$$

Then, we define the Lyapunov function to study the system stability in order to generalize the control law [11][18].

$$V_1 = \frac{1}{2}e^2 > 0 \quad (6)$$

The derivative of the Lyapunov function must be negative to ensure the system stability.

$$\begin{aligned} \dot{V}_1 &= e.\dot{e} < 0 \\ &= e.\left(\dot{\lambda}_d - f(\lambda, t) - h(\lambda, t).u(\lambda, t)\right) \end{aligned}$$

We assume that:

$$\dot{V}_1 = -\alpha.e^2 \leq 0, \quad (7)$$

where $\alpha > 0$ is a constant coefficient.

Then, we define the control law of the system:

$$u(\lambda, t) = \frac{1}{h(\lambda, t)}\left(\dot{\lambda}_d - f(\lambda, t) + \hat{\alpha}(\lambda, \theta_\alpha).e\right), \quad (8)$$

where $\hat{\alpha}(\lambda, \theta_\alpha)$ is the optimal objective function that will be studied using the T-S Fuzzy Logic technique in the next section.

4. T-S fuzzy Logic

In this section, we present the T-S Fuzzy Logic method used in the ABS system to optimize the objective function that keeps the system in a desired level of stability, in order to achieve better results respecting the conditions of system stability using Lyapunov approach [19-21].

We define first the membership functions chosen as follows:

$$\mu_i = e^{-(-\left(\frac{\lambda_j - c_i}{(2\sigma_i)^2}\right))}; \; i = 1,2 \tag{9}$$

Then, the inference phase consists on a collection of IF-THEN rules which are defined in the following form [22-24], if x_1 is α_1^j and....., ... and x_n is α_n^j then α_j is θ_j

Finally, it is necessary to deduce the output of the fuzzy system using Lyapunov approach to ensure the system stability, which is expressed as follows:

$$\hat{\alpha}(\lambda, \theta_\alpha) = \frac{\sum_{j=1}^{k} \theta_j (\prod_{i=1}^{n} \mu_{\alpha_i^j}(\lambda_i))}{\sum_{j=1}^{k} (\prod_{i=1}^{n} \mu_{\alpha_i^j}(\lambda_i))} = {\theta_\alpha}^T . \xi(\lambda) \tag{10}$$

We assume the expression of the Lyapunov function:

$$V_2 = \frac{1}{2} e^2 + \frac{1}{2\gamma} . \Phi_\alpha . {\Phi_\alpha}^T > 0 \tag{11}$$

with:

$$\Phi_\alpha = \theta_\alpha - {\theta_\alpha}^* , \tag{12}$$

where θ_α is the optimal parameter, and:

$${\theta_\alpha}^* = \arg\min(\sup_{\lambda \epsilon R} |\alpha(\lambda, t) - \hat{\alpha}(\lambda, \theta_\alpha)|) \tag{13}$$

The derivative of the Lyapunov function must be negative [12][18].

$$\begin{aligned} \dot{V}_2 &= e . \dot{e} + \frac{1}{\gamma} . \Phi_\alpha . \dot{\Phi}_\alpha \leq 0 \\ &= e . \left(\dot{\lambda}_d - f(\lambda, t) - h(\lambda, t) . u(\lambda, t)\right) \\ &\quad + \frac{1}{\gamma} . \Phi_\alpha . \dot{\Phi}_\alpha \\ &= e . \left((\hat{\alpha}(\lambda, {\theta_\alpha}^*) - \hat{\alpha}(\lambda, \theta_\alpha)) . e\right. \\ &\quad \left. - \hat{\alpha}(\lambda, {\theta_\alpha}^*) . e\right) \\ &\quad + \frac{1}{\gamma} . \Phi_\alpha . \dot{\Phi}_\alpha \end{aligned} \tag{14}$$

From (10) we find:

$$\begin{aligned} \dot{V}_2 &= e . (-\Phi_\alpha . \xi(\lambda) . e - \hat{\alpha}(\lambda, {\theta_\alpha}^*) . e) + \frac{1}{\gamma} . \Phi_\alpha . \dot{\Phi}_\alpha \\ &= \frac{1}{\gamma} . \Phi_\alpha . \left(\dot{\Phi}_\alpha + e^2 . \gamma . \xi(\lambda)\right) - \hat{\alpha}(\lambda, {\theta_\alpha}^*) . e^2 \end{aligned}$$

Taking $\dot{\Phi}_f + e^2 . \gamma . \xi(\lambda) = 0$, we extract the expression of θ_α.

After calculations we obtain:

$$\dot{V}_2 = -\hat{\alpha}(\lambda, {\theta_\alpha}^*) . e^2 \tag{15}$$

Then $\hat{\alpha}(\lambda, {\theta_\alpha}^*)$ must verify the following condition to ensure the system stability.

$$\hat{\alpha}(\lambda, {\theta_\alpha}^*) \geq 0 \tag{16}$$

and

$$\theta_\alpha = \gamma . e^2 . \xi(\lambda) \tag{17}$$

5. Simulation of Results

In order to evaluate the performance of our control strategy proposed, we did many simulations of results found.

First, we employed the Backstepping control method in the ABS system to control the wheel slip and regulate it to its optimum value, which is chosen as follows: $\lambda_d = 0.15$. Then, we add the T-S Fuzzy Logic method to optimize the objective function that provides a desired level of stability to the system.

We simulate the braking torque T_b generated by the Backstepping control method using Fuzzy Logic method.

Fig. 3 shows the evolution of the control law obtained using our control strategy proposed.

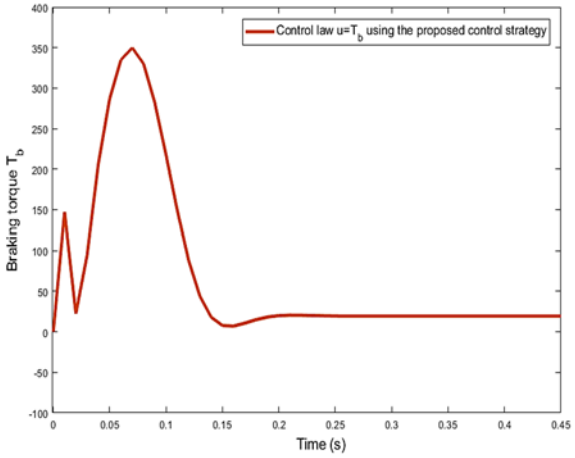


Fig. 3. The control law obtained by the proposed control method using Fuzzy Logic.

We employed the Fuzzy Logic method in the system control for the aim to achieve better results by getting a fast response of convergence.

Fig. 4 represents the evolution of the wheel slip using the control strategy proposed with and without Fuzzy Logic method, which it can be seen that using the Fuzzy Logic in the system control is efficient; the convergence is faster than without using it.

We simulate the tracking error between the desired value to reach and the wheel slip reached using our control strategy with and without the Fuzzy Logic.

Fig. 5 shows that the tracking error converges to 0 in a finite time using the control strategy proposed, but faster when using the Fuzzy Logic method.

After that, we simulate the speed obtained using the proposed backstepping control method with and without Fuzzy logic to demonstrate the accuracy of our proposed control strategy.

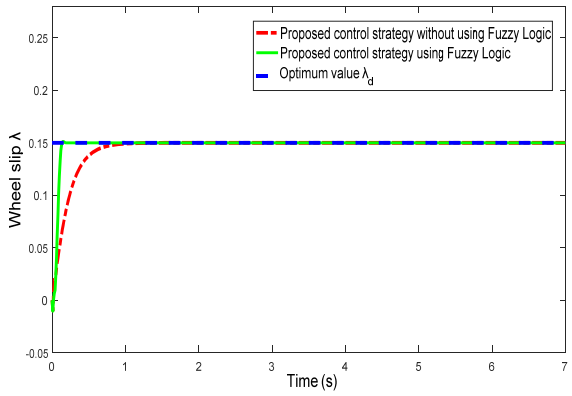


Fig. 4. The evolution of the wheel slip obtained by the proposed control strategy with and without Fuzzy Logic.

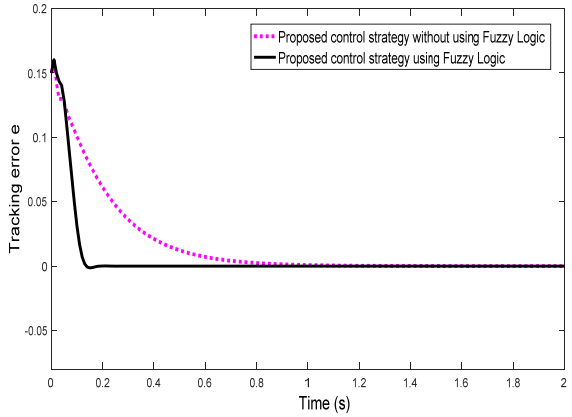


Fig. 5. The evolution of the tracking error between the wheel slip and the desired value.

Fig. 6 shows the evolution of the speed achieved using our control strategy proposed where the effectiveness of the Fuzzy Logic method in the system control is clearly shown, which the speed converges to 0 in faster time when using our control strategy proposed.

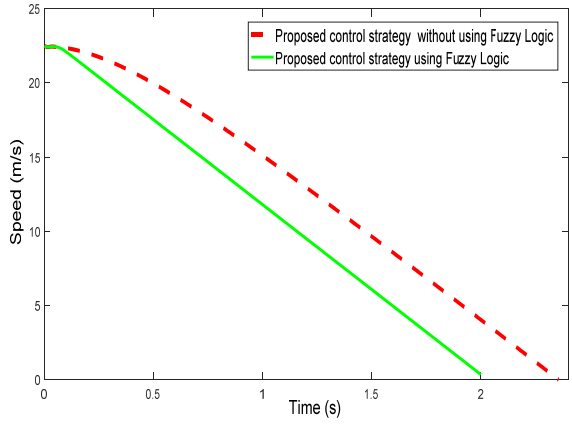


Fig. 6. The evolution of the speed obtained using the control strategy proposed.

The results show the efficiency of our proposed control strategy using the Backstepping control method combined with the T-S Fuzzy Logic method.

6. Conclusion

In this work, we presented the Backstepping control method for controlling an Anti-Lock Braking System, combined with T-S Fuzzy Logic method to optimize the system dynamics in order to reach better results. The generalization of the control law requires the study of system stability using Lyapunov approach.

The efficiency of our proposed control strategy is shown in the results simulation, and adding Fuzzy Logic method makes the system control more accurate.

References

[1]. F. Pretagostini, L. Ferranti, G. Berardo, V. Ivanov, B. Shyrokau, Survey on Wheel Slip Control Design Strategies, Evaluation and Application to Antilock Braking Systems, *IEEE Access,* 8, 2020, pp. 10950-10971.

[2]. W. Sun, J. Zhang, Z. Liu, Two-Time-Scale Redesign for Antilock Braking Systems of Ground Vehicles, *IEEE Transactions on Industrial Electronics*, 66, 6, 2018, pp. 4577-4586.

[3]. L. He, W. Ye, Z. He, K. Song, Q. Shi, A Combining Sliding Mode Control Approach for Electric Motor Anti-Lock Braking System of Battery Electric Vehicle, *Control Engineering Practice,* 102, 2020, 104520.

[4]. B. R. Lee, K. H. Sin, Slip-Ratio Control of ABS Using Sliding Mode Control, in *Proceedings of the 4th Korea-Russia International Symposium on Science and Technology (KORUS' 2000),* 2000, pp. 72-77.

[5]. A. M. Fihakhir, A. Mokhtari, Modeling and Backstepping Control of a New Quadrotor Unmanned Aerial Vehicle Type Heliplane, in *Proceedings of the International Conference Technological Advances in Electrical Engineering (ICATEE' 14),* 2014.

[6]. Y. Qiu, X. Liang, Z. Dai, Backstepping dynamic surface control for an anti-skid braking system, *Control Engineering Practice*, 42, 2015, pp. 140-152.

[7]. X. Zhang, H. Lin, Backstepping Fuzzy Sliding Mode Control for the Antiskid Braking System of Unmanned Aerial Vehicles, *Electronics*, 9, 10, 2020, p. 1731.

[8]. E. M. Mellouli, I. Boumhidi, Direct adaptive fuzzy sliding mode controller without reaching phase for an uncertain three-tank-system, *International Journal of Modelling, Identification and Control*, 25, 4, 2016, pp. 335-342.

[9]. M. A. Soliman, H. M. Hasanien, H. Z. Azazi, E. E. El-Kholy, S. A. Mahmoud, An Adaptive Fuzzy Logic Control Strategy for Performance Enhancement of a Grid-Connected Pmsg-Based Wind Turbine, *IEEE Transactions on Industrial Informatics,* 15, 6, 2018, pp. 3163 - 3173.

[10]. E. M. Mellouli, M. Alfidi, I. Boumhidi, Fuzzy sliding mode control for three-tank system based on linear matrix inequality, *International Journal of Automation and Control*, 12, 2, 2018, pp. 237-250.

[11]. Z. Cai, L. Huang, Generalized Lyapunov approach for functional differential inclusions, *Automatica*, 113, 2020, p. 108740.
[12]. S. Ding, K. Mei, X. Yu, Adaptive Second-order Sliding Mode Control: A Lyapunov Approach, *IEEE Transactions on Automatic Control,* 67, 10, 2022, pp. 5392-5399.
[13]. F. Adıgüzel, T. V. Mumcu, Adaptive Backstepping Sliding Mode Control for ABS with Nonlinear Disturbance Observer, *Electrica*, 21, 2021, pp. 121-128.
[14]. Y. He, C. Lu, J. Shen, C. Yuan, A second-order slip model for constraint backstepping control of antilock braking system based on Burckhardt's model, *International Journal of Modelling and Simulation*, 40, 1, 2019, pp. 1-13.
[15]. H. Yu, Z. Qi, J. Duan, S. Taheri, Multiple model adaptive backstepping control for antilock braking system based on LuGre dynamic tyre model, *International Journal of Vehicle Design*, 69, 1, 2015, pp. 168-184.
[16]. J. P. Fernández, M. A. Vargas, J. M. V, García, J. A, Cabrer, Coevolutionary Optimization of a Fuzzy Logic Controller for Antilock Braking Systems Under Changing Road Conditions, *IEEE Transactions on Vehicular Technology,* 70, 2, 2021, pp. 1255-1268.
[17]. E. M. Mellouli, J. Boumhidi, I. Boumhidi. Using fuzzy logic for eliminating the reaching phase on the fuzzy H∞ tracking control, *International Journal of Modelling, Identification and Control*, 20, 4, 2013, pp. 398-406.
[18]. X. Li, X. Yang, Lyapunov stability analysis for nonlinear systems with state-dependent state delay, *Automatica*, 112, 2020, p. 108674.
[19]. M. Montazeri, M. R Yousefi, K. Shojaei, G. Shahgholian, Fast adaptive fuzzy terminal sliding mode control of synergistic movement of the hip and knee joints (air-stepping) using functional electrical stimulation: A simulation study, *Biomedical Signal Processing and Control,* 66, 2021, p. 102445.
[20]. R. Naoual, E. M. Mellouli, S. Sefriti, I. Boumhidi, Fuzzy sliding mode control for the two-link robot, *International Journal of Systems, Control and Communications*, 6, 1, 2014, pp. 84-96.
[21]. E. M. Mellouli, S. Sefriti, I. Boumhidi, Combined fuzzy logic and sliding mode approach's for modelling and control of the two link robot, in *Proceedings of the IEEE International Conference on Complex Systems (ICCS)*, 2012, pp. 1-6.
[22]. E. M. Mellouli, R. Naoual, I. Boumhidi, A New Modified Sliding Mode Controller Based Fuzzy Logic for A Variable Speed Wind Turbine, *International Journal of Ecology & Development,* 32, 1, 2017, pp. 44-53.
[23]. R. Sharma, S. Bhasin, P. Gaur, D. Joshi, A Switching-Based Collaborative Fractional Order Fuzzy Logic Controllers for Robotic Manipulators, *Applied Mathematical Modelling,* 73, 2019, pp. 228-246.
[24]. E. M. Mellouli, S. Massou, I. Boumhidi, Optimal Robust Adaptive Fuzzy Tracking Control without Reaching Phase for Nonlinear System, *Journal of Control Science and Engineering*, 2013, 498461.
[25]. N. Jennan, E. M. Mellouli, Backstepping Control Method Combined with Fuzzy Logic for an Anti-Lock Braking System, in *Proceedings of 3rd IFSA Winter Conference on Applications, Robotics & Communications for industry 4. 0 / 5. 0 (ARCI' 2023),* Chamonix-Mont-Blanc, France, 22-24 February 2023, pp. 204-206.

Published by International Frequency Sensor Association (IFSA) Publishing, S. L., 2023
(http://www.sensorsportal.com)



Sensors & Transducers, Vol. 261, Issue 2, June 2023, pp. 15-24

www.sensorsportal.com

Sensors & Transducers

Published by IFSA Publishing, S. L., 2023
http://www.sensorsportal.com

Multi-Complex Robot Interaction with Homothetic Human Feedback in a Virtual Environment

[1, *] Taha HOUDA, [2] Ayman BEGHDADI, [2] Lotfi BEJI and [2] Ali AMOURI

[1] ESIEE-IT, 8 Rue Pierre de Coubertin, 95300 Pontoise, France
[2] IBISC EA 4526 Laboratory, University of Paris-Saclay, 91080 Evry-Courcouronnes, France
[1] Tel.: +33788596730
E-mail: thouda@esiee-it.fr, aymanaymar.beghdadi@univ-evry.fr,
lotfi.beji@univ-evry.fr, ali.amouri@univ-evry.fr

Received: 10 April 2023 Accepted: 7 June 2013 Published: 26 June 2023

Abstract: In recent years, the interaction between mechatronic systems and humans, such as human-robot and robot-robot interaction, has gained considerable momentum. The integration and coupling of virtual reality and virtual reality has become very important in Industry 4.0 and 5.0 in general. Motion simulators present a concrete system for the integration and interaction of mechatronic subsystems. Different types of simulators are increasingly being integrated in the various application areas in aviation, at sea and on land. The extension of the application of the simulator in the field of the sport and in particular of the functional rehabilitation has taken a great interest in the public and private sectors. In this context, our team objective is to study the design and to realize a simulator mastering all the low level elements in order to explore the integration of a virtual environment in a complex interactive robotic system. In this paper, we aim to study robot-robot interaction and validate the accuracy and shape tracking of motion perception in skiing for simulator users using the Nao robot.

Keywords: Handiski, Motion simulator, Robot-Robot interaction, Motion cueing algorithm, Humanoid robot, Disabled people, Washout filter.

1. Introduction

Handiski (Handicap, Alpine Skiing), means the adaptation of alpine skiing practice to people with disabilities, is a new sport that arouses a huge interest among enthusiasts, who enjoy practicing it every year. However, there are many restrictions to ski training, especially for people with disabilities. There are environmental dependencies, as skiing requires a good amount of snow and slopes, which limits the sport to certain seasons and suitable resorts.

For that, the ski simulators are becoming increasingly popular in the sliding sports industry due to their ability to replicate real-world sliding conditions and provide users with an immersive experience. They use advanced technologies to replicate the sliding motions, gravity, and vibrations of snow, such as the Motion Cueing Algorithm (MCA) [1]. These simulators can be used for sports training, injury recovery, mental preparation, and functional rehabilitation [2]. Ski simulators can also be coupled with virtual reality to increase immersion and human sensation [3]. To the best of our knowledge, all existing ski simulators use only a 2 DoF mechatronic system which is not sufficient to reproduce all the movements of the skier. We propose a VR-based indoor ski high degree of freedom training system 8 DoF simulator. Using this training system, we replay the movement of an expert skier recorded on a virtual track and we can reproduce this movement in the simulator as faithfully as possible.

MCAs are computer-based techniques used to simulate the effects of motion in skiers. These algorithms are designed to mimic the physical sensation of motion, such as acceleration and deceleration, by adjusting the visual cues that the skier receives. These cues can include changes in the skier's body position, speed, and slope angle, as well as changes in the skier's body position and motion itself. The MCA produces a trajectory that maximizes human sensation while respecting the physical limitations of the simulator.

In general, motion simulators are a multidisciplinary engineering system that can be traced back to the early 20th century. One of the first such devices was the Gough-Stewart platform [4], which was primarily used for military training and research [5, 6]. This platform has a six-degree-of-freedom range of motion. The upper platform can be mounted in a cockpit and uses a combination of rotating and linear actuators to simulate motion. Over time, motion simulators have evolved significantly thanks to advances in technology and engineering. The hybrid platform was introduced by coupling the Gough-Stewart platform with the X-rail or XY table to create a more realistic and immersive experience. For example, the Renault Driving Simulator, which adds an X-rail at Technocentre Renault, France [7] and the National Advanced Driving Simulator (NADS) at IOWA, USA [8] and the XY-6 DOF from IBISC Laboratory [9], which adds an XY table. The aim of the project is to contribute to technological progress in the field of rehabilitation and to provide a unique approach to physiotherapy for people with disabilities. For that, a low-cost simulator called the XY-6 DoF was designed and built from scratch in the IBISC laboratory [10]. The XY-6 DoF simulator is characterized by being completely open and allowing low-level access to the platform, which enables the development and adaptation of new algorithms.

In this paper, we aim to validate the precision and shape tracking of motion perception in skiing for simulator users and evaluate the effectiveness of the simulator as a rehabilitation tool. The humanoid robot Nao has a skeletal structure that mimics a human, which enables it to emulate human-like motion patterns. It is also equipped with appropriate sensors to perceive and interact with its environment. The Nao humanoid robot has been used to interact with humans for many years and has proven its efficiency. Nowadays, it is more and more used in robot-robot interaction, replacing humans, such as in the paper [11], which uses the Nao robot for gesture-based interaction between humans and multi-robot swarms. For all these reasons and for human safety, Nao is a good choice to replace humans with a good similarity.

This paper is organized as follows: Section 2 describes the technical and system architecture of the XY-6 DoF simulator. Section 3 discusses the robot coupling and interaction between the XY-6 DoF and the humanoid robot Nao. Finally, Section 4 presents simulations and discussions.

2. Technological Presentation

The ski simulator system integrates complex multi-robot interaction through the XY-6 DoF platform and the Nao humanoid robot. The XY-6DoF simulator presented in Fig. 1 and Fig. 2, was designed and developed from scratch by our research team in the IBISC laboratory [11].

The association of these two complex robotic systems with very different characteristics required a deep understanding of the low and high-level software and hardware system. The XY-6DoF simulator presented in Fig.1 and Fig.2, was designed and developed from scratch by our research team in the IBISC laboratory [11].

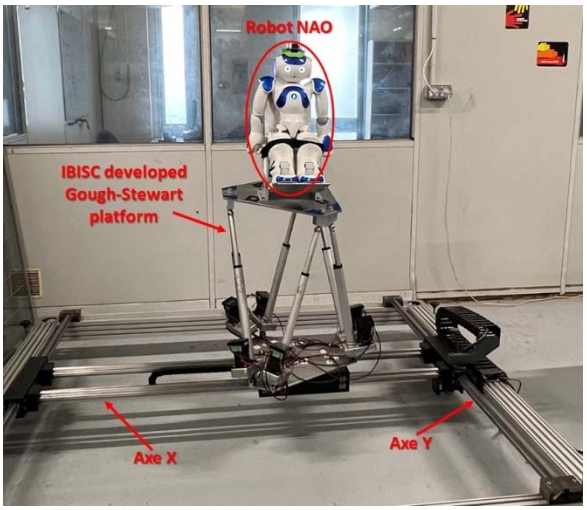


Fig. 1. The XY-6 DoF physical ski simulator with NAO robot.

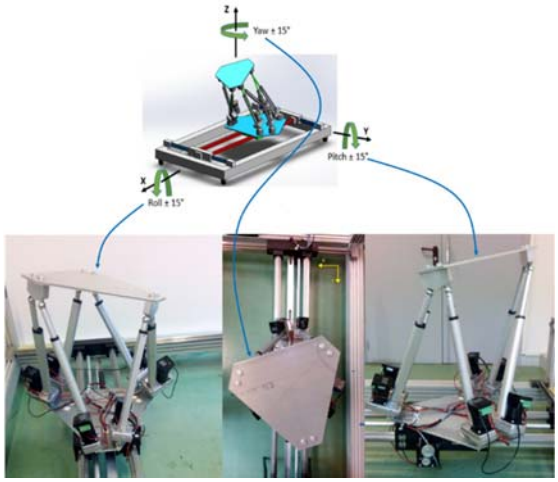


Fig. 2. The pseudo-rotation of the XY-6 DoF simulator.

2.1. Gough-Stewart Platform

The main advantage of the XY-6 DoF Simulator is that it is a completely open low-level access platform

that makes it very easy to create, develop, and evaluate new algorithms.

Our hybrid XY-6 DoF simulator takes advantage of the XY Table and the parallel Gough-Stewart platform characteristics.

Linear XY motions from the bottom of the platform and rotational motions from the upper part are generated by 8 PD4- CB Nanotec motors, guaranteeing the system a total of 6 degrees of freedom. Cylinders actuated by the six motors of the upper part allow rotational movements with an angular amplitude of +/- 15°.

The following table shows the characteristics of the XY-6 degrees of freedom in each direction.

Table 1. XY-6 DoF simulator characteristics.

Axis	Acceleration	Trajectory
X	1.25 (m/s²)	115 (cm)
Y	0.71 (m/s²)	115 (cm)
Z	0.52 (m/s²)	30 (cm)
Roll	0.17 (rad/s²)	+/- 15 (°)
Pitch	0.17 (rad/s²)	+/- 15 (°)
Yaw	0.17 (rad/s²)	+/- 15 (°)

The PD4-CB is a brushless DC motor integrating controller and absolute encoder with an incremental position encoder. The factor β of passage from the incremental position to an absolute position is 1000 for 1 centimeter.

2.2. Platform Workspace and Singularities

The workspace can generally be defined by two types of workspaces: reachable workspace and dexterous workspace. The reachable workspace is defined as the region in which every point can be reached by the upper platform in at least one orientation. In other words, only those points for which there is a solution to the inverse displacement problem are included. Fig. 3 and Fig. 4 show the translational and rotational reachable workspace of the Gough-Stewart platform used in the XY - 6 DoF.

The dexterous workspace is defined as a region of the reachable workspace in which every point can be reached by the upper platform in all possible orientations.

In this work, the reachable and dexterous workspaces of the manipulators are obtained by discretizing the region and locating all points in the region that lie within the boundaries of the corresponding workspace. The dexterous workspace is presented in Fig. 5. The purpose of adding the XY sliding axis is to increase the workspace of the Gough-stewart robot and increase its kinematic and dynamic capability. Fig. 6 shows the dexterous workspace of the XY-6 DoF platform and how the workspace is greatly increased up to ten times.

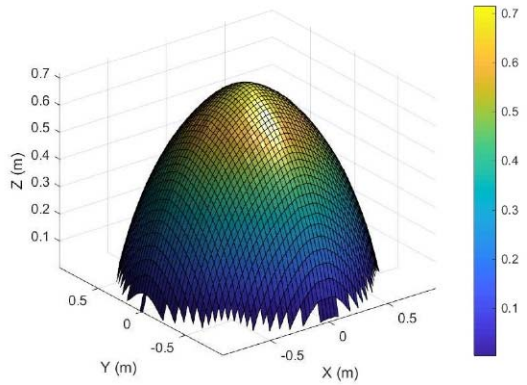


Fig. 3. Gough-Stewart reachable translation workspace.

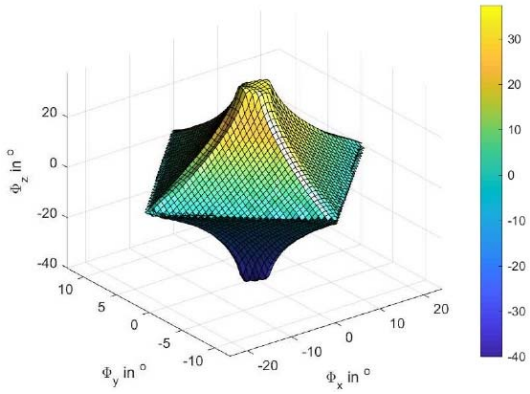


Fig. 4. Gough-Stewart rotation workspace.

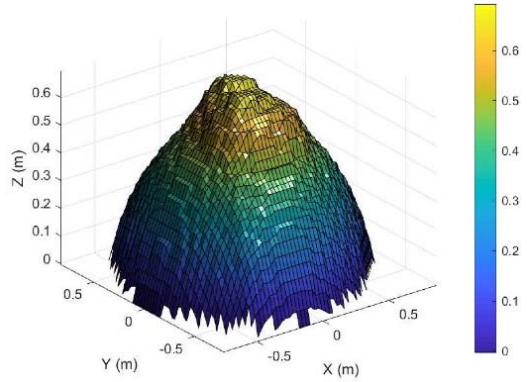


Fig. 5. Gough-Stewart dexterous workspace.

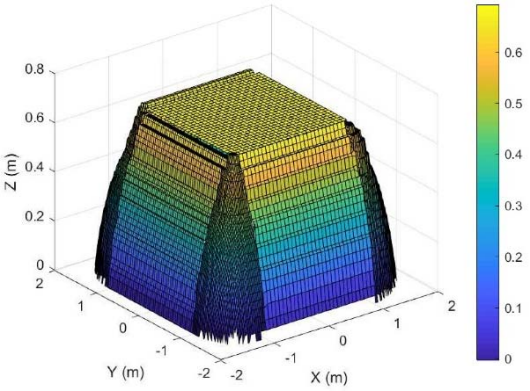


Fig. 6. Dexterous workspace of the XY-6 DoF.

Singularity equations are difficult to obtain for mechanisms with more than three degrees of freedom because the determinant of the Jacobian matrix becomes very complex. For the first time, the singularity equation for the general Gough-Stewart platform was derived from [12]. In fact, it is also a complete singularity equation because the 20 coefficients are functions of the 3 orientation angles. Later, based on the cascade expansion of the determinant of the Jacobian matrix. A procedure was developed in [13] to obtain the explicit expressions of the 20 coefficients as functions of the orientation angles. Unfortunately, the singularity equations obtained in [12, 13] are very complex because they contain too many geometrical parameters. Moreover, this method lacks flexibility because the considered point P is chosen as origin O' of the moving frame.

To solve this problem, [14] proposes that the origin O' of the moving frame should be separated from the point under consideration P and chosen to coincide with a special point on the platform in order to minimize the number of geometric parameters of the platform. Similarly, the fixed frame should also be chosen to be at a special point on the base to minimize the number of geometric parameters of the base.

Recall that, the inverse kinematics can be expressed by $J_q\dot{q} = J_x\dot{x}$ and for the parallel robot $\det(J_x) \# 0$. By using the condition for the direct singularity for our simulator (J_x = identical matrix, $J_q = {}^{R_b}J_{R_p}^{-1}$), $\det({}^{R_b}J_{R_p}^{-1} = 0)$, [14] has expressed the singularity equation as follow:

$$\begin{aligned} f_1x^3 + f_2x^2y + f_3x^2yz + f_4x^2 + f_5y^2x + f_6xyz + f_7xy \\ + f_8xz^2 + f_9xz + f_{10}x + f_{11}y^3 \\ + f_{12}y^2z + f_{13}y^2 + f_{14}yz^2 + f_{15}yz \\ + f_{16}y + f_{17}z^3 + f_{18}z^2 + f_{19}z + f_{20} \\ = 0 \end{aligned} \quad (1)$$

This is a surface of the third order in three-dimensional space, where the coefficients f_i, $i = 1, \ldots, 20$ are functions of the geometric parameters and of the orientation angles ϕ_x, ϕ_y, ϕ_z . Thus, the fi coefficients can be expressed as follows: $f_i = g(\theta_x, \theta_y, \theta_z)$ and they are explicitly presented in Jiang (2008) [93]. For the Gough-Stewart architecture (Simplified Symmetric Manipulator – Semiregular hexagons) used in the XY - 6 DoF simulator, and as recommended in [14] the reference frame O_{xyz} is attached to the base by selecting the midpoint of line segment B_1B_2 as the origin O and B_1B_2 as the x-axis. The O_{xy} plane coincides with the base plane. The mobile frame $O'_{x'y'z'}$ is attached to the platform by taking the midpoint of line segment P_1P_2 as the origin O′and P_1P_2 as the x′ axis. The $O'_{x'y'}$ plane coincides with the platform plane. Hence, the positions of B_i $(i = 1, 2, \ldots, 6)$ in the fixed frame are respectively

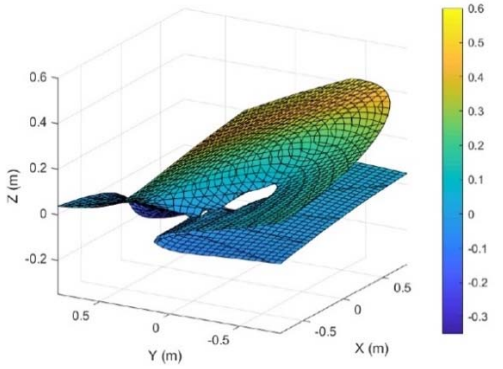
$$b_1 = [-t_1, 0, 0]^T, b_2 = [t_1, 0, 0]^T,$$
$$b_3 = [t_2, t_3, 0]^T, b_4 = [t_4, t_5, 0]^T,$$
$$b_5 = [-t_4, t_5, 0]^T, \text{and } b_6 = [-t_2, t_3, 0]^T.$$

The number of geometric parameters defining the base is only 5. Similarly, the position of P_i $(i = 1, 2, \ldots, 6)$ in the mobile frame are respectively.

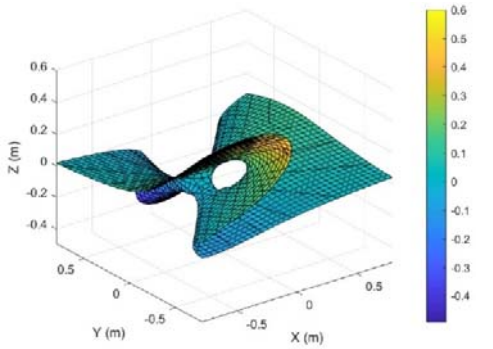
$$p'_1 = [-t_6, 0, 0]^T, p'_2 = [t_6, 0, 0]^T$$
$$p'_3 = [t_7, t_8, 0]^T, p'_4 = [t_9, t_10, 0]^T$$
$$p'_5 = [-t_9, t_10, 0]^T, \text{and } p'_6 = [-t_7, t_8, 0]^T.$$

The number of geometric parameters defining the mobile platform is also 5. Hence, the total number of geometric parameters for the hexagon used in the XY - 6 DoF is about 10.

Thanks to the equation (1), we are able to plot the Singularity loci in 3D Cartesian space with constant orientations, as shown in Fig. 7. Similarly, we have also depicted the Singularity loci in 3D Cartesian space with constant positions in Fig. 8. Additionally, we have represented the Singularity loci by defining two orientations and one position in Fig. 9.



(a) $\phi_x = \phi_z = 25^o$, $\phi_y = 25^o$



(b) $\phi_x = \phi_y = 25^o$, $\phi_z = 0^o$

Fig. 7. Singularity loci in 3D Cartesian space with constant orientations.

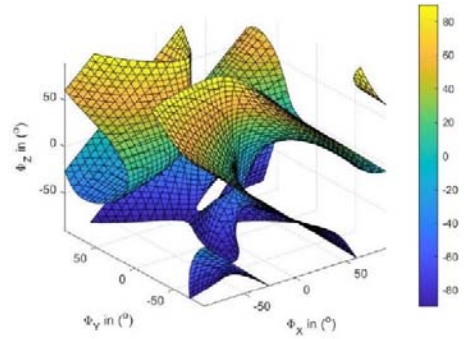


Fig. 8. (a). Singularity loci in 3D Cartesian space with constant positions. $P_0 = [0.5, 0.5, 0.5]^T$ in m.

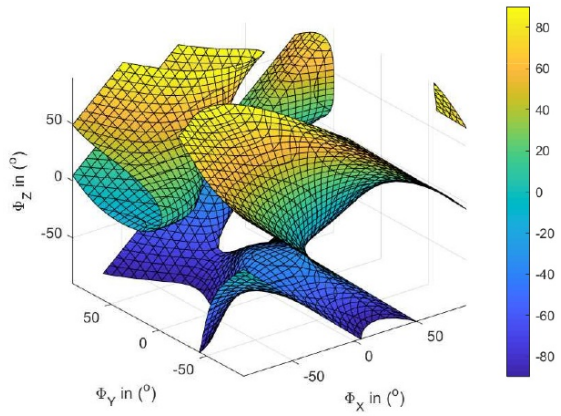
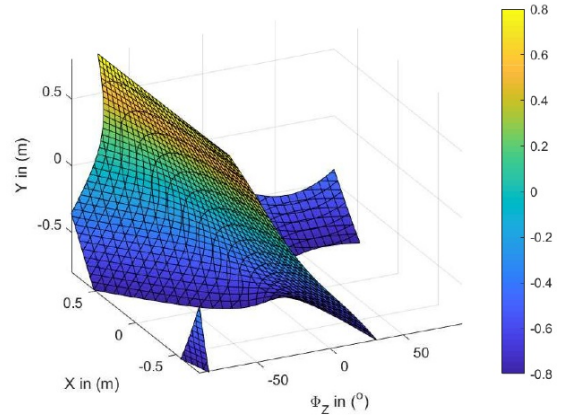
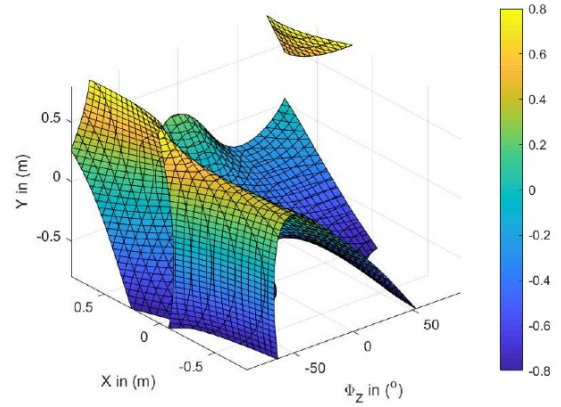


Fig. 8 (b). Singularity loci in 3D Cartesian space with constant positions. $P_0 = [0.1,\ 0.1,\ 0.1]^T$ in m.



(a) $\phi_x = \phi_y = 10^o$, z = 0.2m



(b) $\phi_x = \phi_y = 25^o$, z = 0.3m

Fig. 9. Singularity locus in 3D Cartesian space.

2.3. Platform Communication

Communication with the Gough-Stewart platform is carried out using a National Instruments card PCI - 8513 CAN, a CAN FD interface (Controller Area Network/Flexible Data-Rate). This device allows communication with the PD4-CB brushless DC motors at 1 Mbps and their control via a special Matlab toolbox. Engine communication is done in C# with the CANopen protocol, which defines motors by node IDs allowing to change and access their state and operating mode.

This protocol is based on sending 3 types of objects namely, PSO (Process Data Object), SDO (Service Data Object) and NMT (Network Management). However, an intermediate communication layer allows motor control with Matlab by mapping C# and Matlab functions. This intermediate layer makes possible to use directly from Matlab the NI PCI card to enhance the communication speed (see Fig. 10). Thus, the position instructions are sent in incremental angular position then converted into hexadecimal value in order to be adapted to the CANopen protocol.

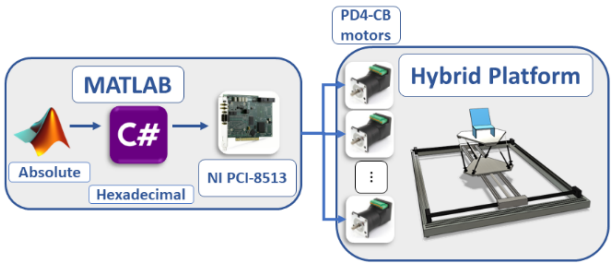


Fig. 10. Platform communication via the CANopen protocol.

The 8 joints are driven by the Nanotec PD4-CB servo motor, where the rotational movement of the leg is converted into a translational movement by the high-quality ball screw system. The motors are controllable in position, speed, and acceleration by instructions sent through the CAN bus.

2.4. Platform Security Protocol

A security protocol has been designed to guarantee the physical integrity of the platform. Each time the platform is powered up, the security protocol runs to determine the edges of the platform and define them as limited in the range of motion with a small safety gap as presented in Fig. 11.



Fig. 11. Security protocol for the platform safety area.

The protocol triggers the movement of the platform along the X-then Y axis successively with low speed. The platform's position is retrieved to determine when

the position difference Δ_p is smaller than a defined threshold value γ. The threshold value is defined as follows:

$$\gamma = 166.7\ \omega\Delta_t \quad (2),$$

where ω is the angular speed assigned to the axis motor and Δ_t the frequency of acquisition of the position. Thus, the platform's edge is assumed to be reached when the distance difference Δ_p is lower than the threshold value γ. Then, we add a safety gap of 5 centimeters at this reference 0 position to ensure a safety area. Verification protocols are built into the motion functions of the platform to ensure the desired range of motion is within the safety area.

2.5. NAO Robot

Fig. 12 presents the complete technological system architecture. illustrating the integration of the Nao robot into our immersive environment simulator XY-6 DoF. Thanks to the advantages of its pelvic kinematics design, the well-known Nao robot [15,16] was chosen to be integrated into the system, respecting the mechatronic constraints related to handi-skiing context (inactive lower limbs).

NAO is a humanoid robot with 25 DoF that includes many sensors and actuators, allowing interaction with its environment. In particular, joint sensors are Magnetic Rotary Encoders (MRE) using Hall-effect sensor technology with an accuracy of 0.1°, which provides reliable information of the angular position of the robot over time. In addition, an IMU sensor is composed of 3-axis gyrometers and accelerometers placed in the torso. A dedicated library named NAOqi provides access to sensors, system information, and actuator control.

Using ROS allows the synchronization of sensors and actuators to perform future postural control. The architecture of the entire NAO system is illustrated in Fig. 13. The connections between mechatronic and software layers presented in Fig. 5 highlight the existing multi-robot interaction and the technical methods that allow its observation.

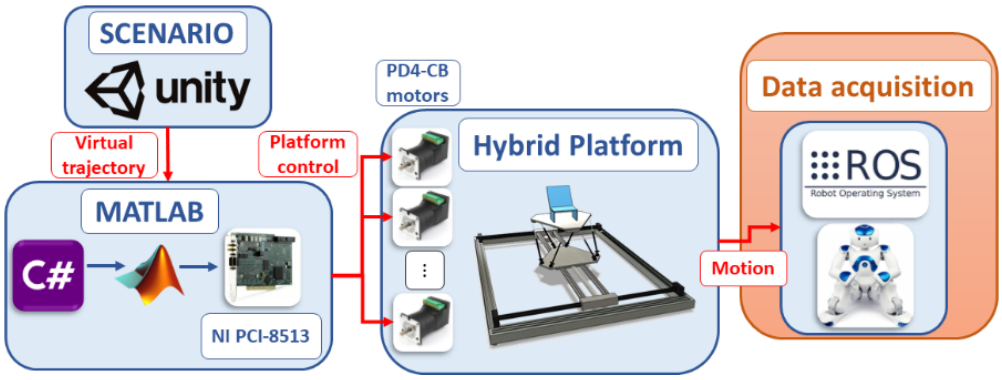


Fig. 12. Technological system architecture.

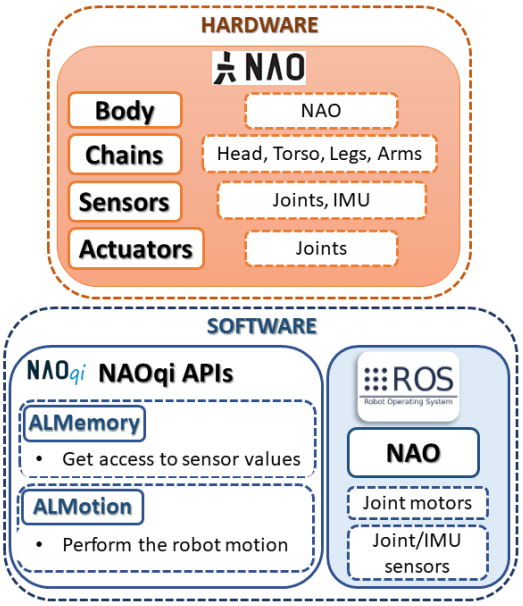


Fig. 13. Architecture of the NAO robot system.

3. Multi-robot Interaction

The XY-6 DoF platform tracks trajectory information from the virtual slide scenario designed using Unity software. The dynamic modeling behavior and sliding mode control of the XY-6 DoF robot simulator were developed and validated in a previous research work [3, 10, 17], where inertial and friction parameters were optimized and identified. The dynamics of the XY-6 DoF simulator can be represented as follows:

$$\Gamma = {}^{b}J_p^T\left({}^{b}F_e + {}^{b}F_p\right) + \sum_{i=1}^{6}\left(\frac{\partial \dot{q}_i}{\partial \dot{q}_a}\right) H_i(q,\dot{q},\ddot{q}), \quad (3)$$

where Γ is the vector of the actuator torques, ${}^{b}J_p^T$ is the Jacobian matrix, ${}^{b}F_e$ is the external wrench exerted on the platform, $\dot{q}_i$ is the passive joints speeds, $\dot{q}_a$ is the active joints speed, $H_i(q,\dot{q},\ddot{q})$ is the inverse dynamic model of leg i considering as serial robot, ${}^{b}F_p$ is the the total forces, is calculated by the following equation:

$${}^{b}F_p = {}^{b}\Pi_p\ {}^{b}\dot{v}_p + \begin{bmatrix} {}^{b}w_p \times ({}^{b}w_p \times {}^{0}MS_p) \\ {}^{b}w_p \times ({}^{b}I_p\ {}^{b}w_p) \end{bmatrix} - \begin{bmatrix} M_p I_3 \\ {}^{b}M\hat{S}_p \end{bmatrix} {}^{b}g, \quad (4)$$

where M_p, ${}^{b}\mathrm{I}_p$, ${}^{b}\Pi_p$, ${}^{0}MS_p$ are mass, inertia tensor, spatial interia matrix moment of inertia vector of the platform, respectively.

Parallel and serial robots are a known challenge which is the large number of dynamic parameters, which requires a lot of processing time, whether in dynamic modeling, identification or control. Therefore, the dynamic parameters of the XY-6 DoF hybrid structure simulator have been optimized and identified in previous works [17]. As a result, the standard 210 inertial parameters are reduced to only 90 basic inertial parameters. The motion of the XY-6 DoF simulator motion is validated by the acceleration data from the NAO IMU and the robot model, as shown in Fig. 14.

Many works [18, 19] highlight interactions in multi-modal robotic systems, such as human-robot and multi-robot interactions, to improve the collaboration and/or the impact between systems. First, the integrated system applies a validation process to the platform motion management algorithms to improve the reliability of virtual trajectory recovery. It provides a reliable solution to assess the motion control of the XY-Gought-Stewart platform and multi-robot interaction.

The interaction evaluation will be done through the inertial and articular information coming from NAO. Afterward, a human motion perception model will be integrated into the system to improve the emulation of human sensory capabilities within NAO.

Figs. 15 and 16 shows the homothety between the present integration of multi-robot interaction and the objective integration of robot-robot human interaction (outlined in red). Visual information will be exploited by a visual SLAM algorithm [20,21] that will mimic how humans perceive their movement through their eyes and the processing of information by the visual cortex. Likewise, inertial information from the NAO IMU and visual information will feed a perception model that mimics the human capacity of self-motion perception through its vestibular system and visual cortex. This future integration will provide a tool for measuring the quality of immersion for simulators by estimating through sensor data the impact of the movements of the virtual scenario and the platform on a human.

4. Experimental Results

The validation of the platform-controlled motion is illustrated in the following figures through the study of multi-robot interaction [22]. In this work, we have neglected the Z-axis and yaw rotation as they have a minor effect on the ski motion sensation comparing to the X and Y axes and roll and pitch rotation. Translation motions on axis X and Y in Fig. 17 and Fig. 18 are oscillatory movements of one meter in amplitude. Similarly, the rotational motions illustrated in Fig. 19 and Fig. 20 are oscillatory angular movements from -10 to 0 degrees. The platform behaviors are obtained by extrapolating the platform position from XY motors through the kinematic model.

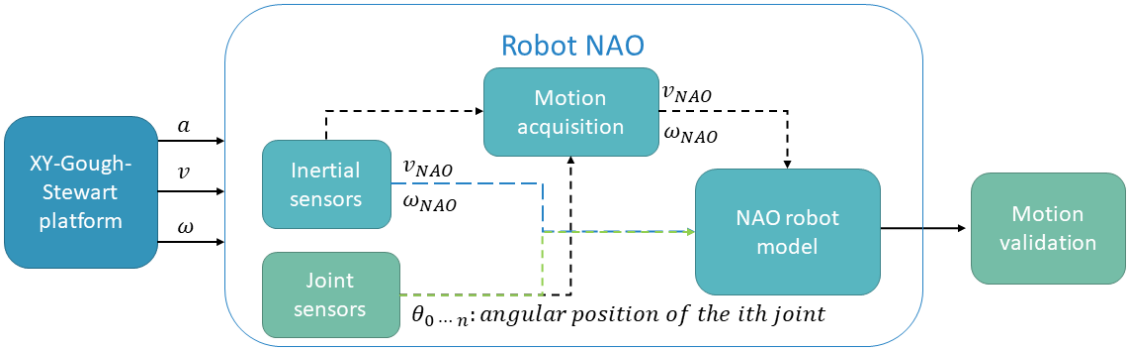


Fig. 14. XY-6 DoF simulator/NAO robot interaction.

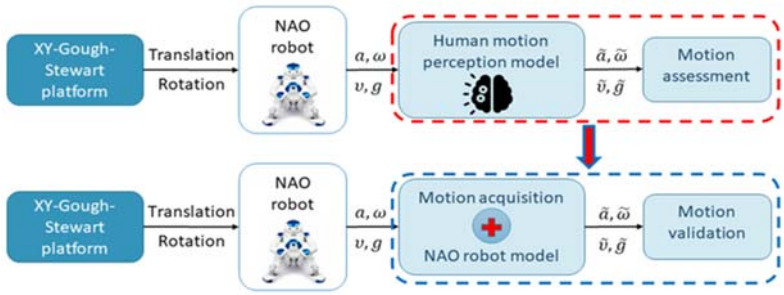


Fig. 15. Multi-robot and robotic human interaction.

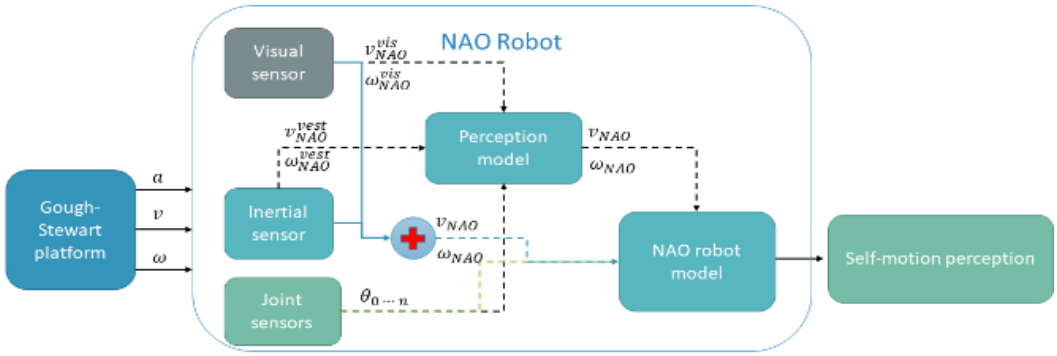


Fig. 16. Human/robot homothety for the self-motion perception.

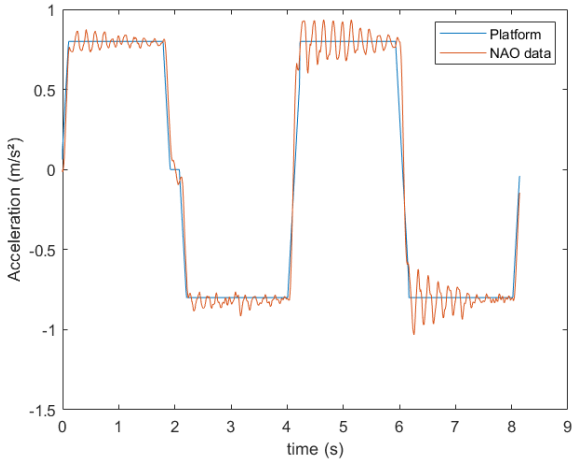


Fig. 17. Motion validation for X-axis movement.

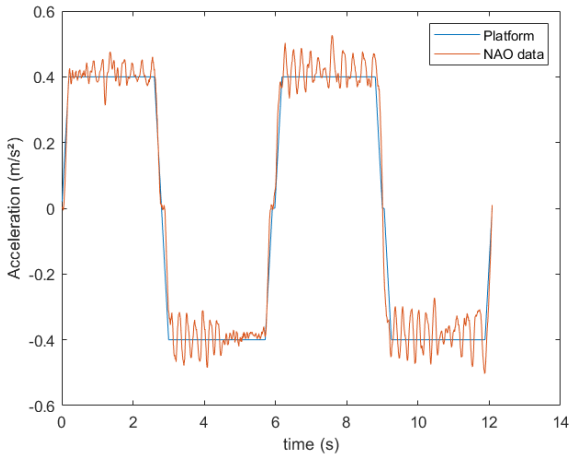


Fig. 18. Motion validation for Y-axis movement.

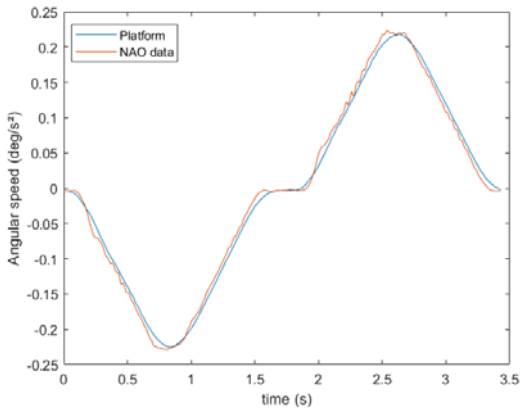


Fig. 19. Motion validation for Pitch movement.

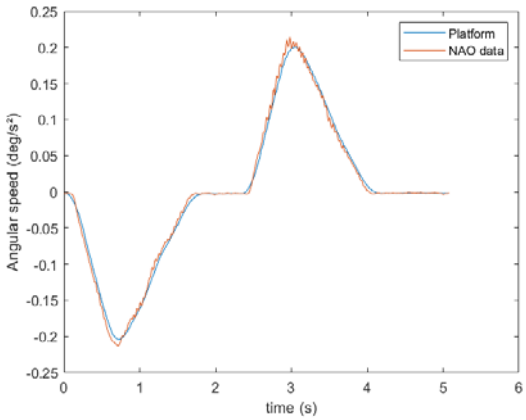


Fig. 20. Motion validation for Roll movement.

Observing the NAO robot's dynamic behavior in Fig. 17 and Fig. 18 validates the platform's accurate behavior tracking for an axis movement. However, some oscillations are observed for high dynamics. They result from slight platform vibrations due to axis friction and IMU acquisition noise.

Rotation motions do not suffer from axis friction. Thus, the angular speed behavior tracking is also precise but also less noisy.

This study validates the ability of NAO to perceive the multi-robot interaction and the interest in integrating it into our system for future work. An additional IMU sensor will be put on the NAO head to simulate the human vestibular system behavior for inertial motion perception. This device will be integrated into the ROS framework that manages the system's sensors. Likewise, a virtual scenario designed with UNITY 3D will provide the visual environment for the visual SLAM algorithm and the virtual trajectories for the platform motions restoring the sensations of acceleration.

5. Conclusion

In this paper, we introduced an original robotic platform combining the advantages of the parallel Gough-Stewart platform and an XY-table. The workspace offers by this hybrid platform is an interesting solution to enhance the motion restitution possibility. This XY-6 DoF simulator provides a comprehensive system to mimic the human self-motion perception behavior for a better immersive sliding simulator. A humanoid NAO robot is added to the upper platform to validate the platform motion acquisition through its intern inertial sensor. This robot, a real human homothetic system, provides information to assess the robot-robot interaction and system behavior properly. Experimentations confirmed the system's reliable feedback, where acceleration response shapes are concordant.

Our future work aims to manage all different parts of the system to achieve human perception integration through inertial and visual senses and realize a better immersive way. This simulator will be completed by a virtual reality scenario which will provide the trajectories to the robotic platform and restore the sensations of acceleration of the virtual trajectories.

References

[1]. Casas, Sergio, Ricardo Olanda and Nilanjan Dey, Motion Cueing Algorithms: A Review: Algorithms, Evaluation and Tuning, *International Journal of Virtual and Augmented Reality,* Vol. 1, Issue 1, 2017, pp. 90–106.

[2]. Petrović, Đorđe, Radomir Mijailović and Dalibor Pešić, How to Improve the Inclusion of Drivers with Disabilities: Measures to Enhance Accessibility, Mobility, and Road Safety, *Journal of Transportation Engineering, Part A: Systems*, 148, 10, 2022.

[3]. Houda, Taha, Lotfi Beji, Ali Amouri and Malik Mallem. Dynamic Behavior of an Interactive XY - 6 DoF Simulator for People with Reduced Mobility, in *Proceedings of the IEEE Conference on Control Technology and Applications (CCTA' 2020)*, 2020, pp. 522-527.

[4]. Nahon, Meyer A. and Lloyd D. Reid, Simulator motion-drive algorithms - A designer's perspective. *Journal of Guidance Control and Dynamics*, 13, 1990, pp. 356-362.

[5]. Pan, C. T., Pei-Yuan Sun, Hao Li, Cheng-Hsuan Hsieh, Zheng-Yu Hoe and Yow-Ling Shiue. Development of Multi-Axis Crank Linkage Motion System for Synchronized Flight Simulation with VR Immersion. *Applied Sciences,* 11, 2021, p. 3596.

[6]. Wei, Ming-Yen, Design and Implementation of Inverse Kinematics and Motion Monitoring System for 6DoF Platform, *Applied Sciences*, 11, 19, 2021, 9330.

[7]. Reymond, Gilles and Andras Kemeny, Motion Cueing in the Renault Driving Simulator, *Vehicle System Dynamics,* 34, 2000, pp. 249 - 259.

[8]. Salaani, Mohamed Kamel, Dennis Guenther and Gary Heydinger, Vehicle dynamics modeling for the national advanced driving simulator of a 1997 jeep Cherokee, *SAE Transactions*, 108, 1999, pp. 443-465.

[9]. Miunske, Tobias, Christian Holzapfel, Edwin Baumgartner and Hans-Christian Reuss. A new Approach for an Adaptive Linear Quadratic Regulated Motion Cueing Algorithm for an 8 DoF Full Motion Driving Simulator, in *Proceedings of the International Conference on Robotics and Automation (ICRA' 2019),* 2019, pp. 497-503.

[10]. Houda, Taha, Lotfi Beji, Ali Amouri and Malik Mallem. Handiski simulator performance under PSO-based washout and control parameters optimization. *Nonlinear Dynamics,* 110, 2022, pp. 649 - 667.

[11]. Amouri, Ali and Fakhreddine Ababsa. Sliding Movement Platform for Mixed Reality Application, *IFAC-PapersOnLine*, 49, 2016, pp. 662-667.

[12]. St-Onge B. M., Gosselin C. M., Singularity Analysis and Representation of the General Gough-Stewart Platform, *The International Journal of Robotics Research*, 19, 3, 2000, pp. 271-288.

[13]. Li, H., Gosselin, C. M., Richard, M. J., and St-Onge, B. M., Analytic Form of the Six-Dimensional Singularity Locus of the General Gough - Stewart Platform, *ASME. J. Mech. Des.,* 128, 1, January 2006, pp. 279–287.

[14]. Q. Jiang, Singularity-free Workspace Analysis and Geometric Optimization of Parallel Mechanisms, PhD thesis, *Laval University*, Quebec, QC, Canada, October 2008.

[15]. Gouaillier, David, Vincent Hugel, Pierre Blazevic, Chris Kilner, Jérôme Monceaux, Pascal Lafourcade, Brice Marnier, Julien Serre and Bruno Maisonnier. Mechatronic design of NAO humanoid, in *Proceedings of the 2009 IEEE International Conference on Robotics and Automation*, 2009, pp. 769-774.

[16]. Kofinas, Nikolaos, Emmanouil Orfanoudakis and Michail G. Lagoudakis. Complete Analytical Forward and Inverse Kinematics for the NAO Humanoid Robot, *Journal of Intelligent & Robotic Systems,* 77, 2015, pp. 251-264.

[17]. Houda, Taha, Ali Amouri, Lotfi Beji and Malik Mallem. Dynamic Parameters Optimization and Identification of a Parallel Robot, *Multibody Dynamics*, 2019, 53, 2019, pp. 367-374.

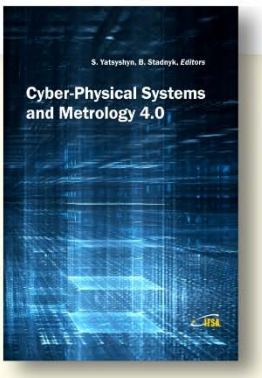
[18]. Darmanin, Rachael N. and Marvin K. Bugeja. A review on multi-robot systems categorised by application domain, in *Proceedings of the 25th Mediterranean Conference on Control and Automation (MED' 2017),* 2017, pp. 701-706.

[19]. Sharkawy, Abdel-Nasser, Human-Robot Interaction: Applications, in *Proceedings of the 1st IFSA Winter Conference on Automation, Robotics & Communications for Industry 4.0,* February 2021, pp. 98-103.

[20]. Bescos, B., Fácil, J. M., Civera, J., and Neira, J., DynaSLAM: Tracking, mapping, and inpainting in dynamic scenes, *IEEE Robotics and Automation Letters*, 3, 4, 2018, pp. 4076-4083.

[21]. Beghdadi, Ayman, Malik Mallem, and Lotfi Beji, D2SLAM: Semantic visual SLAM based on the influence of Depth for Dynamic environments, *arXiv:2210.08647*, 2022.

[22]. Houda Taha, Beghdadi Ayman, Beji Lotfi and Amouri Ali, Complex Multi Robot Hybrid Platform for Augmented Virtual Skiing Immersion, in *Proceedings of the 3rd IFSA Winter Conference on Automation, Robotics & Communications for Industry 4.0/5.0 (ARCI'2023).* 2023, pp. 95-99.



Cyber-Physical Systems and Metrology 4.0

S. Yatsyshyn and B. Stadnyk, Editors

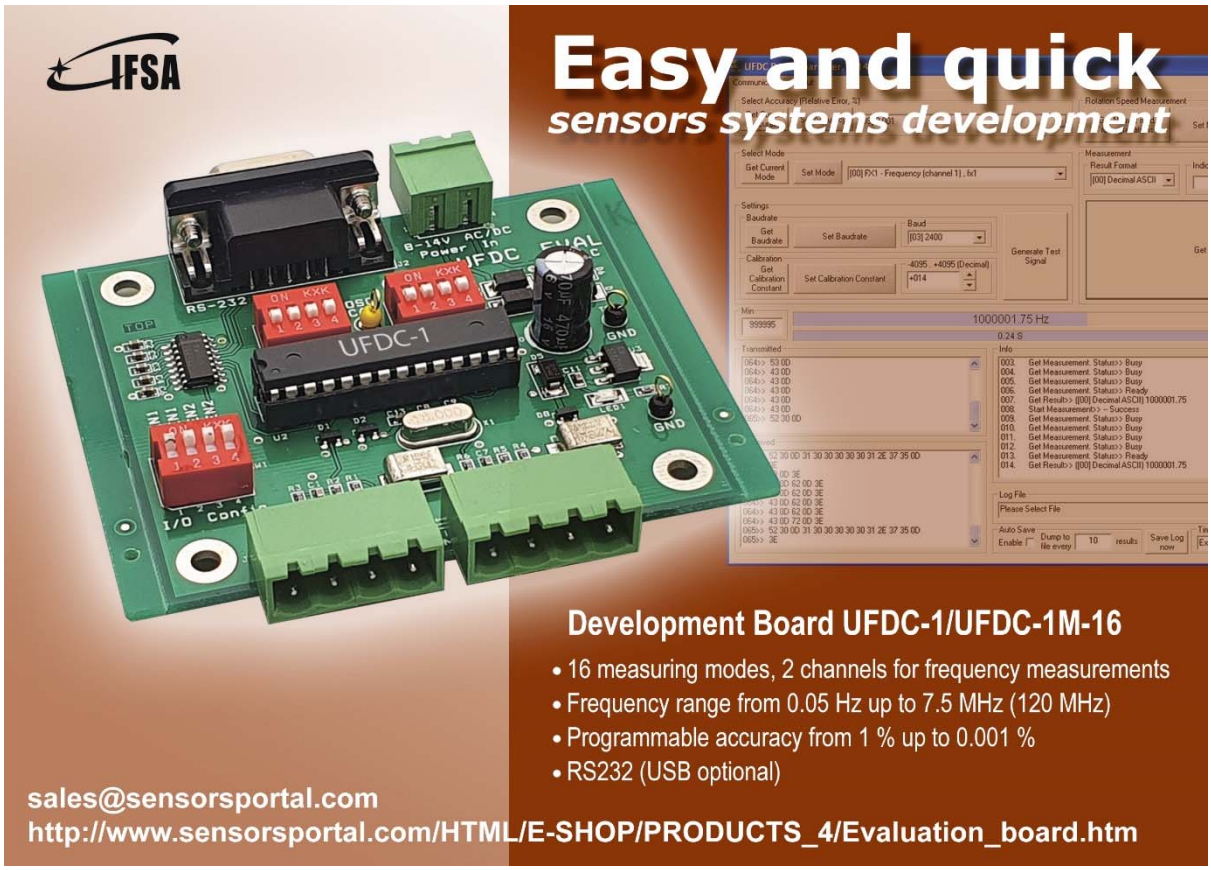
The book is written by 30 authors whose scientific achievements for the last 5 years cover a significant information technology and measurement science areas.

The purpose of this title is to present and consider the main trends in the field of metrology of Cyber-Physical Systems, which are becoming a key element of everyday life. At the first, the book is intended for engineers, lecturers, students, persons who are not acquainted enough with the specificity of Cyber-Physical Systems and their Metrology, but are interested in it.

Formats: hardcover (print book) and PDF, 332 pages
ISBN: 978-84-09-26899-3, e-ISBN: 978-84-09-26898-6

IFSA Publishing

https://www.sensorsportal.com/HTML/BOOKSTORE/Cyber-Physical_Systems_and_Metrology_4_0.htm



Sensors & Transducers, Vol. 261, Issue 2, June 2023, pp. 25-32

www.sensorsportal.com

Sensors & Transducers

Published by IFSA Publishing, S. L., 2023
http://www.sensorsportal.com

Learning from Demonstration and Safe Cobotics Using Digital Twins

[1*] A. RIZZOTTI-KADDOURI, [1] L. JEANNERET, [1] B. STUDER, [1] J. BRACAMONTE, [1] N. OUERHANI and [2] M. KUNZE

[1] School of Engineering Neuchâtel, University of Applied Sciences and Arts Western Switzerland, HES-SO/HE-ARC, Espace de l'Europe 11, 2000 Neuchâtel, Switzerland
[2] School of Engineering and Management Vaud, University of Applied Sciences and Arts Western Switzerland, HES-SO/HEIG-VD, Route de Cheseaux 1, 1401 Yverdon-les-Bains, Switzerland
[1] Tel.: +41 32 930 22 94, fax: +41 32 930 22 94
E-mail: aicha.rizzotti@he-arc.ch

Received: 14 April 2023 /Accepted: 30 May 2023 /Published: 26 June 2023

Abstract: The use of collaborative robots, or cobots, is nowadays continually increasing, especially in the small- and medium-sized manufacturing sector. For each particular use case, the integration and deployment of a cobot into a collaborative workspace faces a certain number of challenges. Programming industrial robots, for example, can be a relatively complex and time-consuming task. In this paper we report an accurate method to robot programming by using an optimized "learning from demonstration" technique. The operator/programmer performs in real-time the corresponding task to be automatized, and by means of a tracker sensor the programmer's motions are captured and transmitted to the robot; the robot registers the trajectories and is now able to reproduce the human movements with high accuracy. Another fundamental issue for cobot deployment is safety. In this paper, we also present a virtual/augmented reality (VR/AR) environment to facilitate the design and operation of cobots in order to maximize human safety. The virtual reality environment operates as an aide tool during the design phase. The human operator and the robot's digital twin work side-by-side while executing a collaborative task in a virtual reality space. Their movements are controlled and registered, and after a given period of test time, the data is analyzed to suggest modifications to ensure a safe workspace (collision free) and to increase productivity. For the regular real-time cobot operation, an augmented reality environment was developed, again, with the purpose of assuring a safe human-robot collaboration. The augmented reality environment keeps tracking permanently the cobot and the human manipulations. This system produces audio and visual alarm signals in unsafe situations and is also able to take actions, such as slowing down or stopping the robot, to preserve the physical integrity of the human operator.

Keywords: Cobot, Human-robot collaboration, Virtual- and augmented reality, Learning from demonstration, Machine learning, Digital twin, Sensors, Smart glasses.

1. Introduction

Collaborative robots represent an effective strategy for promoting human-machine interaction to increase productivity in the manufacturing room. Cobots relieve humans of repetitive, dangerous, non-ergonomic or heavy-load tasks. The goal is that cobots and humans collaborate side-by-side sharing the same workspace in a safe and efficient manner.

Depending on the use case, the design and deployment of a cobot faces a certain number of challenges. In this paper we address some of those challenges.

This paper is an extended version of the conference publication [1] in which we presented a solution to the complex task of programming robots. In this paper we report the general context and additional research on the development of both a virtual- reality and an augmented-reality environment. The objective of these two systems is to design and operate safer workspaces (e.g., zero collisions) in industrial human-robot collaboration. The virtual reality environment is used specifically for the human-cobot workspace design while the augmented reality environment is rather used during the operation phase (real-time, real-world human-robot collaboration).

2. Related Works

The LfD (Learning from Demonstration) robot-programming approach has attracted a lot of interest in the field of human-robot interaction [2, 3]. This topic encompasses several disciplines and scientific fields.

In general, there are two main approaches for LfD. The first one is based on observational learning which usually exploits a vision system for the perception of movements and gestures, by using for example, cameras. The second approach is based on kinesthetic guidance which refers to the manual movements of the robot by interaction through haptic sensors.

It should be noted that the second approach simplifies the corresponding learning task, but the movements remain spatially limited. Moreover, it is not possible to perform kinesthetic guidance on all types of robots. Therefore, in this study we favored the vision-based learning approach. We note that there are several important phases in this workflow, namely:

data capture and fusion > learning phase > reproduction by the robot of the learned movement or action.

Relevant existing work in this area is reported below.

In the framework of the European project PRACE (Productive Robot ApprentiCE), whose aim is the development of a mobile robotic platform for the automation of assembly operations, a system based on several Kinect-type cameras to calculate 3D positions has been investigated. In this work [4], the author adopted a top-down approach: first, an estimation of the positions was made, and then, a refinement of the data captured by each sensor was performed.

In the LfD domain, there are other approaches [5] that are based on the fusion of data recorded with gloves and video cameras. The work in [6] up to a certain point inspired our approach of fusing data from Microsoft's Kinect V2 to get the 3D data in skeletal form and supplementing it with data from Intel's RealSense sensor to refine the depth.

One example of this approach is also reported in [7], where the robot must perform assembly tasks in the industrial Peg-in-Hole (PiH) domain. Here, a learning phase and a reproduction phase reinforced by a kinesthetic guidance phase are listed. With a camera on the robot's wrist, the object is detected, located and captured. The objects are labelled, and the detection algorithms are based on conventional computer vision algorithms such as SIFT (Scale-Invariant Feature Transform) and KNN (K-Nearest-Neighbors) for classification.

We note that in [8] the human arm and the robot arm are physically attached for learning. The trajectory of each action is followed by the robot arm giving a representation of the trajectory in space. For the demonstration, the authors used the 3D coordinates of the three joints (shoulder, elbow, and wrist) for the tracking. They also used the procedure named Gaussian Process Latent Variable Model (GPLVM) and RANSAC (RANdom SAmple Consensus) to map the motion behavior.

In [18] the imitation is done by decomposing the main task into hierarchical subtasks, based on an RNN neural network to predict the next task to be performed. This will of course depend on the observed input of the current state with the control of a closed loop.

The work reported in [19] is carried out by using the ABB YuMi robot which is the same robot we used to develop our approach. The aim of the experiment was to test the effects of reusing non-expert programming parameters and skills for assembly tasks on industrial robots.

Our approach of course leveraged the results from previously reported studies. Our objective nonetheless was to increase accuracy (a recurrent problem in the cited works) either by using multi-channel vision systems for the data captures (unlike [3, 8]), or to obtain finer resolution movements (unlike [4, 5, 6]).

3. Demonstration-based Robot Learning

Efficient robot programming is one of the challenges faced during the deployment of cobots. Demonstration-based robot learning [9] is an active research area which studies robot programming. In this area, capturing and replicating the motion with high accuracy remains a recurrent issue. Our approach [1] to tackle the accuracy problem was to use a system composed of multiple sensors [10] and then to extract a trajectory from the motions and the (programmer's) fingers' positions using machine learning.

We tested different sensors including gloves and cameras. Due to accuracy and occlusion problems, we opted for a solution which uses an HTC Vive Tracker sensor [17], which is indeed accurate enough for robotic applications [11]. In our workflow, the HTC VIVE Tracker sensor is attached to the application-dependent tool which is used by the operator "to demonstrate" the motion. The Tracker sensor can then

track the movement of the tool in three dimensions by locating its position relative to a VIVE Base Station.

Since the tool position and rotation is directly tracked, it is not necessary to interpret (or to process) the intent and gestures of the user, which would have required more complex machine learning models. Moreover, our solution is coupled with AR smart glasses which allows the user to have immediate feedback. The used AR glasses (the Microsoft HoloLens 2) also provide tools to correct, in an intuitive way, possible recording errors.

3.1. Safe Human-robot Collaboration Testing

Robotic Task Planning, which is a sub-category of automated planning and scheduling, aims at solving complex robot use-case scenarios [12]. While some problem solvers such as STRIPS [13] can integrate human safety (as described in [14]) we cannot integrate such a system when a task is learned from demonstration. As an alternative, we approached this issue by testing the learned tasks in a high-fidelity virtual reality environment, where the human operator does not risk any harm. In our safe testing environment multiple digital twins can be placed in the scene along with a real human operator. The digital twins can be connected either to an alternative real simulator or to real robots located in a separate room.

4. VR and AR Environments for Safe Cobotics

Safety is a non-negotiable requirement for any human-robot collaboration in the workplace. One of the main challenges for a wide deployment of robots/cobots is related to safety issues. To unlock the full potential of collaborative robotics in industry and society, human safety must be guaranteed. At the same time, investment in the safety of human-robot collaboration must not reduce the promised return on investment.

Below we report the current status of the development of a VR/AR system intended for achieving safer workspaces (e.g., zero collisions) and increased productivity in industrial human-robot collaborations.

During the real-time cobot operation phase, the same digital twin used in Virtual Reality is used in Augmented Reality with AR smart glasses (in this case, the Microsoft HoloLens 2), while simultaneously calculating and displaying other kinds of metrics. One, for example, is the *Safety Score* metric. This score indicates to the operator the degree of safety of the current situation (or position). If the situation is deemed too risky, or when the operator crosses a dangerous zone, the smart glasses can send a signal to slow down or to stop the robot.

4.1. System Architecture

The system is composed of two main sub-systems as can be seen in Fig. 1. Each of the two main parts of this figure can operate independently on its own. They communicate together through robots and simulators by sharing programmed trajectories.

The “Common Digital Twin Library” component (on the right side of Fig. 1) provides a generic way to define robots for Virtual Reality and Augmented Reality called *Robot Components*. Robot Components allow us to define an existing robot or to prototype a new one by using small re-usable parts.

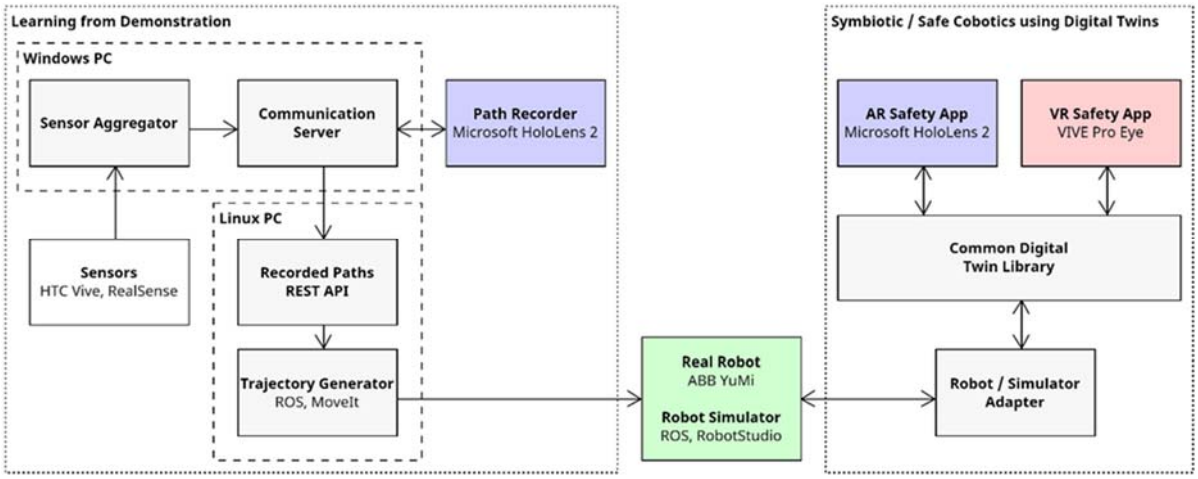


Fig. 1. Learning from demonstration and safe cobotics using digital twins.

Robot Components can be very specific and accurate (e.g., an accurate 3D model of an existing robot) or very generic and re-usable (e.g., a robotic joint, a 3D collider, a generic gripper, etc.). They can then be combined, using a parent/child system to define a fully working robot. This allows us to add

support for many robots' features with minimal effort, as long as the simulator or the real robot provides an API for it.

Robot Components can communicate to real robots and simulators through the "Robot / Simulator Adapter" component, which is a custom NodeJS server with an adapter system.

Plugins can add new adapters, which permits to communicate with both real robots and simulators. Robot Components and the plugin system make it possible and easy to add support for new robots if they have a public API.

Robots are *stored* in a modeled room (which represents a real-life industrial room), which can then be loaded in Virtual Reality to test the scenario, or in Augmented Reality (without furniture) to show to the operator where the robots are. Fig. 2 shows the class diagram of how robots are stored in a room.

Our *Learning from Demonstration* system (on the left in Fig. 1) is composed of multiples modules and several physical sensors. Two *sensor aggregator applications* retrieve and merge data from the sensors. A communication bus exchanges data between the HoloLens 2 module, the web server, and the sensor aggregators. The server module stores the recorded trajectories. It is then accessed by the ROS (Robot Operating System) module, which converts the operator trajectories into robot trajectories, before sending them to the robot. The sensor aggregator is built in a way that makes it easy to add new sensors, by allowing each sensor to validate or improve the accuracy of previous sensors.

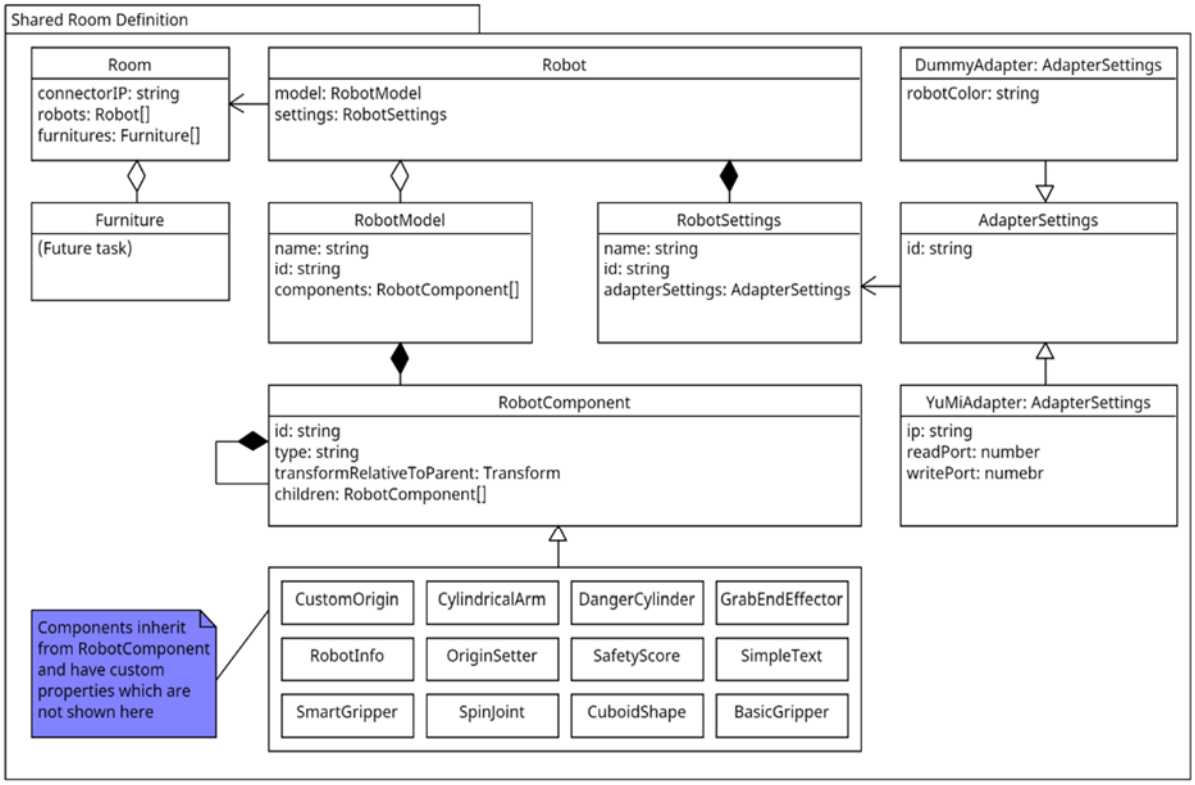


Fig. 2. Room definition class diagram used in the VR and AR environments.

4.2. Sensors

4.2.1. Leap Motion and Deep Learning

The goal of this part is to set up a system for the detection and classification of gestures performed by a human hand. The acquisition of gesture data is done using a *Leap Motion*, and the analysis and classification with a deep learning model (see Fig. 3). The process is carried out in three parts: The first one is the data acquisition, the second one is the creation and training of an MLP (Multilayer Perceptron) neural network, and the third part consists in importing the previously created model and making predictions on the fly with it. The features used are the relative distances between the fingers, which allows reducing the neural network complexity.

The main objectives for this part were successfully attained. For example, the "pinch" and "thumb up" hand gestures were correctly recognized. Other hand signs can of course be added at the expense of longer training and slightly lower performance. One recurrent issue we had was the misinterpretation of gestures that are differentiated only by hand rotation. A straightforward solution to this problem and/or a possible improvement will be the inclusion of hand orientation as an additional feature for the neural networks training.

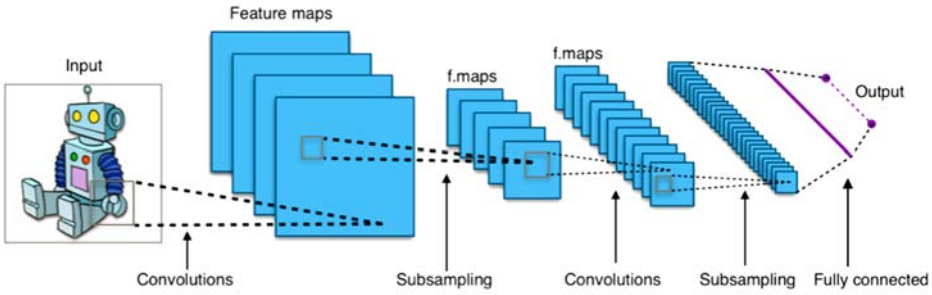


Fig. 3. Classification with the deep learning model.

4.2.2. Camera

In order to increase accuracy, we opted to use the RealSense D435 sensor (depth camera), which allows the detection of objects with high precision. Subsequently we merged the captured information with the Trackers' data. The depth camera is placed above the workspace. An algorithm detects the plane of the table and then a threshold is applied to the depth of each pixel. This allows to detect items dimensions with accuracy (±3 mm delta error) on different types of boxes. See Fig. 4.

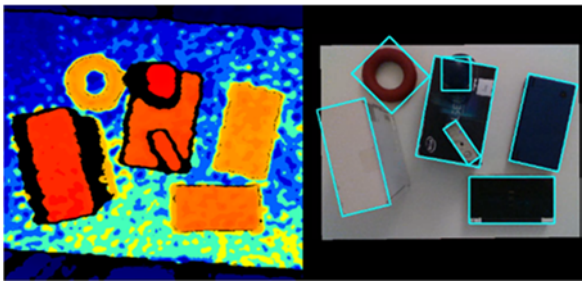


Fig. 4. Camera sensor and boundary detection algorithm.

4.2.3. Hand Tracking with Gloves

Multiple hand tracking sensors were tested, including the Hi5 Glove and the Senso Gloves before settling for the HTC VIVE Tracker. The main disadvantages of the non-selected ones were that they could be cumbersome to wear and that they featured a lower tracking accuracy. Additionally, their main purpose is to track the fingers and hand position of the operator, and for our application, it was not always possible to convert (post-process) the obtained data to accurately describe the motion of the *tool*.

To solve this in a pragmatic way, we decided to attach the tool to the Tracker. Since we could not use the gripper of the robot directly, we 3D-printed a "pen" representing a gluing tool (see use-case in the next section). However, in future work, it will be possible to print custom tips, either to attach existing tools, or to print "smart" tools. For example, a gripper with a small electronic circuit could automatically track the opening of the clamp during the recording, which would be feasible via the HTC VIVE Trackers' programmable pins.

4.2.4. HTC VIVE Tracker and AR Smart Glasses

A pair of Augmented-Reality/Mixed-Reality glasses were used in combination with two HTC VIVE Trackers. The selected AR/MR glasses were the Microsoft Hololens 2 glasses [20]. The system architecture is, all the same, open to the use of other types of glasses or models from other manufacturers.

One of the HTC VIVE trackers was used to track the tool and the other to define the origin. A quick response QR code (see Fig. 5) was used to synchronize the origins of the Tracker and the HoloLens 2. The operator can view the limits of the workspace through the AR/MR smart glasses and use controls to start and stop recording (Fig. 5).

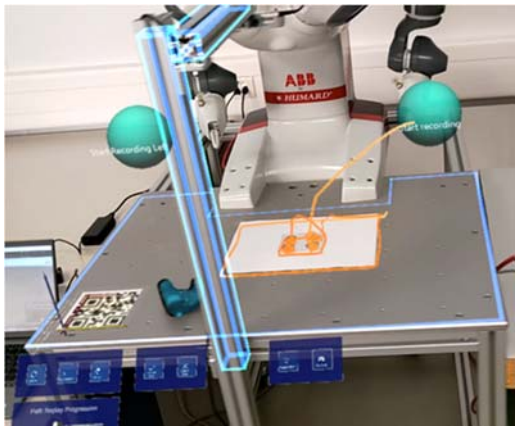


Fig. 5. AR smart glasses screen capture.

Once the task is recorded, it can be uploaded to a web server for future usage. The communication between the web server, the HoloLens 2, and the Trackers is done in a modular way.

The accuracy of the Tracker with the pen was measured by touching with the tip of the pen at specific (known distance) points drawn on a sheet of paper. The results of the positions are summarized below in Fig. 6.

x	y	z	x	y	z	x	y	z
Expected			Measured			Absolute error		
0	0	0	1	1	1	1	1	1
0	0	53	0	0	54	0	0	1
0	0	143	3	8	145	3	8	2
(More lines truncated...)								
HTC Tracker			Average :			1.875 [mm]		
			Max :			8 [mm]		

Fig. 6. Accuracy of the HTC Vive Tracker.

The use case for our demonstration was a "gluing task", which has the following sequence: the operator picks up an item, moves it, applies glue on it, and then glues the other half together. Fig. 7 shows the operator during the recording of the trajectory, which is displayed in orange color. While this figure displays a 2D path, the path recorded is indeed three-dimensional.

For the reported use case, an ABB YuMi robot was used. This robot has two arms. The operator can decide which arm is used while *in teaching mode* by simply touching the arm of the robot with the pen. Technically, two Trackers could be used to record trajectories for both arms at the same time.

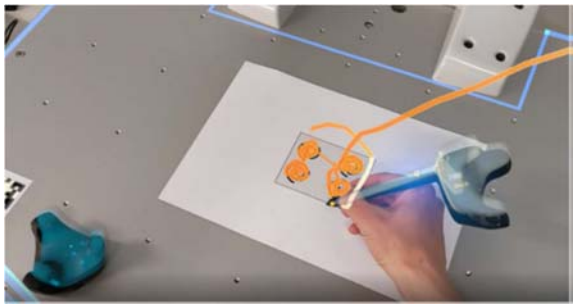


Fig. 7. Recording the trajectory.

4.3. VR environment for a Safe and Efficient Human-robot Workspace

Once the trajectories are recorded using the method described in the previous sections, they are validated in a Virtual Reality environment. Contrary to traditional approaches that would try to test the trajectories in real conditions with a physically present robot, we opted to equip the operator with an HTC Vive Pro eye head mounted display [15] and use Unity's Virtual Reality features [16] coupled with digital twins. Such a system reduces the injury risks of the human operator to practically zero when testing new trajectories. This riskless procedure also minimizes the overall testing time. Furthermore, a virtual environment permits to create new testing scenarios that would be complex and/or more expensive to set up in real life. The VR system also facilitates the testing of different or alternative configuration scenarios in search of increasing productivity.

The following paragraphs describe the operation of the VR system in more detail:

1) The operator can (virtually) observe both the robot and the surrounding environment.
2) The operator can then at real-time speed interact with the robot and the environment as in a classic Virtual Reality application. The simulation is as close as possible to the real-world case from the operator's standpoint. A connection with the Robot Adapter allows the robot to mimic real-life robot trajectories.
3) For post-analysis and optimization purposes, the VR system offers the capability of recording the scenario and all the involved actors (e.g., the robot(s), the operator in the room).
4) Diagnostic tools and metrics are also constantly shown to the human operator. For example, we can display the minimum distance between the operator and the robot(s) for every timestamp during the execution of the use case scenario; or the number of occurred human-robot (virtual) collisions. Other metrics can be easily implemented and added in graphs to the displayed information. Fig. 8 shows the diagnostic view for a very simple use-case example. On the top left part of the display the number of collisions is reported. On the right part, the minimum distances and robot speed plots are displayed.



Fig. 8. Diagnostic view in a simple use case.

4.3.1. Testing the System: Results

In order to test our system on a practical application, a pick-and-place (robot-executed) task with an intermediate assembly task (human-executed) was successfully implemented. We used multiple sensors and a real (not a virtual one) ABB YuMi robot.

During the tests, it was confirmed that the hand-tracking accuracy (by using the Microsoft HoloLens 2) was high enough to control the ABB YuMi robot.

Our plugin-based system allows us to quickly add new robots and simulators. For example, we exercised this feature by providing multiple plugins for multiple entities: a) a plugin that can communicate with a real ABB YuMi, b) another plugin with a simulated ABB robot, and c) a third plugin with a modeled "dummy" (robot) which was used to simply test the feasibility with any prototyped robot.



Fig. 9. Screen capture of the AR smart glasses during regular human-robot operation. The human operator can visualize in real-time the danger zone, the safety score, and other valuable information.

The developed modular Robot Components system was used to define an ABB Robot, which can be animated using data from real robots and simulators. These digital twins can be viewed in Virtual Reality and in Augmented Reality.

The implemented solution allows managing tasks on a running robot. When the robot is stopped, it can be controlled in an intuitive manner.

Safety features were implemented. For example, displaying a danger zone (the circular yellow strips in Fig. 9); or slowing or stopping the robot depending on the value of the *safety score* or on the distance of the operator to the robot.

Furthermore, the robots can be visualized in the real world, in virtual reality or in a third-party 3D application.

5. Conclusions

In this paper we reported an accurate "Learning from Demonstration" robot programming method. By means of a series of sensors, the robot programmer's movements are accurately captured and then transmitted to the robot, which is then able to exactly reproduce the learned movements.

We also introduced current work on the development of a virtual- and an augmented-reality environments that facilitate cobots workspace design and robot real-time operation, in view of a maximum-safety collaboration. Our system is still open for further developments, and we are adding new features on a periodic basis. For the real-time robot operation, the goal of our approach is not to replace traditional security measures such as safety switches and lasers. The purpose is rather to add an effective security layer for maximum operator safety and to reduce the need to interrupt the production.

The developed system also includes the following features: 1) Hazardous areas are shown directly on the scene, as can be seen in Fig. 9. This should reduce the risks of the operator walking into a protected area. 2) A *safety score*, which is based on the combination of multiple inputs, such as: a) the operator's distance to the robot, b) the safety level of the current robot's task, c) the operator's attention (e.g., tracking the operator's eyes) relative to the robot, and d) the operator's (next/imminent) movement prediction. The value of the *safety score* is used to warn the operator by using audio and visuals cues (when the score is too low). 3) The system can also be equipped with a signal to communicate with the robot to slow it down or stop it when the operator gets too close. We consider that our solution may lead to increased productivity, as it provides a common User Interface (UI) directly in front of the robot, which allows the operator to manage tasks and eventually stop the robot. Additionally, when the robot is stopped, the operator can jog the robot from a safe distance, without touching it, simply by moving 3D spheres around in augmented reality.

References

[1]. A. Rizzotti-Kaddouri, M. Kunze, L. Jeanneret, L. Depierraz, Collaborative Robots and Set of Sensors for Learning by Demonstration, in *Proceedings of the 3rd ISFA Winter Conference on Automation, Robotics, & Communications for Industry 4.0/5.0 (ARCI 2023)* Chamonix-Mont Blanc, France, 22-24 February 2023, pp. 207-209.

[2]. J. Lee, A survey of robot learning from demonstrations for human-robot collaboration, *arXiv preprint arXiv:1710.08789*, 2017.

[3]. Z. Zhu, H. Hu, Robot learning from demonstration in robotic assembly: A survey, *Robotics*, 2018, Vol. 7, No. 2, pp. 17-42.

[4]. J-T. Masse, Capture de mouvements humains par capteurs RGB-D, Thèse de doctorat, *Université Paul Sabatier-Toulouse III*, 2015.

[5]. K. Bernardin, K. Ogawara, K. Ikeuchi, A sensor fusion approach for recognizing continuous human grasping

sequences using hidden Markov models, *IEEE Transactions on Robotics*, 2005, Vol. 21, No. 1, pp. 47-57.
[6]. Y. Lan, J. Li, Z. Ju, Data fusion-based real-time hand gesture recognition with Kinect V2, in *Proceedings of the 9th IEEE International Conference on Human System Interactions (HIS' 2016)*, 2016, pp. 307-310.
[7]. Z. Zhu, H. Hu, D. Gu, Robot performing peg-in-hole operations by learning from human demonstration, in *Proceedings of the 10th Computer Science and Electronic Engineering (CEEC' 2018)*, 2018, pp. 30-35.
[8]. M. Koskinopoulou, S. Piperakis, P. Trahanias, Learning from demonstration facilitates human-robot collaborative task execution, in *Proceedings of the 11th ACM/IEEE International Conference on Human-Robot Interaction (HRI' 2016)*, 2016, pp. 59-66.
[9]. H. Ravichandar et al., Recent advances in robot learning from demonstration, *Annual review of control, robotics, and autonomous systems*, 3, 2020, pp. 297-330.
[10]. S. E. Ovur, et al., Novel adaptive sensor fusion methodology for hand pose estimation with multileap motion, *IEEE Transactions on Instrumentation and Measurement*, 70, 2021, pp. 1-8.
[11]. I. Soares, et al., Accuracy and repeatability tests on HoloLens 2 and HTC Vive, *Multimodal Technologies and Interaction*, Vol. 5, No. 8, 2021, pp. 47-62.
[12]. Automatic planning and scheduling: https://en.wikipedia.org/wiki/Automated_planning_and_scheduling#Classical_planning
[13]. STRIPS: https://en.wikipedia.org/wiki/Stanford_Research_Institute_Problem_Solver
[14]. M. Faroni et al., A layered control approach to human-aware task and motion planning for human-robot collaboration, in *Proceedings of the 29th IEEE International Conference on Robot and Human Interactive Communication (RO-MAN' 2020)*, 2020, pp. 1204-1210.
[15]. HTC. Vive website. Vive Pro Eye. https://www.vive.com/
[16]. Unity Technologies, https://unity.com
[17]. HTC. Vive website, Vive Tracker sensor, https://www.vive.com/
[18]. D. Xu, S. Nair, Y. Zhu, Neural task programming: Learning to generalize across hierarchical tasks, in *Proceedings of the IEEE International Conference on Robotics and Automation (ICRA' 2018), 2018*, pp. 3795-3802.
[19]. M. Stenmark, E. A. Topp, From demonstrations to skills for high-level programming of industrial robots, in *Proceedings of the 2016 AAAI Fall Symposium*, 2016, pp. 75-78.
[20]. Microsoft HoloLens 2. https://en.wikipedia.org/wiki/HoloLens_2

Published by International Frequency Sensor Association (IFSA) Publishing, S. L., 2023 (http://www.sensorsportal.com).

Advances in Robotics and Automatic Control: Reviews

Sergey Y. Yurish, Editor

Industrial robots offer many benefits, including cost reduction, increased rate of operation and improving quality, along with improved manufacturing efficiency and flexibility. The demand for industrial robotics is majorly observed in industries such as automotive, electrical & electronics, chemical, rubber & plastics, machinery, metals, food & beverages, precision & optics, and others. In its turn, industrial automation control market will witness considerable growth during the same period with the growing demand of products such as sensors, drives and various robots.

The first volume of the 'Advances in Robotics and Automatic Control: Reviews', Book Series started by IFSA Publishing in 2018 contains ten chapters written by 32 contributors from 9 countries: Belgium, China, Germany, India, Ireland, Japan, Serbia, Tunisia and USA.

This book will be a valuable tool for those who involved in research and development of various robots and automatic control systems.



IFSA Publishing

http://www.sensorsportal.com/HTML/BOOKSTORE/Advances_in_Robotics_and_Automatic_Control_Vol_1.htm

Sensors & Transducers, Vol. 261, Issue 2, June 2023, pp. 33-40

www.sensorsportal.com

Sensors & Transducers

Published by IFSA Publishing, S. L., 2023
http://www.sensorsportal.com

Controlling a Two-Link Robot using Sliding Mode Control Combined with Neural Network

Ayoub Belkheir and El Mehdi Mellouli
Laboratory of Engineering, Systems, and Applications (LISA)
Sidi Mohamed Ben Abdellah University Fez, Morocco
E-mail: belkheir.ayoub@usmba.ac.ma, mellouli_elmehdi@hotmail.com

Received: 25 May 2023 /Accepted: 23 June 2023 /Published: 26 June 2023

Abstract: This research focuses on designing and controlling a MIMO (Multiple Input and Multiple Output) two-link robot using a mix of Sliding Mode Control (SMC) and artificial intelligence (specifically, Radial Basis Function Neural Network (RBFNN)). In the first section, we present the model dynamics of this system in the state space. Then, in the second section, we provide a new approach in which we attempt to identify the optimum performance and attain stability in finite time by predicting the nonlinear dynamics of the system and also reducing the disturbance and uncertainty impacts on the system using artificial intelligence. And, by examining the Lyapunov function we can prove the stability of the system. Based on the simulations of the new technique presented in the latter portion of this work, we illustrate and enhance the superiority of our methodology over existing ways, their positive outcomes, and their effectiveness in time tracking, stability, and robustness.

Keywords: Two-link robot, Normal sliding mode control, Artificial intelligence, Lyapunov function, Non-linear function.

1. Introduction

In all industrial sectors, automatic systems are becoming increasingly crucial. This makes quality control in terms of speed, security, and resilience extremely important, and as a result, this sector has become increasingly vital over the past 20 years. Because of this, commercial enterprises research this area in an effort to create new techniques that will lessen disturbance, perturbations, and uncertainties and therefore improve system stability.

One of the most common robots in the industrial sector is the two-link robot [3, 4, 5, 8, 12, 14, 26, 27], which is specifically employed in the manufacture of cars and airplanes. Due to the fact that speed and stability are crucial for this sort of robot, various societies attempt to research this type of robot in order to provide alternative methods for its optimum control and application.

Since sliding mode control has been researched for so long, it is currently one of the most popular technics used in nonlinear control theory. The literature has numerous studies on sliding mode control and its extensions, including [1, 2, 4, 7, 8, 10, 11, 15, 24]. The goal of sliding mode control in recent years has been to produce finite-time convergence to the equilibrium of the relevant closed-loop system.

Artificial neural networks [3, 12, 14, 22] have been used to model nonlinearities rather frequently. A neural network is among the strongest approximators because it can estimate any nonlinearities with arbitrary precision as its size and complexity increase. Due to their effectiveness, neural networks are also widely used to identify and control nonlinear systems. For the underlying nonlinearity, neural networks are

used in the majority of these works as nonlinear models.

The combination of SMC and neural networks is applied in many research, but in this work, we will try to use SMC as a sliding manifold and RBFNN [21, 22, 23] to estimate the unknown dynamics of the hidden state in order to make the system more robust and stable.

To guarantee the stability of the two-link robot system using normal Sliding Mode Control, and RBF neural network, we study the Lyapunov function [3, 4], to know the strength of this strategy.

At the begging of this paper, we will present the two link-robot models, in the second part we will describe the proposed strategy, after that, the third part will show the results of our proposed two-link robot control strategy, and, the conclusion and perspective will be the last part.

2. Two-link Robot Model

The two-link robot represented in Fig. 1. model is expressed as follows [4, 26, 28]:

$$M(q)\ddot{q} + C(q,\dot{q})\dot{q} + G(q) = T$$
$$\dot{T} = J.i - B.T - E.\dot{q}, \quad (1)$$

where q, i, and T are the angle, current, and torque respectively of the two-link robot.

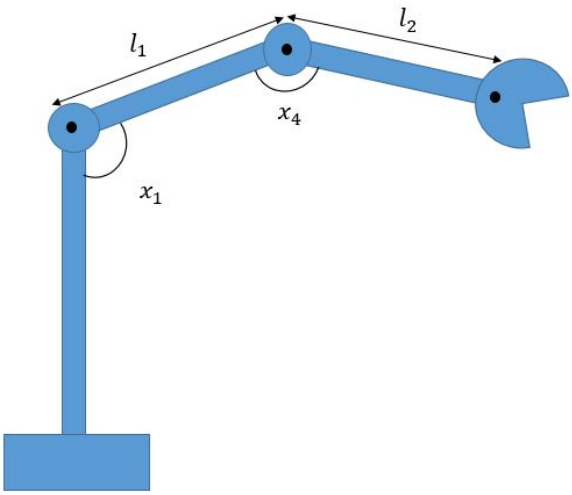


Fig. 1. Two-link robot model.

And B, J, and E represent the diagonal matrices that depend on the temperature, the thermo- dynamics parameters, and the initial conditions.

$M(q)$, $C(q,\dot{q})$, and G(q) are the positive-definite symmetric inertia matrix, the centrifugal forces, and the gravitational matrices respectively. Here

$$M(q) = \begin{bmatrix} M_{11} & M_{12} \\ M_{21} & M_{22} \end{bmatrix},$$

where

$$M_{11} = I_1 + I_2 + 4m_2l_1^2 + 4m_1m_2l_1l_2\cos(q_2)$$
$$M_{12} = I_2 + 2m_2l_1l_2\cos(q_2)$$
$$M_{21} = I_2 + 2m_2l_1l_2\cos(q_2)$$
$$M_{22} = I_2$$

and $C(q,\dot{q}) = \begin{bmatrix} C_{11} & C_{12} \\ C_{21} & C_{22} \end{bmatrix}$,

where

$$C_{11} = -2m_2l_1l_2\dot{q}_2\sin(q_2)$$
$$M_{12} = -2m_2l_1l_2(\dot{q}_1 + \dot{q}_2)\sin(q_2)$$
$$M_{21} = -2m_2l_1l_2\dot{q}_1\sin(q_2)$$
$$M_{22} = 0$$

and

$$G(q) = \begin{bmatrix} m_2gl_2\sin(q_1+q_2) + m_1gl_1\sin(q_1) \\ m_2gl_2\sin(q_1+q_2) \end{bmatrix}$$

This system is represented in state space as follows:

$$\begin{aligned} \dot{x}_1 &= x_2 \\ \dot{x}_2 &= x_3 \\ \dot{x}_3 &= f_1(x) + g_{11}(x_1,x_4)u_1 + g_{12}(x_1,x_4)u_2 \\ \dot{x}_4 &= x_5 \\ \dot{x}_5 &= x_6 \\ \dot{x}_6 &= f_2(x) + g_{21}(x_1,x_4)u_1 + g_{22}(x_1,x_4)u_2, \end{aligned} \quad (2)$$

where

$$\mathrm{x} = [x_1 \quad x_2 \quad x_3 \quad x_4 \quad x_5 \quad x_6]^T$$
$$\mathrm{U} = [u_1 \quad u_2]^T$$
$$f(x) = [f_1(x) \quad f_2(x)]^T$$

$$g(x_1,x_4) = \begin{bmatrix} g_{11}(x_1,x_4) & g_{12}(x_1,x_4) \\ g_{21}(x_1,x_4) & g_{22}(x_1,x_4) \end{bmatrix}$$

3. The Control Strategy

3.1. Control Law

Let's take the two following sliding surfaces:

$$S_1 = \ddot{e}_1 + \lambda_1\dot{e}_1 + \lambda_2e_1$$
$$S_2 = \ddot{e}_2 + \lambda_3\dot{e}_2 + \lambda_4e_2, \quad (3)$$

where λ_1, λ_2, λ_3 and λ_4 are the positives constants and $e_1$and e_2 are the angle errors of q_1 and q_2 respectively which are expressed as following:

$$e_1 = x_1 - x_{1d} \text{ and } e_2 = x_4 - x_{4d} \quad (4)$$

and x_{1d}, x_{4d} are the desired trajectories, which are represented in Fig. 2.

Now, we derive the sliding surface:

$$\dot{S}_1 = \dddot{e}_1 + \lambda_1\ddot{e}_1 + \lambda_2\dot{e}_1$$
$$\dot{S}_2 = \dddot{e}_2 + \lambda_3\ddot{e}_2 + \lambda_4\dot{e}_2 \quad (5)$$

From equations (4),

$$\begin{aligned} \dot{S}_1 &= \ddot{x}_1 - \ddot{x}_{1d} + \lambda_1 \ddot{e}_1 + \lambda_2 \dot{e}_1 \\ \dot{S}_2 &= \ddot{x}_4 - \ddot{x}_{4d} + \lambda_3 \ddot{e}_2 + \lambda_4 \dot{e}_2 \end{aligned} \tag{6}$$

And from equation (6) and using equation (2), we find:

$$\begin{aligned} \dot{S}_1 &= f_1(x) + g_{11}(x_1, x_4)u_1 + g_{12}(x_1, x_4)u_2 \\ &\quad - \ddot{x}_{1d} + \lambda_1 \ddot{e}_1 + \lambda_2 \dot{e}_1 \\ \dot{S}_2 &= f_2(x) + g_{21}(x_1, x_4)u_1 + g_{22}(x_1, x_4)u_2 \\ &\quad - \ddot{x}_{4d} + \lambda_3 \ddot{e}_2 + \lambda_4 \dot{e}_2 \end{aligned} \tag{7}$$

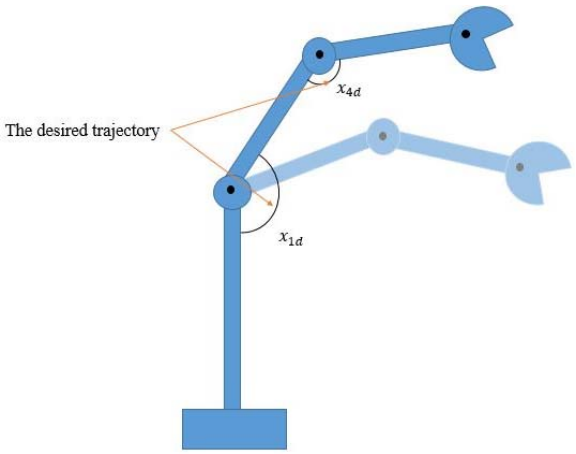


Fig. 2. Desired trajectory x_{1d} and x_{4d}.

To guarantee the stability of the system we define the Lyapunov function:

$$V_1 = \frac{1}{2} S_1^2 \quad \text{and } V_2 = \frac{1}{2} S_2^2 \tag{8}$$

The system is stable if the derivative of the Lyapunov function $\dot{V}$ is negative, which means that:

$$\dot{V}_1 = \dot{S}_1 S_1 < 0 \text{ and } \dot{V}_2 = \dot{S}_2 S_2 < 0 \tag{9}$$

That's why we define the sliding surface derivative:

$$\dot{S}_1 = -K_1 \text{sgn}(S_1) \text{ and } \dot{S}_2 = -K_2 \text{sgn}(S_2) \tag{10}$$

where K_1 and K_2 are the positive constants.

Using the equations of (7), and to be satisfying to the condition (9), we can write the control laws as follows,

$$\begin{aligned} U_1 &= \frac{1}{g_{11}(x_1, x_4)} [\ddot{x}_{1d} - f_1(x) - g_{12}(x_1, x_4)u_2 \\ &\quad - \lambda_1 \ddot{e}_1 - \lambda_2 \dot{e}_1 \\ &\quad - K_1 sgn(S_1)] \\ U_2 &= \frac{1}{g_{22}(x_1, x_4)} [\ddot{x}_{4d} - f_2(x) - g_{21}(x_1, x_4)u_1 \\ &\quad - \lambda_3 \ddot{e}_2 - \lambda_4 \dot{e}_2 \\ &\quad - K_2 sgn(S_2)] \end{aligned} \tag{11}$$

In order to force the system to track the desired trajectory, minimize errors, guarantee stability, and use artificial intelligence as a way to estimate the unknown dynamics and the nonlinear dynamics of the system to define new control laws more performances and efficiencies.

3.2. Approximating the Unknown Dynamics and Nonlinear Functions using Artificial Intelligence

In this section, we will see how we develop the algorithm using a neural network, which their role is to approximate the nonlinear f_1 and f_2 of the system, in order to force the system to track the desired trajectory x_{1d} and x_{4d}.

To approximate f_1 and f_2 we build an RBFNN network, which is based on radial basic function, their role is to give an approach to a non-linear function (Fig. 3).

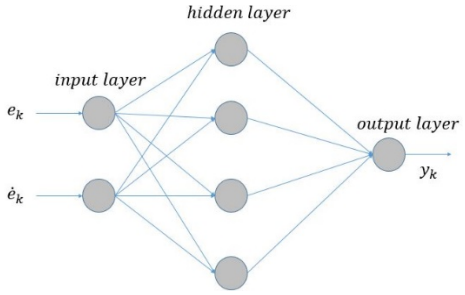


Fig. 3. Radial Basis Function Neural Network or RBFNN.

The RBFNN is a neural network that contains three layers: the input layer, is to take the data from the feedback errors e_1 and e_2, the hidden layer where each node contains a radial basic function as an activation function, and the output of each node is defined as a Gaussian function.

$$h_i(y) = \exp\left(-\frac{\|y_k - c_i\|^2}{b_i^2}\right) \tag{12}$$

where $y_k = [e_k \quad \dot{e}_k]^t$ (k=1,2) is the input of the neural network, c_i is a center vector of each hidden layer node with the same dimension as y, $\|y_k - c_i\|$ represent the Euclidean distance the input and each hidden node, and b_i is a positive scalar of each hidden node.

And the output layer calculates the estimated function based on the output of each node on the hidden layer using the following expression:

$$Y_i(y) = \sum_{j=1}^{N} w_{ij} h_j(x) \tag{13}$$

From equations (12) and (13), the nonlinear estimates are as follows:

$$\begin{aligned}\hat{f}_1(\mathrm{x}) &= \hat{w}_1{}^t.[\,h_i(y)] \text{ and } f_1(\mathrm{x}) = w_1{}^t.[\,h_i(y)]\\ \hat{f}_2(\mathrm{x}) &= \hat{w}_2{}^t.[\,h_i(y)] \text{ and } f_2(\mathrm{x}) = w_2{}^t.[\,h_i(y)],\end{aligned} \tag{14}$$

where $\hat{w}_1{}^t$, $\hat{w}_2{}^t$, and $w_1{}^t$and $w_2{}^t$are the approximated weights and the ideal weights of the network respectively.

The control lows will be as follow:

$$\begin{aligned}U_1 = \frac{1}{g_{11}(\hat{x}_1,\hat{x}_4)}[\ddot{x}_{1d} - \hat{f}_1(x) - g_{12}(\hat{x}_1,\hat{x}_4)u_2 \\ - \lambda_1\ddot{e}_1 - \lambda_2\dot{e}_1 - K_1 sgn(S_1)]\\ U_2 = \frac{1}{g_{22}(\hat{x}_1,\hat{x}_4)}[\ddot{x}_{4d} - \hat{f}_2(x) - g_{21}(\hat{x}_1,\hat{x}_4)u_1 \\ - \lambda_3\ddot{e}_2 - \lambda_4\dot{e}_2 \\ - K_2 sgn(S_2)]\end{aligned} \tag{15}$$

So,

$$\begin{aligned}\dot{S}_1 &= -\tilde{f}_1(\mathrm{x}) - K_1.sgn(S_1)\\ \dot{S}_2 &= -\tilde{f}_2(\mathrm{x}) - K_2.sgn(S_2),\end{aligned} \tag{16}$$

where

$$\begin{aligned}\tilde{f}_1(\mathrm{x}) &= (w_1{}^t - \hat{w}_1{}^t).[\,h_i(x)]\\ \tilde{f}_2(\mathrm{x}) &= (w_2{}^t - \hat{w}_2{}^t).[\,h_i(x)]\end{aligned} \tag{17}$$

Then,

$$\tilde{f}_1(\mathrm{x}) = \tilde{w}_1{}^t.[\,h_i(y)] \text{ and } \tilde{f}_2(\mathrm{x}) = \tilde{w}_2{}^t.[\,h_i(y)] \tag{18}$$

where $\tilde{f}_1(\mathrm{x})$ and $\tilde{f}_2(\mathrm{x})$ are the difference between the ideal and estimated unknown dynamic function, $\tilde{w}_1{}^t = w_1{}^t - \hat{w}_1{}^t$ and $\tilde{w}_2{}^t = w_2{}^t - \hat{w}_2{}^t$ are the difference between the ideal and the approximated weight.

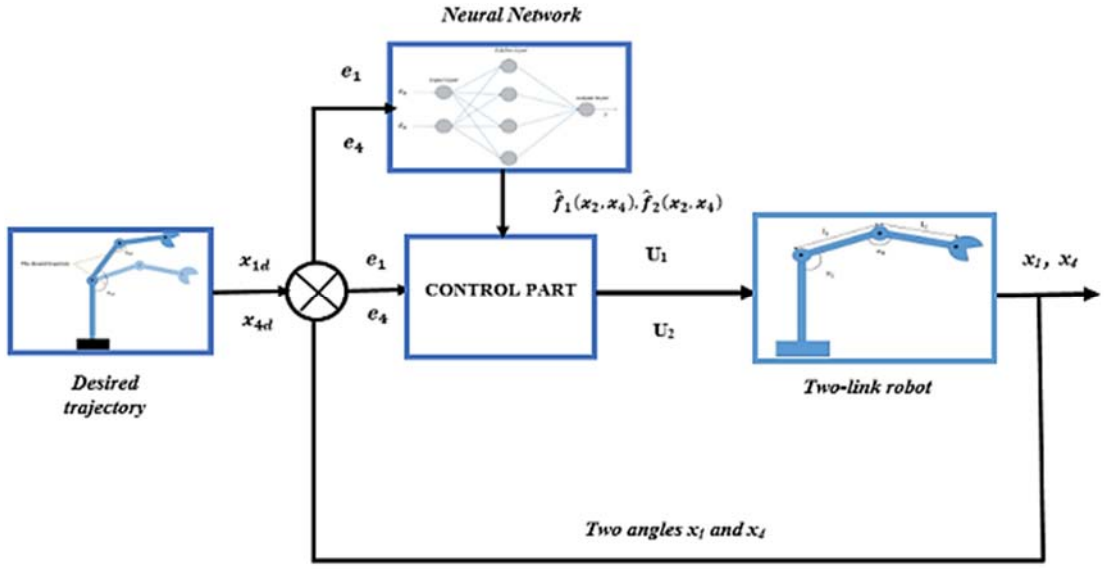


Fig. 4. Proposed approach.

3.3. Stability Analysis

To make the system stable we define the Lyapunov function as in [10]:

$$\begin{aligned}V_{1_rbnn} &= \frac{1}{2}S_1{}^2 + \frac{1}{2}\beta_1\tilde{w}_1{}^t\tilde{w}_1\\ V_{2_rbnn} &= \frac{1}{2}S_2{}^2 + \frac{1}{2}\beta_2\tilde{w}_2{}^t\tilde{w}_2,\end{aligned} \tag{19}$$

where β_1 and β_2 are the positive constants.

The derivative of the equation of the Lyapunov functions is written as follows:

$$\begin{aligned}\dot{V}_{1_rbnn} &= \dot{S}_1S_1 - \beta_1\tilde{w}_1{}^t\hat{w}_1\\ \dot{V}_{2_rbnn} &= \dot{S}_2S_2 - \beta_2\tilde{w}_2{}^t\hat{w}_2\end{aligned} \tag{20}$$

From (16) and (18), we find:

$$\begin{aligned}\dot{V}_{1_rbnn} = -\tilde{w}_1{}^t(S_1.[\,h_i(x)] + \beta_1\dot{\hat{w}}_1) - \\ K_1.sgn(S_1)\\ \dot{V}_{2_rbnn} = -\tilde{w}_2{}^t(S_2.[\,h_i(x)] + \beta_2\dot{\hat{w}}_2) - \\ - K_2.sgn(S_2)\end{aligned} \tag{21}$$

We assume that the terms $\dot{\hat{w}}_1$ and $\dot{\hat{w}}_2$ are:

$$\begin{aligned}\dot{\hat{w}}_1 &= -\frac{1}{\beta_1}S_1[\,h_i(x)]\\ \dot{\hat{w}}_2 &= -\frac{1}{\beta_2}S_2[\,h_i(x)]\end{aligned} \tag{22}$$

So, using the results of (22) and the equations in (21), the system will be stable and the derivative of V_{1_rbnn} and $\dot{V}_{2_rbnn}$ are satisfied to the Lyapunov theory

$$\dot{V}_{1_rbnn} = -K_1.\mathrm{sgn}(S_1) \leq 0$$
$$\dot{V}_{2_rbnn} = -K_2.\mathrm{sgn}(S_2) \leq 0 \quad (23)$$

From equations (20) and (24), we can assume that the system is stable and it will obtain the sliding manifold in finite time.

4. Simulation

In this section, we share the findings as well as the criteria that guided the creation of our plan. We test the strength of the neural network structure we suggest and evaluate its effectiveness using the sliding mode control.

4.1. Simulation 1

In this simulation we will take the parameter gain values of the sliding manifold λ_1 =25, λ_2 = 2000, λ_3 = 20, and λ_4 = 1500, then we find the following results with $x_{1d} = \cos(t)$ and $x_{1d} = \cos(t)$ are desired trajectory (Figs. 5-10).

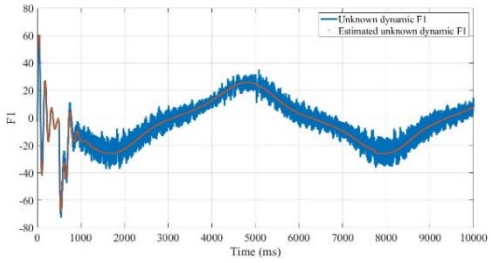


Fig. 5. Estimated dynamic unknown function F_1.

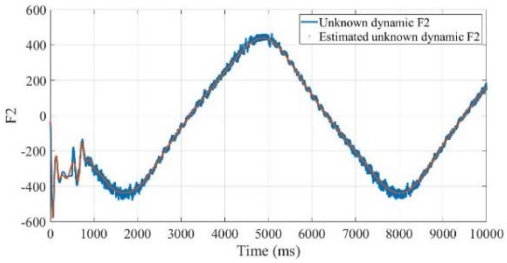


Fig. 6. Estimated dynamic unknown function F_2.

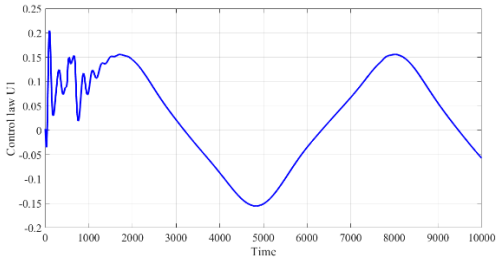


Fig. 7. The control law u_1 generated using the dynamic functions estimates.

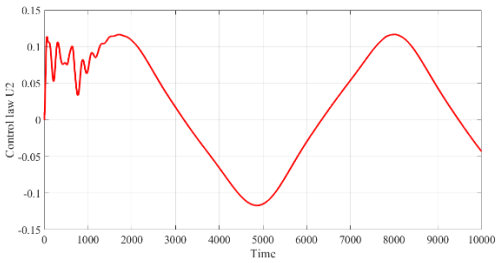


Fig. 8. The control law u_2 generated using the dynamic functions estimates.

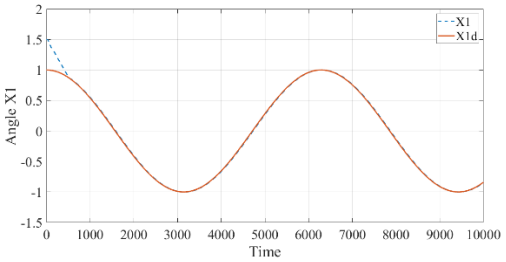


Fig. 9. Desired trajectory x_{1d} and estimate trajectory x_1.

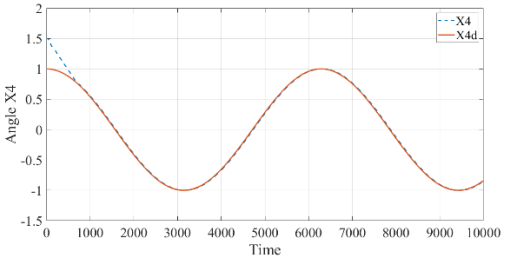


Fig. 10. Desired trajectory x_{4d} and estimate trajectory x_4.

4.2. Simulation 2

Now, let's take the parameter gain values λ_1 = 12.5, λ_2 = 1000, λ_3 = 10, and λ_4 = 750 of the sliding manifold, then we find the following results (Figs. 11-16).

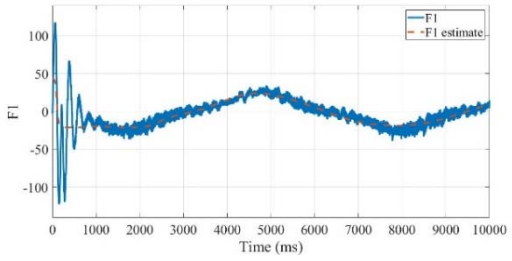


Fig. 11. Estimated dynamic unknown function F_1.

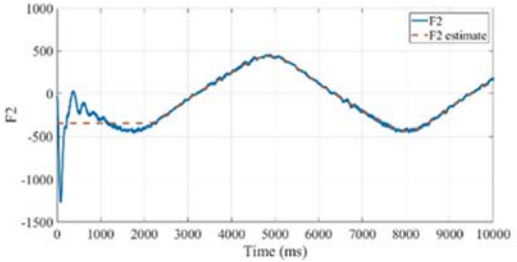


Fig. 12. Estimated dynamic unknown function F_2.

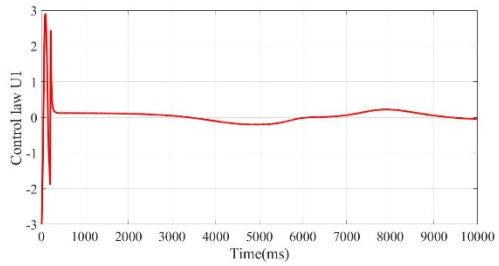


Fig. 13. The control law u_1 generated using the dynamic functions estimates.

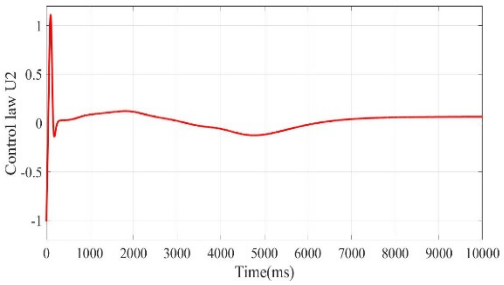


Fig. 14. The control law u_2 generated using the dynamic functions estimates.

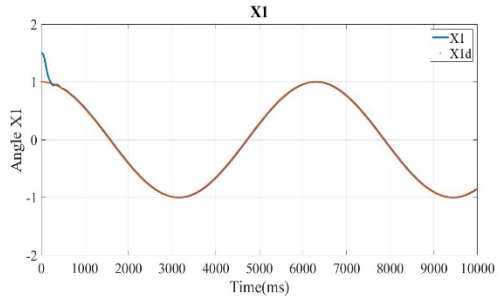


Fig. 15. Desired trajectory x_{1d} and estimate trajectory x_1.

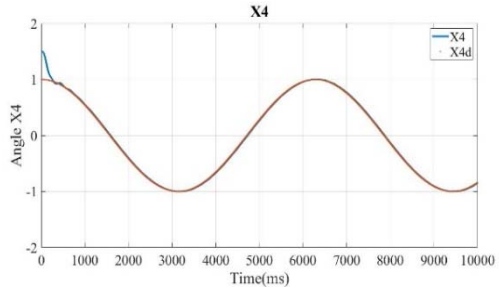


Fig. 16. Desired trajectory x_{4d} and estimate trajectory x_4.

4.3. Simulation 3

Now, let's take the same parameter gains as simulation 2, with $x_{1d} = 2\cos(t)$ and $x_{4d} = 2\cos(t)$ being the new desired trajectory, then we find the results (Control laws and estimate trajectories) as following (Figs. 17-20).

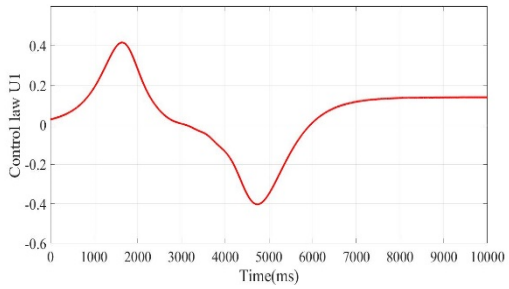


Fig. 17. The control law u_1 generated using the dynamic functions estimates.

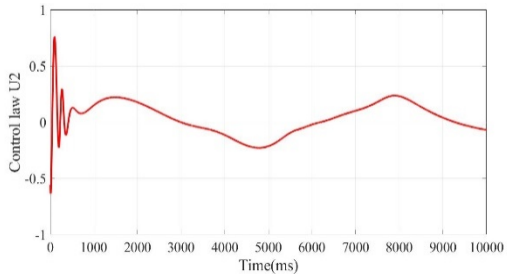


Fig. 18. The control law u_2 generated using the dynamic functions estimates.

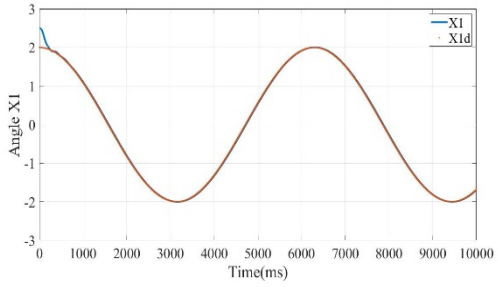


Fig. 19. New desired trajectory x_{1d} and estimate trajectory x_1.

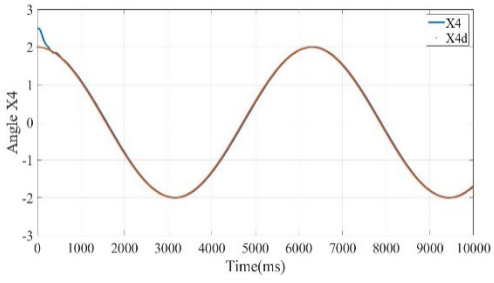


Fig. 20. New desired trajectory x_{4d} and estimate trajectory x_4.

5. Conclusions and Perspective

The paper presents a controller that estimates the dynamic functions of the two-link robot with two control laws using SMC and radial basis function neural networks. This newly designed controller performs well in terms of time convergence and stability, as illustrated by the simulation as in [8] and

[12]. To get the greatest outcomes for this task, we will attempt to improve it by utilizing new and more relevant methods in future works.

References

[1]. L. El Hajjami, E. M. Mellouli, M. Berrada, Robust adaptive non-singular fast terminal sliding-mode lateral control for an uncertain ego vehicle at the lane-change maneuver subjected to abrupt change, *International Journal of Dynamics and Control,* 9, 4, pp. 1765-1782.

[2]. E. M. Mellouli, R. Naoual, I. Boumhidi, A New Modified Sliding Mode Controller Based Fuzzy Logic for A Variable Speed Wind Turbine, *International Journal of Ecology & Development,* 32, 1, pp. 44-53.

[3]. Z. Zhekov, Inverse Kinematics Neural Approximation and Neural Control of Two-link Planar Robot, in *Proceedings of the International Conference Automatics and Informatics (ICAI' 2020),* 2020, pp. 1-5.

[4]. R. Naoual, E. M. Mellouli, S. Sefriti, I. Boumhidi, Fuzzy sliding mode control for the two-link robot, *International Journal of Systems, Control and Communications,* 6, 1, 2014, pp. 84-96.

[5]. A. U. Darajat and S. Istiqphara, Control of Two-Link Robot Manipulator with Uncertainty Parameter using Self-Tuning Sliding Mode Control, in *Proceedings of the 3rd International Conference on Mechanical, Electronics, Computer, and Industrial Technology (MECnIT' 2020),* 2020, pp. 376-380.

[6]. E. M. Mellouli, S. Massou, I. Boumhidi, Optimal Robust Adaptive Fuzzy Tracking Control without Reaching Phase for Nonlinear System, *Journal of Control Science and Engineering*, 2013, art. 498461.

[7]. B. Sarsembayev, T. Kalganova, A. Kaibaldiyev, T. Duc Do and Y. Zhetpissov, Sliding Mode Control with High-Order Disturbance Observer Design for Disturbance Estimation in SPMSM, in *Proceedings of the International Conference on System Science and Engineering (ICSSE' 2019),* 2019, pp. 531-536.

[8]. A. U. Darajat and S. Istiqphara, Control of Two-Link Robot Manipulator with Uncertainty Parameter using Self-Tuning Sliding Mode Control, in *Proceedings of the 3rd International Conference on Mechanical, Electronics, Computer, and Industrial Technology (MECnIT' 2020)*, 2020, pp. 376-380.

[9]. Jun-Fei, Q., and Hong-Gui, H.. Identification and modeling of nonlinear dynamical systems using a novel self-organizing RBF-based approach, *Automatica*, 48, 8, 2012, pp. 1729–1734.

[10]. D. Cruz-Ortiz, I. Chairez and A. Poznyak, Sliding-Mode Control of Full-State Constraint Nonlinear Systems: A Barrier Lyapunov Function Approach, *IEEE Transactions on Systems, Man, and Cybernetics: Systems,* Vol. 52, No. 10, Oct. 2022, pp. 6593-6606.

[11]. X. Zhao, Z. Liu, B. Jiang and C. Gao, Switched Controller Design for Robotic Manipulator via Neural Network-Based Sliding Mode Approach, *IEEE Transactions on Circuits and Systems II: Express Briefs*, Vol. 70, No. 2, Feb. 2023, pp. 561-565.

[12]. E. M. Mellouli, S. Sefriti, I. Boumhidi, Combined fuzzy logic and sliding mode approach's for modelling and control of the two link robot, in *Proceedings of the IEEE International Conference on Complex Systems (ICCS' 2012),* 2012, pp. 1-6.

[13]. Naira, H., Bong-Jun, Y., & Anthony J. Calise, Adaptive output feedback control methodology applicable to non-minimum phase nonlinear systems, *Automatica*, 42, 4, 2006, pp. 513–522.

[14]. Z. Zhekov and E. Marinov, Neural Control of Two-link Planar Robot, in *Proceedings of the 16th Conference on Electrical Machines, Drives and Power Systems (ELMA' 2019),* 2019, pp. 1-4.

[15]. E. M. Mellouli, M. Alfidi, I. Boumhidi, Fuzzy sliding mode control for three-tank system based on linear matrix inequality, *International Journal of Automation and Control*, 12, 2, 2018, pp. 237-250.

[16]. Xin, X., and Yannian, L., Reduced-order stable controllers for two-link underactuated planar robots. *Automatica*, 49, 7, 2013, pp. 2176–2183.

[17]. Tajdari, F., Khodabakhshi, E., Kabganian, M., Golgouneh, A., Switching controller design to swing-up a two-link underactuated robot, in *Proceedings of the 4th IEEE International Conference on Knowledge-Based Engineering and Innovation (KBEI' 2017),* 2017, pp. 595–599.

[18]. Xiang-Gui, G., Wei-Dong, X., Jian-Liang, W., & Ju H. Park, Distributed neuroadaptive fault-tolerant sliding-mode control for 2-D plane vehicular platoon systems with spacing constraints and unknown direction faults, *Automatica*, 129, 2021, 109675.

[19]. A. U. Darajat and S. Istiqphara, Control of Two-Link Robot Manipulator with Uncertainty Parameter using Self-Tuning Sliding Mode Control, in *Proceedings of the 3rd International Conference on Mechanical, Electronics, Computer, and Industrial Technology (MECnIT' 2020)*, Medan, Indonesia, 2020, pp. 376-380.

[20]. M. Bagheri, I. Karafyllis, P. Naseradinmousavi and M. Krstic, Adaptive control of a two-link robot using batch least-square identifier, in *IEEE/CAA Journal of Automatica Sinica,* Vol. 8, No. 1, January 2021, pp. 86-93.

[21]. Y. Wan, L. Xiao and C. Wu, A New Self-Adaptive Control Model and Application Basis on Optimum Fuzzy-RBFNN, in *Proceedings of the International Conference on Artificial Intelligence and Computational Intelligence*, Shanghai, China, 2009, pp. 582-585.

[22]. H.-P. Ren, S. -S. Jiao, X. Wang and O. Kaynak, Fractional Order Integral Sliding Mode Controller Based on Neural Network: Theory and Electro-Hydraulic Benchmark Test, in *IEEE/ASME Transactions on Mechatronics*, Vol. 27, No. 3, June 2022, pp. 1457-1466.

[23]. W. Yang, F. Meng, S. Meng, S. Man and A. Pang, Tracking Control of Magnetic Levitation System Using Model-Free RBF Neural Network Design, in *IEEE Access*, Vol. 8, 2020, pp. 204563-204572.

[24]. Mondal, S., & Mahanta, C., Adaptive second-order terminal sliding mode controller for robotic manipulators, *Journal of the Franklin Institute*, 351, 4, 2014, pp. 2356–2377.

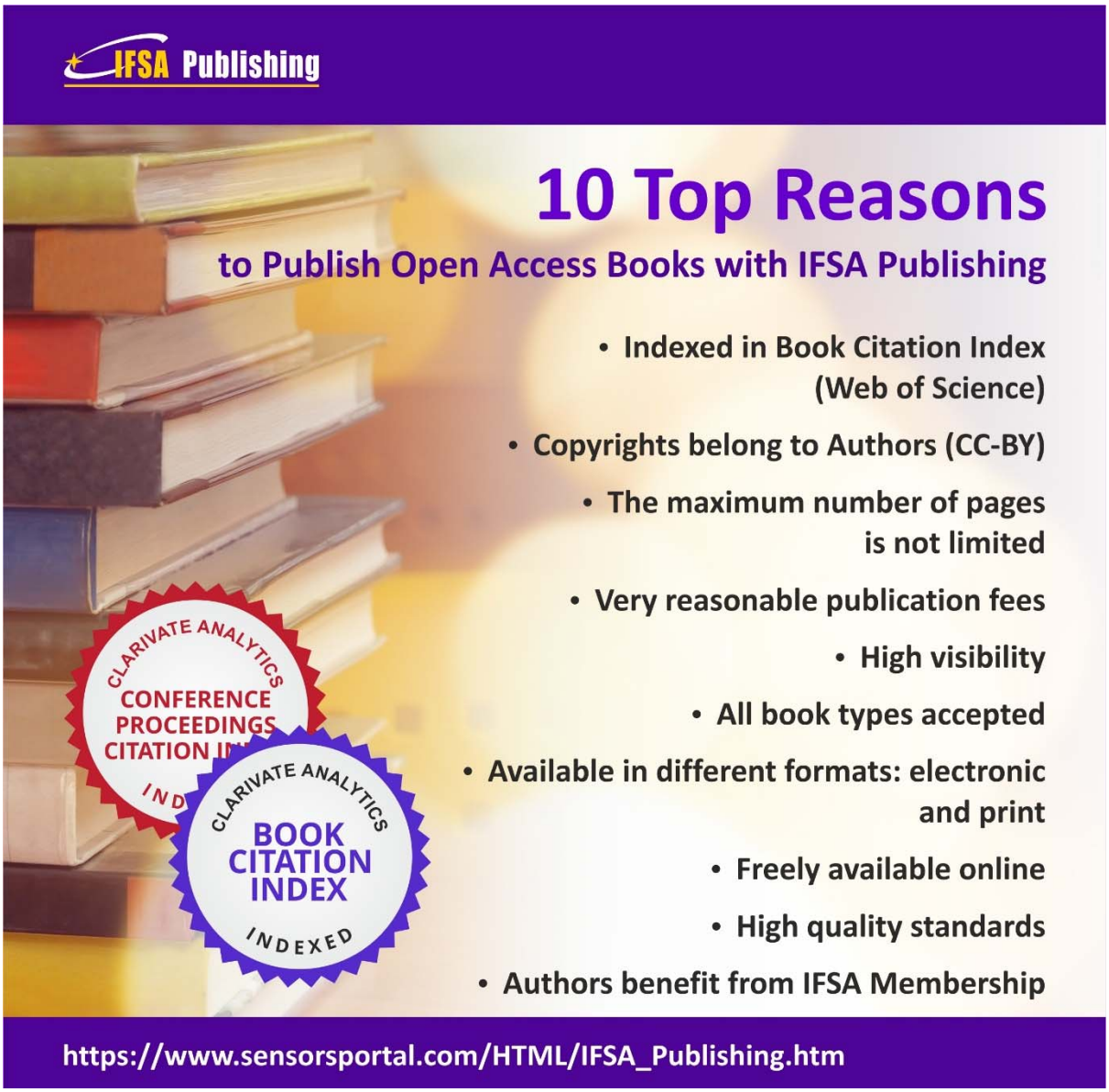
[25]. Chen, Z., Zhang, Y., Nie, Y., Tang, J., & Zhu, S. Adaptive Sliding Mode Control Design for Nonlinear Unmanned Surface Vessel Using RBFNN and Disturbance - Observer, *IEEE Access*, 8, 2020, pp. 45457–45467.

[26]. Bajd, T., Mihelj, M., Lenarcic, J., Stanovnik, A., and Munih, M., Robotics, *Springer*, Netherlands, 2010.

[27]. Jeon, W., Chakrabarty, A., Zemouche, A., and Rajamani, R., Simultaneous State Estimation and Tire Model Learning for Autonomous Vehicle Applications, *IEEE/ASME Transactions on Mechatronics*, 26, 4, 2021, pp. 1941–1950.

[28]. Belkheir, A., and Mellouli, E. M. Sliding Mode Control Combined with Neural Networks for a Two-Link Robot, in *Proceedings of the 3rd IFSA Winter Conference on Automation, Robotics & Communications for Industry 4.0 / 5.0 (ARCI' 2023)*, 22-24 February 2023, Chamonix-Mont-Blanc, France, 2023, pp. 1-2.

Published by International Frequency Sensor Association (IFSA) Publishing, S. L., 2023 (http://www.sensorsportal.com).



Sensors & Transducers, Vol. 261, Issue 2, June 2023, pp. 41-45

www.sensorsportal.com

Sensors & Transducers

Published by IFSA Publishing, S. L., 2023
http://www.sensorsportal.com

The Triangular Observer-Based Integral Sliding-Mode Wind System Energy Control

*** Sanae EL BOUASSI, Zakaria CHALH and El Mehdi MELLOULI**
Laboratory of Artificial Intelligence, Data Sciences and Emerging Systems,
School of Applied Sciences, Sidi MohamedBen Abdellah University, Fez, Morocco
E-mail: sanae.elbouassi@usmba.ac.ma

Received: 13 April 2023 Accepted: 19 June 2023 Published: 26 June 2023

Abstract: We describe a fresh way to constructing a dependable controller utilizing a modified integrated sliding mode control technique in this research. Our proposed solution is intended to address the problem of attaining phase in systems with matching disturbances. As a starting point for demonstrating the usefulness of our technique, we propose replicating a wind turbine system. The inbuilt sliding mode control system is therefore used, which just requires the rotor speed as an accessible measurement. We use an asymptotic observer design that lowers observing errors over time to predict the unknown rotor acceleration required for the control law. The control law is based on Lyapunov stability analysis, which ensures the system's stability. We compare the performance of our proposed system to that of typical sliding mode control using simulation results in terms of settling time, tracking precision, energy usage, and input smoothness. Our findings show that the proposed technique outperforms classic sliding mode control across various performance parameters, showing its potential for developing a reliable controller in real applications.

Keywords: Integral sliding mode control, Lyapunov stability, Nonlinear control, Triangular observer, Wind turbine.

1. Introduction

Wind energy is an abundantly available source of electricity by converting the kinetic energy of moving air mass into electricity. The deployment of solar and wind is characterized as tributed/distributed local production, excluding huge offshore wind farms are considered as local when they are power plants having ratings in the range of more than 100 MW [1-3, 23].

Wind turbines (WTs) are progressing toward the trend of large size and huge capacity in order to fulfil the growing needs of wind power consumption. To enhance the overall performance of big WTs in this trend, numerous sophisticated yaw control solutions have been put out; however, their analysis and summaries are still missing [22].

Since the high rise in energy consumption and the threat of the depletion of natural resources, renewable energy production methods have drawn considerably greater attention, particularly in nations without access to natural energy resources. One of the major sources of clean, renewable energy for producing power is wind energy [4, 5].

It's believed that Sliding Mode Control (SMC) is one of the majorities of system performances, comprising disturbance and insensitivity to parameter changes rejection and have been implemented effectively in several fields.

Practical nonlinear plants, making the task of designing controls for nonlinear systems challenging [6, 10]. Thus, a variety of nonlinear control techniques, including sliding mode control and integral sliding mode control, have been developed for

nonlinear systems to get around the challenge of designing a controller for a real system.

Sliding mode control is a robust control technology that is increasingly used in wind turbine control. It is intended to handle the uncertainties and disturbances associated with wind energy conversion systems, making it an appropriate alternative for wind turbine control [7-9]. A sliding surface is defined as a function of the system states and desired references in sliding mode control, and the control rule is designed to drive the system states onto this sliding surface. The basic concept is to drive the system to slide down the surface towards the desired operating point, resulting in fast and accurate control. Sliding mode control for wind turbines has various advantages, including resistance to parameter changes, changes in wind speed, and other environmental disturbances.

Sliding mode control (SMC), a nonlinear control technique, induces a nonlinear system to "slide" over a cross-section of its typical behaviour by delivering a discontinuous control signal [10, 11].

Integral sliding mode control (ISMC) is a sophisticated control technique that has been developed to address the challenges associated with designing controllers for nonlinear systems, such as practical nonlinear plants. Unlike traditional sliding mode control, ISMC allows the system trajectory to start from the sliding plane, eliminating the arrival phase and promising robustness across the entire state space. ISMC is a combination of sliding mode control with another controller, and was initially developed with the goal of ensuring a sliding mode response from the start of the system's reaction or providing compensation for matching uncertainty response throughout the system [12, 15]. This makes ISMC a powerful approach for controlling nonlinear systems with matched disturbances, as it can effectively handle uncertainties and disturbances in the system dynamics. ISMC has been successfully applied in various fields, including renewable energy systems like wind energy, to improve system performance in terms of tracking accuracy, disturbance rejection, and robustness against parameter changes. In the context of wind energy systems, ISMC has shown promising results in optimizing the performance of large wind turbines and enhancing the overall efficiency and reliability of wind energy generation. The use of ISMC in wind energy systems is an active area of research, and ongoing studies continue to explore its potential for further advancements in renewable energy production.

The integral sliding mode control (ISMC) is a technique which was first proposed in [13, 14] as a solution to the reaching phase problem for systems with matched disturbances. It can be considered a technique for combining the use of the sliding mode controller with another controller.

When ISMC was first developed, the main goal was to compel a sliding mode from the start of the system's reaction, or an ISMC-based controller can give the entire system compensation for matching uncertainty response [16, 17].

The triangular observer is a popular state estimation approach in control systems. It is a special sort of observer, also known as an extended state observer, that is well suited for estimating the states of nonlinear systems with unknown or uncertain dynamics [22]. The triangular observer is based on the concept of a system's "triangular form," in which the state variables are represented as a combination of their original and derivative values. The observer estimates the system states using the system's input-output data and an estimated input. The key concept is to design the observer dynamics so that the estimation error converges to zero, resulting in accurate state estimation. The capacity of triangular observers to deliver resilient and accurate state estimates even in the presence of model uncertainties and disruptions is well established. They've found use in a variety of fields, including robotics, power systems, and automotive systems, where precise state estimate is critical for control and monitoring. The triangular observer is a potent tool for nonlinear system state estimation, contributing to improved system performance, fault detection, and control.

The system's motion is same in dimension to the state space, in contrast to traditional sliding mode control. In integral sliding mode control (ISMC), the system trajectory starts usually from the planning plane. Hence eliminates the arrival phase and promises robustness across the state space.

In this work, the first section covers the modelling of the wind energy system [23, 20] then we present the suggested strategy then we applied it on our system, and we present some simulations of the sliding mode control and the integral to make a comparison between the two modes of sliding control. Finally, a conclusion is reached from the results.

2. Wind Turbine Modeling

The variable speed wind turbine's aerodynamic torque is given by [8, 23]:

$$\text{Ta} = \frac{1}{2}\rho\pi R^3 \frac{Cp(\lambda,\beta)}{\lambda(t)} v(t)^2, \quad (1)$$

where ρ is the density of air, R is the rotor radius, V is the wind speed, C_p is the power coefficient and $\boldsymbol{\lambda}$ is defined as:

$$\lambda\,(\text{t}) = \text{R}.\dot{w}_t \,/\, v\,(\text{t}) \quad (2)$$

The rotor's dynamics is determined by:

$$J_r\dot{w}_t = T_a - T_{ls} - k_r w_t, \quad (3)$$

where J_r, k_r and w_t are the sequentially, the rotor's inertia, external damping, and rotational speed.

The speed w_g of the generator is provided by the following expression:

$$J_g\dot{w}_g = T_{hs} \dot{-} k_g w_g - T_{em}, \quad (4)$$

where J_g, k_g are the generator inertia and friction coefficient and T_{em} is the control law ofthe system.

Expecting a perfect transmission, we define n_g :

$$n_g = \frac{Tls}{Ths} \tag{5}$$

3. Integral Sliding Mode Control

The maximum point on the power coefficient curve corresponds to the ideal amount of wind energy which corresponds to w_{topt} [23, 22], where w_{topt} is given by:

$$y_r = w_{topt} = \frac{v(t).\lambda_{opt}}{R} \tag{6}$$

The system in (Fig. 1) is represented by (7) with disturbances:

$$\begin{cases} \dot{w}_t = w_g \\ \dot{w}_g = f(x) * w_g + g\ .u(x,t) + \frac{1}{10} * \frac{K_g}{J_g} randn \\ y_1 = w_t \end{cases} \tag{7}$$

The control law u=T_{em}, y=w_t.

The errors of the system are provided by [23]:

$$e_1 = w_{topt} - w_t\ , e_2 = \dot{w_{topt}} - \dot{w_t} \tag{8}$$

The sliding surface is defined as:

$$\sigma(t) = \lambda e_1(t) + e_2(t) + ki * \int_0^{\infty} e_1(t)dt \tag{9}$$

Such as ki is the sliding gain.
Assuming the function of stability given by [23]

$$e_1 = w_{topt} - w_t\ , e_2 = \dot{w_{topt}} - \dot{w_t} \tag{10}$$

By using the following equation's derivative, we have

$$\dot{V} = \sigma\dot{\sigma} = \sigma(\lambda(\dot{w_{topt}} - \dot{w_t}) + ki * e_1(t)) \tag{11}$$

The condition of stability

$$\dot{V} \leq 0 \tag{12}$$

This condition satisfies the following requirement [18]

$$\lambda(\dot{w_{topt}} - \dot{w_t}) + ki * e_1 = \begin{cases} < 0 \text{ for } \sigma > 0 \\ = 0 \text{ for } \sigma = 0 \\ > 0 \text{ for } \sigma < 0 \end{cases} \tag{13}$$

K is the designer's chosen sliding control positive gain [19].

$$Tem = Jg\left(-\lambda e_2(t) - \ddot{w_{topt}} + \frac{1}{Jg}(Ths - kgw_g)\ kie_1(t)\right) - ksign(\sigma). \tag{14}$$

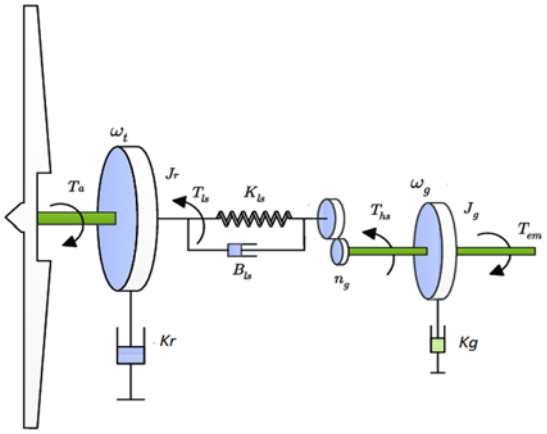


Fig. 1. The representation of the two-mass model wind turbine (10 m/s).

4. Triangular Observer Structure

For the system model stated in (7), the triangle observer that causes the observing errors to go to zero after a finite length of time can be expressed as follows [6][23]:

$$\begin{cases} \dot{\hat{w}}_t = \hat{w}_g + \lambda_1 sign(w_t - \hat{w}_t) \\ \dot{\hat{w}}_g = \dot{w}_g + \lambda_2 sign(\tilde{w}_g - \hat{w}_g) \end{cases},$$

where

$$\tilde{w}_g = \hat{w}_g + \lambda_1 sign_1(w_t - \hat{w}_t)$$

and

$$\tilde{w}_t = w_t$$

Such as $sign_i$ is characterized by:

$$sign_i(..) = \begin{cases} 0 & \text{if } \tilde{x}_j - \hat{x}_j \neq 0 \\ & j \in [1, i] \\ sign(..) & \text{elsewhere} \end{cases}$$

5. Simulation Results

The Fig. 2 depicts the wind speed used in our study (10 m/s), the second depicts the two curves, one for the rotor speed and the other for the target rotor speed, and the third depicts the error between the two rotor speeds, the normal and the desired. The Fig. 6 describes an asymptotic observer triangular; that causes the observing errors to go toward zero over a finite period of time which shown in Fig. 7; to roughly estimate the unknown rotor acceleration needed to build the control law. Fig. 6 depicts the difference between the generator speed and the observed state.

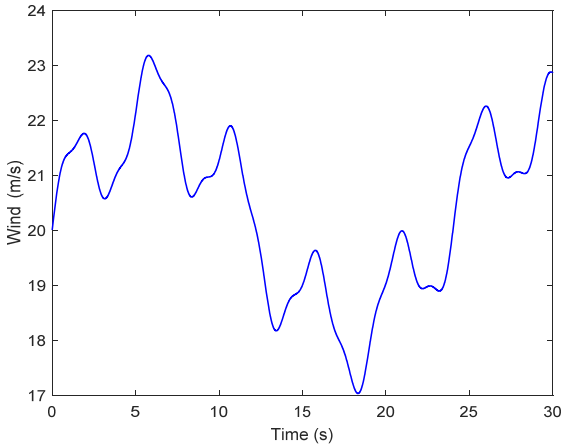


Fig. 2. The representation of the wind for (10 m/s).

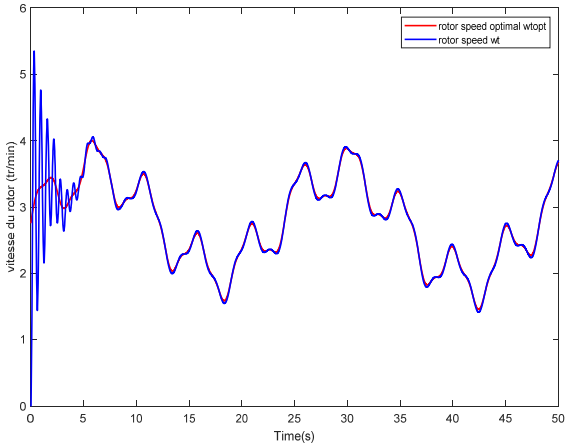


Fig. 3. Responses of the calculate and desired (optimal) rotor speed.

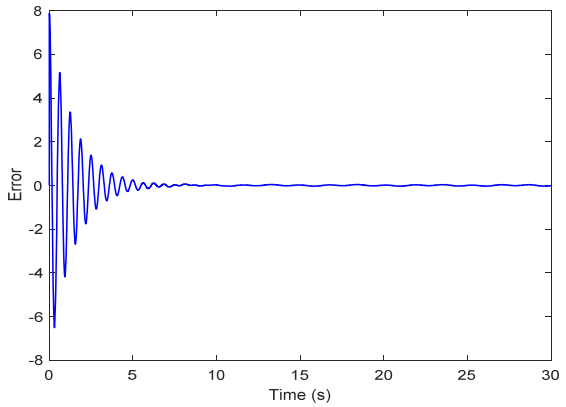


Fig. 4. Responses of tracking error between the rotor speed and the rotor speed desired.

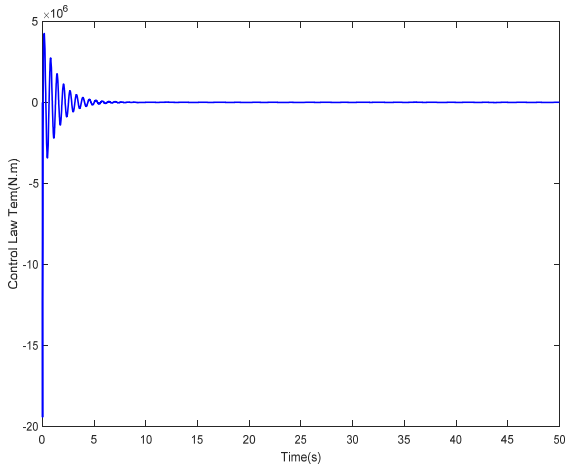


Fig. 5. The response of the control law with integral sliding mode control.

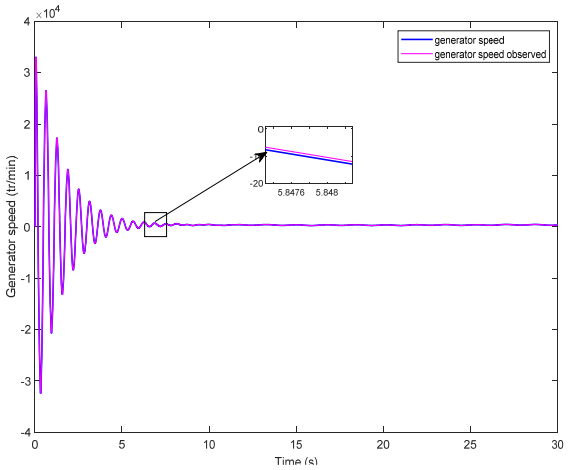


Fig. 6. The generator speed and the generator speed observed.

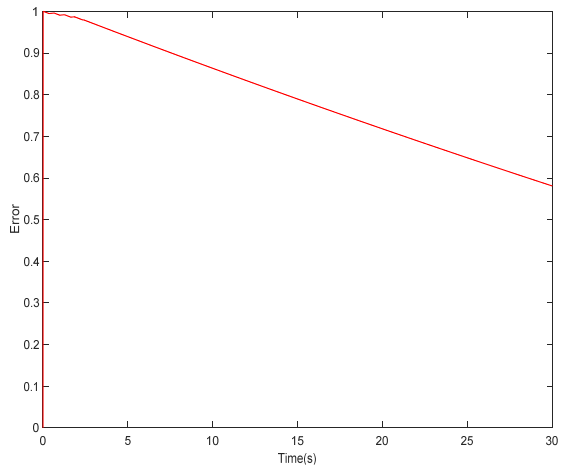


Fig. 7. The observatory error.

6. Conclusion

In this article, we explored the operating mode for the two-mass model system that is connected to the integral sliding mode control (ISMC). The simulation results demonstrate the distinction between the two strategies. The Lyapunov technique ensures the stability of the system. In this optics, we can make and

search for approximations to key parameters and gains in order to improve our system's performance and efficiency.

7. References

[1]. A. Sellami, D. Arzelier, R. M'hiri, J. Zrida, A Sliding Mode Control Approach for Systems Subjected to a Norm-Bounded Uncertainty, *International Journal of Robust and Nonlinear Control*, Vol. 17, Issue 4, 2007, pp. 327-346.

[2]. A. Aissaoui, A. Tahour, M. Abid, N. Essounbouli, F. Nollet, Power Control of Wind Turbine based on Fuzzy Controllers, *The Mediterranean Green Energy Forum (MGEF-13)*, 2013, pp. 163-172.

[3]. C. Chatri, M. Ouassaid, M. Labbadi, Y. Errami, Integral-type terminal sliding mode control approach for wind energy conversion system with uncertainties, *Computers and Electrical Engineering*, 2022, p. 107775.

[4]. R. Naoual, E. M. Mellouli, S. Sefriti, I. Boumhidi, Fuzzy sliding mode control for the two-link robot, *International Journal of Systems, Control and Communications*, 6, 1, 2014, pp. 84-96.

[5]. E. M. Mellouli, M. Alfidi, I. Boumhidi, Fuzzy sliding mode control for three-tank system based on linear matrix inequality, *International Journal of Automation and Control*, 2018, pp. 237-250.

[6].

[7]. E. M. Mellouli, Z. Chalh, M. Alfidi, A New Robust Adaptive Fuzzy Sliding Mode Controller for a Variable Speed Wind Turbine, *International Review of Automatic Control*, 8, 5, 2015, pp. 338-345.

[8]. J. Mérida, Luis T. Aguilar, J. Dávila, Analysis and synthesis of sliding mode control for large scale variable speed wind turbine for power optimization, *Renewable Energy*, 2014, pp. 715-728.

[9]. Yujun Li, Zhao Xu, Ke Meng, Optimal Power Sharing Control of Wind Turbines, *IEEE Transactions on Power Systems*, 32, 1, 2017, pp. 824 - 825.

[10].H. Chen, Q. Li, S. Tang, N. AÏT-Ahmed, J. Han, T. Wang, Z. Zhou, T. Tang, M. Benbouzid, Adaptive super-twisting control of doubly salient permanent magnet generator for tidal stream turbine, *International Journal of Electrical Power & Energy Systems*, Vol 128, June 2021, 106772.

[11]. W. Du, G. Yang, C. Pan, P. Xi, Y. Chen, A Sliding-Mode-Based Duty Ratio Controller for Multiple Parallelly-Connected DC–DC Converters with Constant Power Loads on MVDC Shipboard Power Systems, *Energies*, Vol 13, 15, 2020, 3888.

[12]. Sami, A. Abid, N. Khan, M. Zaid, H. Ahmad, H. Ali, Supertwisting Sliding Mode Control of Multi-converter MVDC power systems under constant power loads, in *Proceedings of the 4th IEEE International Conference on Computing, Power and Communication Technologies* (GUCON), 2021, pp. 1-5.

[13]. Y. Shtessel, M. Taleb, F. Plestan, A novel adaptive-gain supertwisting sliding mode controller: Methodology and application, *Automatica*, Vol 48, May 2012, pp. 759-769.

[14]. F. Qiao, Q. Zhu, A. FT Winfield, C. Melhuish, Adaptive sliding mode control for MIMO nonlinear systems based on fuzzy logic scheme, *International Journal of Automation and Computing*, 1, 2004, pp. 51-62. E. M. Mellouli, S. Sefriti, I Boumhidi, Combined fuzzy logic and sliding mode approach's for modelling and control of the two link robot, in *Proceedings of the IEEE International Conference on Complex Systems (ICCS)*, 2012, pp. 1-6.

[15]. W. Zhang, L. Zhao, Survey and tutorial on multiple model methodologies in modelling, *Identification and Control*, 32, 2019, pp 1-9.

[16]. B. Wang, T. Wang, Y. Yu, C. Luo, D. Xu, Convergence Trajectory Optimization of Supertwisting Sliding-Mode Current Control for Induction Motor Drives, *IEEE Transactions on Industrial Electronics*, Vol. 69, 2021, pp. 12292 – 12304.

[17]. S. El Bouassi, Z. Chalh, E. M. Mellouli, A New Robust Adaptive Control for Variable Speed Wind Turbine, *Artificial Intelligence and Smart Environment*, Vol 635, 2023, pp. 90-96.

[18]. Soufi Y., Kahla S., Bechouat M., Particle swarm optimization based sliding mode control of variable speed wind energy conversion system, *International Journal of Hydrogen Energy*, 41, 45, 2016, pp. 20956-20963.

[19]. M. Ayadi, O. Naifar, N. Derbel, High-order sliding mode control for variable speed PMSG-wind turbine-based disturbance observer, *International Journal of Modelling, Identification and Control*, 32, 1, 2019, pp. 85-92.

[20]. Carlos Arturo Martínez-Fuentes et al., Saturated Lipschitz Continuous Sliding Mode Controller for Perturbed Systems with Uncertain Control Coefficient, *IEEE Transactions on Automatic Control*, 66, 8, 2021, pp. 3885 – 3891.

[21]. J. Mérida, L. Aguilar, J. Dávila, Analysis and synthesis of sliding mode control for large scale variable speed wind turbine for power optimization, *Renewable Energy*, Vol. 71, No. 11, 2014, pp. 715-728.

[22]. A. Norouzi, R. Kazemi, S. Azadi, Vehicle lateral control in the presence of uncertainty for lane change maneuver using adaptive sliding mode control with fuzzy boundary layer, *Proceedings of the Institution of Mechanical Engineers Part I: Journal of Systems and Control Engineering*, Vol 232, 2018, pp. 12–28.

[23]. S. El Bouassi, Z. Chalh, E. M. Mellouli, Triangular observer-Based Integral Sliding-Mode Control for wind system energy, in *Proceeding of the 3rd IFSA Winter Conference on Applications, Robotics and Communications for industry 4.0/5.0 (ARCI'2023)*, Charmonix-Mon-blanc, France, 22-24 February 2023, pp. 20-22.

[24]. S.El Bouassi, Z. Chalh, E. M. Mellouli, A New Robust Adaptive Control for Variable Speed Wind Turbine, in Artificial Intelligence and Smart Environment, *Springer*, 2022, pp 90–96.

Published by International Frequency Sensor Association (IFSA) Publishing, S. L., 2023 (http://www.sensorsportal.com).

Sensors & Transducers, Vol. 261, Issue 2, June 2023, pp. 46-54

www.sensorsportal.com

Sensors & Transducers

Published by IFSA Publishing, S. L., 2023
http://www.sensorsportal.com

Comparison of LMI Solvers for Robust Control of a DC-DC Boost Converter

[1, *] Jérôme BOSCHE, [2] David LARA ALABAZARES and [1] Abdelhamid RABHI

[1] Modeling, Information and Systems, UPJV, 33 rue Saint-Leu, 80000, Amiens, France
[2] Instituto Tecnológico Superior de Misantla, Carretera a Loma del Cojolite, 93821 Misantla, Veracruz, México
[1] Tel.: + 33322825915, fax: + 33322825905
[*] E-mail: jerome.bosche@u-picardie.fr

Received: 17 April 2023 Accepted: 19 May 2023 Published: 26 June 2023

Abstract: This work deals with a robust Fault-Tolerant Control (FTC) design for a class of uncertain systems. Fault resilience is associated with a robustness bound generated by a sufficient Linear Matrix Inequality (LMI) condition for static state feedback stabilization. This design control approach is based on solving an optimization problem expressed in terms of LMI with three different programming solvers which are *mincx* (MATLAB), *lmisolver* (SCILAB) and *cvxopt* (PYTHON). Numerical validations were carried out, first on an academic model, then on the model of a PV energy conversion system connected to a DC-DC boost converter. Then, a robustness analysis for fault resilience associated with a control law gains, obtained using the three solvers, was realized to investigate the best performance. This approach was finally validated on an experimental test bench.

Keywords: Fault, Tolerant control, Robust state feedback control, LMI, DC/DC boost converter, MATLAB, SCILAB, PYTHON.

1. Introduction

Cyber-physical Systems (CBS) are increasingly complex and sophisticated. The challenge is to exploit new technologies and hardware to make them more efficient and autonomous [1]. Sensors are associated with CBS to get precise environment information, allowing the system to be autonomous, as much as possible. However, this poses two major problems: (a) how to make the system react effectively based on real-time sensor data? (b) how to take into account a fault sensor during operation? Fault Tolerant Control (FTC) studied in the field of control theory, can solve this problem. It is applied as a tool in transport [2], energy [3], industry 4.0 [4], etc. In the case of a partial fault, the FTC problem can be formulated as a state feedback control (SFC) problem for an uncertain system with a norm-bounded uncertainty. Then, a controller guaranteeing a certain level of performance for the largest uncertainty domain is designed. When the fault is total, a SFC augmented with an observer or outright, an output feedback control (OFC) law, are suitable. Finally, it is possible to consider the general case of partial and/or total faults by using a robust OFC. Concerning partial fault, the approach of [5] can be exploited to design an FTC. In this work, a α-stabilization technique is used to compute a passive fault-tolerant control law that guarantees the asymptotic stability of the system in the presence of faults.

On the other hand, the pole placement of the closed-loop system in a region α of the complex

plane, allows the process to react efficiently to the fault. Whatever the technique, it must lead to a control law as robust as possible, the capacity of the system to tolerate the fault depending on this robustness. In fact, most of the work relating to this issue tends to reduce the conservatism induced by the sufficient conditions, related to a LMI problem, and leading to the gain of the controller. Some LMI-based conditions consider non-quadratic Lyapunov functions [6], other works rather exploit homogeneous polynomial Lyapunov functions [7] while promising results are obtained with fuzzy Lyapunov functions [8]. Then, significant advances have been made in this area, but these new conditions, less conservative, consist in LMI systems that are increasingly complex to solve from a numerical point of view. However, it is interesting to note that the robustness of these control laws may depend on the numerical computation software used to solve the problem, and more globally, on the associated LMI solver. Solving an LMI amounts to a semidefinite programming problem (SDP). There are many algorithms for solving SDP and many of them use the interior-point method [9]. Interior point algorithms are often combined with second-order optimization methods using Newton's method. They are particularly efficient for small SDP. For more complex problems, first-order optimization methods using the gradient descent method are more suitable. In [10], an efficient randomized first-order algorithm for solving SDP is proposed and compared to the CVXOPT solver of PYTHON [11] and the Splitting Conic Solver algorithm [12]. This work considers rather small-dimensional SDP and we will solve our LMI problems using PYTHON's CVXOPT solver [11], SCILAB's LMISOLVER solver [13] and MATLAB's MINCX solver [14]. The robustness of a control law associated with a DC-DC boost converter is then analyzed according to the solver used.

The paper is organized as follows: Section 2 is dedicated to some preliminaries which present the uncertainty models considered in this work as well as the concept of robust $\alpha - stabilization$. Section 3 deals with the modeling of the DC-DC boost converter considering sensor faults and the control objectives. Section 4 compares the efficiency of the three LMI solvers. Initially, the $\alpha - stabilization$ of a numerical model is considered, then the problem of the voltage regulation of a PV module is dealt with. Section 5 presents an experimental validation of the FTC control approach on photovoltaic energy conversion chain while section 6 gives conclusions and perspectives.

2. Preliminaries

We denote by M^T, the transpose of M. $\mathbb{I}_n$ is the identity matrix of order n. $\mathbb{O}$ is a null matrix of suitable dimension. $\{\blacksquare\}^T$ standing block (i,j) in a matrix corresponds to the transposed term of block (j,i). $\Gamma(A)$ is the spectrum of the matrix A, that is to say, the set of its eigenvalues. $\mathcal{C}$ is the complex plane and $\mathcal{C}^-$ stands for $Re(\mathcal{C}) < 0$.

2.1. Polytopic and Norm-Bounded Representation

The Polytopic and Norm-Bounded (PNB) representation is used to robust analysis and control dedicated to systems affected by both polytopic and structured uncertainties, represented in the state space by the following model:

$$\begin{cases} \dot{x}(t) = A(\theta).x(t) + B(\theta).u(t) + T.\varphi(t). & (1) \\ y(t) = C(\Delta).x(t), & (2) \end{cases}$$

where $x(t) \in \mathbb{R}^n$, $u(t) \in \mathbb{R}^m$, $y(t) \in \mathbb{R}^p$, and $\varphi(t) \in \mathbb{R}^v$ are respectively the state, input, output and measurable disturbance vectors. $A(\theta) \in \mathbb{R}^{n\times n}$ and $B(\theta) \in \mathbb{R}^{n\times m}$ represent the state and control matrices, belonging to a polytopic of matrices with N vertices:

$$[A(\theta)B(\theta)] = \sum_{i=1}^{N} \theta_i \, [A_i B_i] \quad (3)$$

with $\sum_{i=1}^{N} \theta_i = 1.$ (4)

$C(\Delta)$ is the output matrix affected by a norm-bounded uncertainty, denoted $\mathcal{JL}$ -structured uncertainty, whose representation is recalled here:

$$C(\Delta) = C_0 + \mathbb{E} = C_0 + J.\Delta.L\,, \quad (5)$$

where C_0 is a nominal matrix, $J \in \mathbb{R}^{nxq}$ and $L \in \mathbb{R}^{rxn}$ are known structured matrices whereas $\Delta \in \mathbb{R}^{qxr}$ is the uncertain matrix belonging to the ball $\mathcal{B}(\rho)$ such that $\|\Delta\|_2 < \rho$. $\mathbb{E}$ is a norm-bounded uncertainty whose structure is defined par J and L.

2.2. α-stabilization

This part addresses the design of robust feedback control for a system with PNB uncertainties and particular attention is paid to the system dynamic performance, such as the time response. Also, the placement of all spectrum of the state-matrix $\Gamma(A_C = A(\theta) + B(\theta).K)$ in a half plane $\mathcal{C}^\alpha$ of $\mathcal{C}^-$ is treated, defined by $x < \alpha$. Then, when $(A_C) \in \mathcal{C}^\alpha$, A_C is said α-stable.

A sufficient condition of robust α-stabilization by static state feedback deduced from that proposed by [5] is recalled here. Therefore, it does not constitute an original contribution in the context of this work but rather a robust control law technique which will be processed by different solvers and analyzed.

Theorem 1. There is a matrix K associated with the robust state control law $u(t) = K.x(t)$ α -stabilizing system (1)-(2), if there is a solution to the following convex optimization problem

$$\underset{X,R,\zeta}{\min} \quad \gamma = \rho^{-2}, \tag{6}$$

where ζ is a positive scalar fixed a priori, $X = X^T > 0$, $X \in R^{n\times n}$, $R \in R^{m\times n}$ and γ are variables verifying the LMI constraints:

$$H_i(A_i, B_i, J_i, L_i, T) < 0\ , \quad \forall i \in \{1, .., N\} \tag{7}$$

with

$$H_i = \begin{bmatrix} Q_i & \{\blacksquare\}^T & \{\blacksquare\}^T & \{\blacksquare\}^T & \{\blacksquare\}^T \\ L_i X & -\mathbb{I}_r & \mathbb{0} & \mathbb{0} & \mathbb{0} \\ X & \mathbb{0} & -\mathbb{I}_n & \mathbb{0} & \mathbb{0} \\ J_i^T & \mathbb{0} & \mathbb{0} & -\gamma\mathbb{I}_q & \mathbb{0} \\ T^T & \mathbb{0} & \mathbb{0} & \mathbb{0} & -\zeta\mathbb{I}_v \end{bmatrix}$$

with $Q_i = \{-\alpha X + A_i X + B_i R\} + \{\blacksquare\}^T$

A static state feedback is then associated with:

$$K = R.X^{-1} \tag{8}$$

and the uncertainty domain for which the α-stability is guaranteed is given by $\|\Delta\|_2 \leq \rho^* = \gamma^{-\frac{1}{2}}$, the optimal value of ρ.

3. FTC for DC-DC Boost Converter

The DC-DC boost converter system, associated with a photovoltaic module, connected to a load is shown in Fig. 1. It fits into our problem and will be used to support a comparison of the fault resilience resulting from the resolutions of control optimization problems.

The converter consists of: a) a power transistor Q and a rectifier diode D (threshold voltage v_D) constituting the switching-mode power device, b) a smoothing inductance L with internal resistance r_L, and c) a filtering voltage capacity C_1 and a bus capacity C_2.

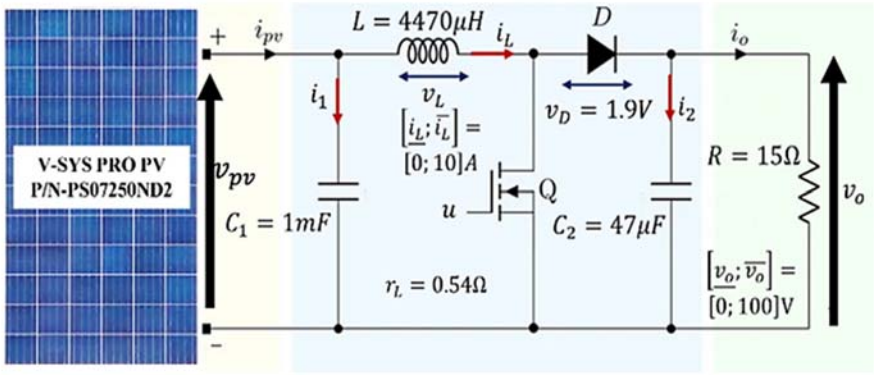


Fig. 1. DC-DC boost converter for a PV module

3.1. PNB Representation of a Boost Converter

The averaged model of this system considers two sub-models: one is associated with an "off state" of the thyristor (u(t)=0), the other with an "on state" (u(t)=1). It can be written in the form (1) with $x(t) = [i_L(t) v_0(t) \quad v_{PV}(t)]^T$, $\varphi(t) = [v_D \quad i_{PV}(t)]^T$ where $i_L(t)$ is the inductor current, $v_0(t)$ is the output voltage, and $v_{PV(t)}$ the PV voltage generated by the module. Basically, the dynamic equations of the boost converter can be expressed by the Linear Parameter-Varying (LPV) state-space equation (1) with:

$$A = \begin{bmatrix} -\frac{r_L}{L} & \frac{(u_0 - 1)}{L} & \frac{1}{L} \\ \frac{(1-u_0)}{C_2} & \frac{-1}{RC_2} & 0 \\ \frac{-1}{C_1} & 0 & 0 \end{bmatrix} \tag{9}$$

$$B(\theta(t)) = \begin{bmatrix} \frac{(v_0(t)+v_D)}{L} \\ \frac{-i_L(t)}{C_2} \\ 0 \end{bmatrix} \tag{10}$$

$$T = \begin{bmatrix} \frac{(u_0-1)}{L} & 0 \\ 0 & 0 \\ 0 & \frac{1}{C_1} \end{bmatrix} \tag{11}$$

Note that the control matrix $B(\theta(t))$ depends on time-varying states $i_L(t)$ and $v_0(t)$, leading to a nonlinear the model. Nevertheless, the range of signal variation is bounded, as shown in Fig. 1, so $B(i_L(t), v_0(t))$ can be considered as a polytope of matrices as in (3) with N=4, $B_1 = B(\overline{i_L}, \overline{v_0})$, $B_2 = B(\overline{i_L}, v_0)$, $B_3 = B(i_L, \overline{v_0})$ and $B_4 = B(i_L, v_0)$.

On the other hand, under normal operating conditions, the states are measured by current and

voltage sensors, respectively noted S_{I_L}, S_{v_0} and $S_{v_{PV}}$. Then, it is assumed that these sensors can be affected by a fault. Depending on the value of $C(\Delta)$ in (5), three cases are considered associated with $C_0 = \mathbb{I}_3$ and the corresponding values for *J* and *L*, as shown Table 1.

Table 1. Three fault cases for the DC-DC boost converter.

Case	J	L	S_{I_L}	S_{v_0}	$S_{v_{PV}}$
1	$B(\theta)$	[1,0,0]	partial	none	none
2	$B(\theta)$	[0,1,0]	none	partial	none
3	$B(\theta)$	[0,0,1]	none	none	partial

3.2. Control Objective

Our control objective is to exploit the α-stabilization condition to develop a proportional-integral regulator, whose architecture is shown in Fig. 2.

$z(t) \in \mathbb{R}^z$ is the controlled output vector and the problem consists in regulating $z(t)$ to a reference value $z_{ref}(t)$. The control law results in *n* proportional actions (one for each state variable) and one integral action (on the error). The corresponding *n*PI controller is then defined by:

$$u(t) = u_0 + K_p.y(t) + K_i.e(t) = u_0 + \delta u(t). \quad (12)$$

$$\text{with } e(t) = \int_0^t (z_{ref}(\tau) - z(\tau)).d\tau \quad (13)$$

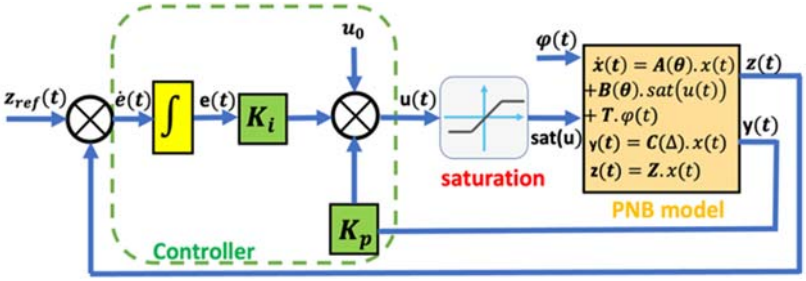


Fig. 2. nPI controller architecture.

The input command is saturated, $u(t) \in \left[\overline{u}; \dot{u}\right]$, with $\overline{\boldsymbol{u}} = u_0 - \delta_u(t)$ and $\boldsymbol{u} = u_0 + \delta_u(t)$, where u_0 is the nominal value of u(t). In order to take into account the integral action inherent in this control architecture, the state-space representation (1)-(2) is extended to an augmented model with a state vector resulting from the concatenation of $x(t)$ and $e(t)$, the integral of the error between the reference signal $z_{ref}(t)$ and $z(t)$,the signals to be regulated. Without difficulty, we obtain the corresponding representation.

$$\begin{cases} \dot{X}(t) = \mathbb{A}.X(t) + \mathbb{B}.u(t) + \mathbb{T}.\varphi(t) + \mathbb{F}.z_{ref}(t) & (14) \\ y(t) = \mathbb{C}(\Delta).X(t) & (15) \end{cases}$$

with

$$\begin{cases} X(t) = \begin{bmatrix} x(t) \\ e(t) \end{bmatrix}, \mathbb{A} = \begin{bmatrix} A(\theta) & \mathbb{O} \\ -Z & \mathbb{O} \end{bmatrix}, \mathbb{B} = \begin{bmatrix} B(\theta) \\ \mathbb{O} \end{bmatrix} \\ \mathbb{T} = \begin{bmatrix} T \\ \mathbb{O} \end{bmatrix}, \mathbb{F} = \begin{bmatrix} \mathbb{O} & \mathbb{O} \\ \mathbb{O} & \mathbb{I}_z \end{bmatrix}, \mathbb{C}(\Delta) = \begin{bmatrix} C(\Delta) & \mathbb{O} \\ \mathbb{O} & \mathbb{I}_z \end{bmatrix} \end{cases} \quad (16)$$

3.3. FTC Controller of a Boost Converter

According to part 3.2, it is clear that $z_{ref}(t) = v_{PVref}$ (t) and $z(t) = v_{PV}$ (t). It leads to $E = [0 \quad 0 \quad 1]$ and then, the augmented DC-DC boost converter model is easily deduced from (14), (15), (16) with (9), (10) and (11). A fault-tolerant control law can then be computed if there is a solution to the convex optimization problem (6) verifying LMI conditions:

$$H_i(\mathbb{A}_i, \mathbb{B}_i, \mathbb{J}_i, \mathbb{L}_i, \mathbb{T}) < 0\ ,\ \forall i \in \{1,..,4\} \quad (17)$$

$$\begin{bmatrix} \mu_1 \mathbb{I}_n & R^T \\ R & \mathbb{I}_m \end{bmatrix} > 0 \quad (18)$$

$$\begin{bmatrix} \mu_2 \mathbb{I}_n & \mathbb{I}_n \\ \mathbb{I}_n & X \end{bmatrix} > 0 \quad (19)$$

where $\mathbb{J}_i = [J_i \quad \mathbb{O}]^T$ and $\mathbb{L}_i = [L_i \quad \mathbb{O}]$ and LMIs (18) and (19) respectively limit the 2-norm of R and X^{-1}, and consequently the controller gain values.

4. Simulation Results

This section is dedicated to simulation results. First, the robust α -stabilization is applied on a numerical model and generated by the three LMI solvers. Subsequently, this same stabilization technique is tested on the photovoltaic energy conversion system presented in Section 3, as in [9].

4.1. Numerical Model Simulations

We consider the polytopic and norm-bounded representation of a numerical model described below:

$$A_1 = \begin{bmatrix} -2 & -1 & 0 \\ 0 & 10 & 1 \\ 0 & 0 & -1 \end{bmatrix} and A_2 = \begin{bmatrix} -2 & -1 & 0 \\ 2 & 10 & 1 \\ 0 & 0 & -1 \end{bmatrix}$$

$$B_1 = B_2 = \begin{bmatrix} 2 \\ -1 \\ 1 \end{bmatrix} and J_1 = J_2 = B_1 = B_2$$

Then three fault sensor cases are considered:

Case 1: $1st$ sensor fault with $L_1 = L_2 = [1 \quad 0 \quad 0]$;
Case 2: $2nd$ sensor fault with $L_1 = L_2 = [0 \quad 1 \quad 0]$;
Case 3: $3rd$ sensor fault with $L_1 = L_2 = [0 \quad 0 \quad 1]$.

Then, the optimization problem (6) considering LMI conditions (7) with $T = \mathbb{0}$ (no disturbance) has been solved using the MATLAB's *mincx* function, the SCILAB's *lmisolver* function and the PYTHON's *cvxopt* function for the three fault sensor cases and for $\alpha = -1, -2, -3 \; and \; -5$. Table 2 shows the robustness bound values obtained for each case. When no value is provided, it means that the LMI system could not be solved by the corresponding solver. Colored cells correspond to the highest bound.

These results show that SCILAB's *lmisolver* leads each time to the best robustness bound, that is to say to the best sensor fault tolerance. However, note that the results obtained with this solver are very close to those obtained with *mincx* from MATLAB. PYTHON's *cvxopt* function seems, in this case, to offer less robustness.

4.2. DC-DC Boost Converter Simulations

It is about computing the nPI controller presented in part 3.2 to regulate the photovoltaic voltage of a PV module. The control objective is to generate the duty cycle of signal $u(t)$ for the gate of Q to regulate the voltage $v_{PV}(t)$ to the reference photovoltaic voltage v_{PVref}(t). An MPPT algorithm (not detailed in this work) generates the reference PV voltage from data (weather, current, voltage) acquired on an experimental set-up. The architecture of this implementation is shown in Fig. 3.

Table 2. Robustness bounds ρ^*.

Case	α	LANGUAGE		
		MATLAB	SCILAB	PYTHON
1	-1	5.0641	5.0777	4.9808
	-2	5.0439	5.0547	4.6120
	-3	4.8956	4.9068	2.5509
	-5	---	---	---
2	-1	5.0631	5.0776	4.9766
	-2	5.0424	5.0562	4.6451
	-3	4.9288	4.9328	3.0610
	-5	2.9135	2.9217	---
3	-1	5.0635	5.0774	4.9583
	-2	5.0420	5.0560	4.6212
	-3	4.9240	4.9299	2.8493
	-5	2.6839	2.6896	---

For this simulation, it is supposed that the corresponding v_{PVref}(t) is computed over a 12 hours period starting at 7:00 am, as showed Fig. 4, with the PV current $i_{PV}(t)$ generated by the panel shown at Fig. 5.

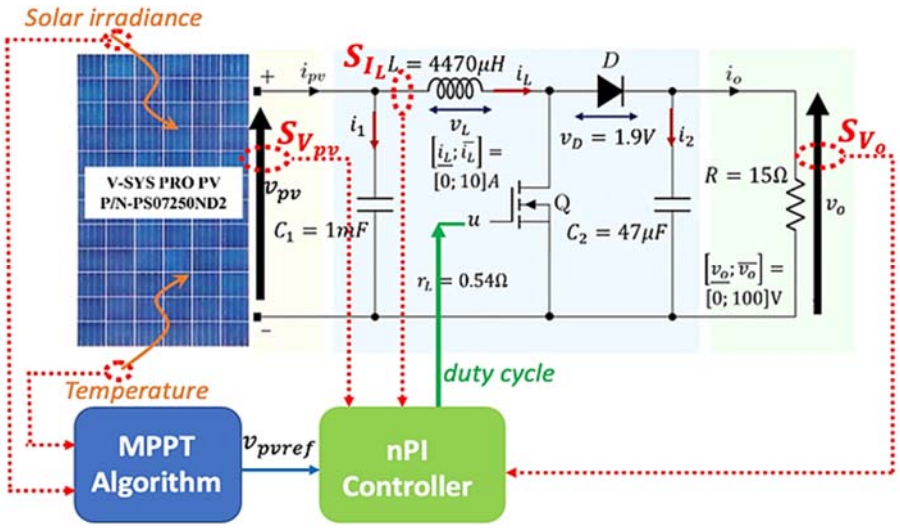


Fig. 3. Controller implementation.

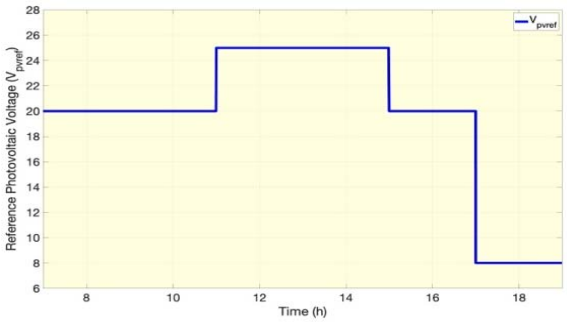


Fig. 4. Reference Photovoltaic voltage v_{PVref}(t).

The Fault-Tolerant Control technique presented in the Section 3.3 has been tested on the DC-DC boost converter of Section 3.1. Once again, three fault sensor cases are considered:

Case 1: i_L sensor fault with $L_1 = L_2 = [1 \quad 0 \quad 0]$;
Case 2: v_0 sensor fault with $L_1 = L_2 = [0 \quad 1 \quad 0]$;
Case 3:v_{pv} sensor fault with $L_1 = L_2 = [0 \quad 0 \quad 1]$.

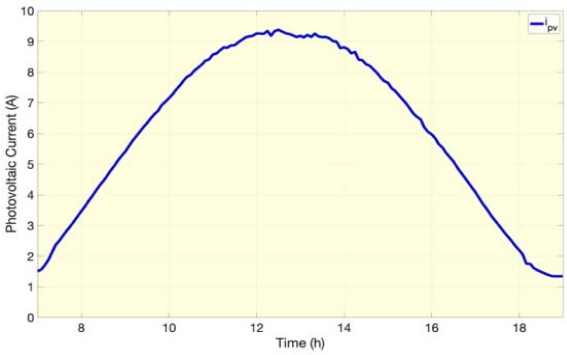


Fig. 5. Photovoltaic current $i_{PV}(t)$.

Then, the optimization problem (6) considering LMI conditions (17), (18) and (19) has been solved using the MATLAB's *mincx* function, the SCILAB's *lmisolver* function and the PYTHON's *cvxopt* function for the three fault sensor cases and for $\alpha = -1, -10 and -100$ (transient performance), $\zeta = 1$ (disturbance rejection) and $\mu_1 = \mu_2 = 1000$ (limitation of gain values). Table 3 show the robustness bound values obtained for each case, respectively for α. In order to facilitate the reading of these results, the values of the robustness bounds appearing in the table are multiplied by 100. Each robustness bound represents the fault tolerance of the remaining sensor affected, S_{I_L}, S_{v_0} or $S_{v_{PV}}$. Colored cells correspond to the highest bound.

Generally, MATLAB seems to give significantly better results for $\alpha = -1$ and $\alpha = -10$ except for case 3 where the best fault tolerance is obtained with PYTHON. It is logical to obtain less robust control laws for $\alpha = -100$, however it should be noted that SCILAB is the most efficient in this case. In order to compare the quality of these FTC control laws, we carried out a simulation with Simulink for case 3 (fault on $S_{v_{PV}}$ sensor) and $\alpha = -10$. The magnitude of the considered fault is the one corresponding to the largest robustness bound, $\rho^{*Py} = 0.00686$, obtained with PYTHON. For information, we give the gains of the controllers obtained by the three solvers and associated with the control law given in Table 4.

$$\begin{cases} u(t) = 0.5 + \delta u(t) \\ \delta u(t) = k_i e(t) + k_{p1} i_L(t) + k_{p2} v_o(t) + k_{p3} v_{PV}(t) \end{cases} \quad (20)$$

Table 3. Robustness bounds $\rho^*.10^2$.

Case	α	LANGUAGE		
		MATLAB	SCILAB	PYTHON
1	-1	1.0836	0.9971	0.9474
	-10	0.4582	0.3824	0.4113
	-100	0.720	0.1346	0.0995
2	-1	0.8935	0.8396	0.75783
	-10	0.7364	0.6713	0.7003
	-100	--	--	--
3	-1	0.4578	0.4198	0.3901
	-10	0.6348	0.5768	0.6860
	-100	0.0848	0.0490	0.0320

Table 4. Gains obtained with the three solvers.

	Gain			
SOLVER	k_i	k_{p1}	k_{p2}	k_{p3}
MATLAB	-28.3943	-0.1921	0.0136	0.1831
SCILAB	-60.5522	-3.2052	0.1301	3.0070
PYTHON	-1644.892	-5.1347	0.4208	4.3108

For simulation purposes, the fault is associated with an additive uncertainty on the output matrix, such as:

$$C(\Delta) = \mathbb{I}_3 + \begin{bmatrix} 0 \\ 0 \\ 1 \end{bmatrix} . \rho^{*Py} . sin(2.\pi.t) . [0 \quad 0 \quad 1] \quad (21)$$

Photovoltaic voltage v^*_{PV}(t) respectively obtained with MATLAB, PYTHON and SCILAB are compared with v_{PVref}(t) in Fig. 6. The three control laws are rather fault resilient but it is clear that the voltage regulation is better with the state feedback matrix K

generated by PYTHON. This is highlighted by the Fig. 7 which presents a zoom of Fig. 6. Finally, Fig. 8 shows the shape of the control inputs associated with the three previous control laws. Note that the signal generated by the controller respects $0 \leq u(t) \leq 1$.

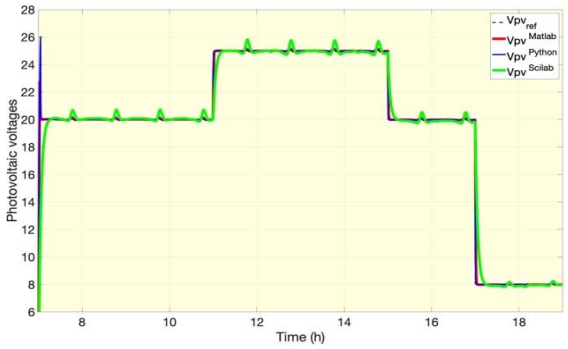


Fig. 6. Regulated photovoltaic voltages v_{PV}^{*}(t).

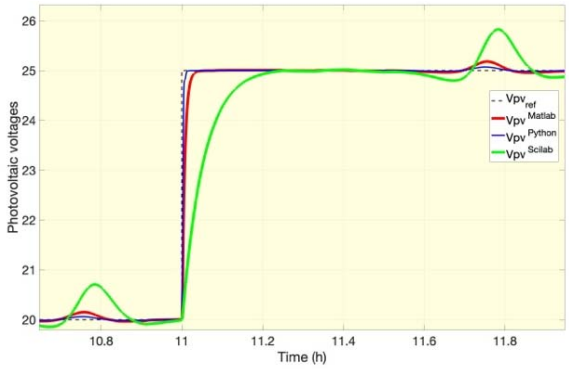


Fig. 7. Zoom of regulated photovoltaic voltages v_{PV}^{*}(t).

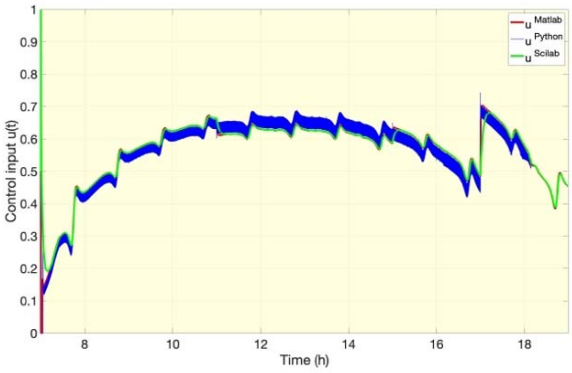


Fig. 8. Control signal $u(t)$.

5. Experimental Tests

The effectiveness of the proposed FTC control approach is approved by experimental tests on an experimental platform. This stand-alone test bench, illustrated in Fig. 9, consists of a photovoltaic chalet equipped, on its roof, with 30 photovoltaic panels with a power of 233Wc and monocrystalline technology.



Fig. 9. SMART-EnR platform: photovoltaic chalet.

The experimental setup, located inside the chalet and shown in Fig. 10 had been implemented with the following equipment:

① PV panel

② *Li-ion* batteries

③ Acquisition of solar irradiance and temperature measurements

④ MicroLabBox-dSPACE card

⑤ *DC-DC* boost converter

⑥ Two bidirectional converters built using S*EMIKRON* power modules

⑦ Voltage and current sensors

⑧ The graphical user interface on *ControlDesk* software.

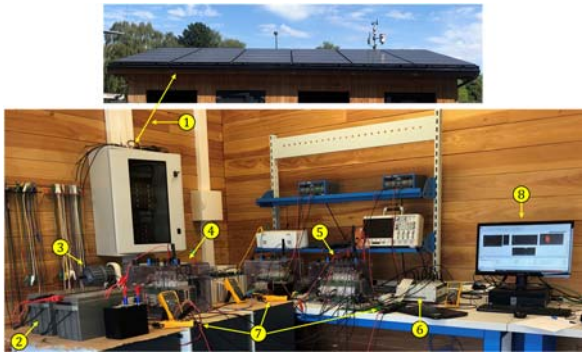


Fig. 9. Experimental test bench of *PV/battery* system.

This test was performed on April 11, 2023 at 11:17 a.m. over a period of 650 seconds. Weather conditions during this period are relatively stable with an ambient temperature of around 15 °C and solar irradiance shown in Fig. 10.

Only one of the 30 photovoltaic panels is connected to the Li-ion batteries. The DC-DC boost converter is the same as the one described section 3 and the control law implemented is the one given in (20) with the coefficients of the PYTHON solver appearing in Table 4. We simulated a fault sensor fault of the photovoltaic voltage by multiplying the value of $v_{pv}(t)$ by $(1-\rho^{*Py})$ between 11:21:46 a.m. and 11:22:26 a.m. The sensor fault period is illustrated by

the blue area in Fig. 10. This fault has the consequence of disturbing the MPPT algorithm which exploits the measurement of $v_{pv}(t)$ to generate $v_{pvref}(t)$.

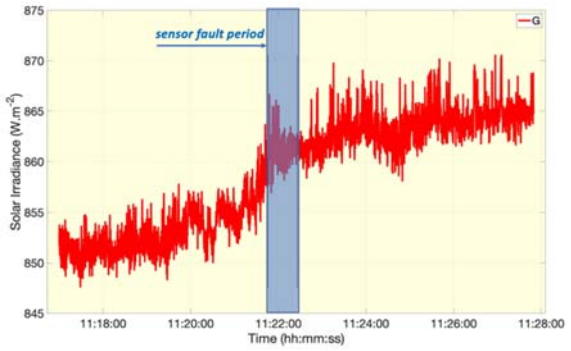


Fig. 10. Solar irradiance and sensor fault period.

Despite this sensor defect, Fig. 11 shows that the regulation of the photovoltaic voltage is excellent. This observation is definitively validated by Fig. 12 which is a zoom of Fig. 11 during the sensor fault period. It is important to remember that the performance of this reference voltage tracking is closely linked to the choice of the half-plane $\mathcal{C}^{\alpha}$. The more the half-plane is offset from the imaginary axis of the complex plane, the better the performance of the controller in terms of response time. For this experimental validation, $\alpha = -10$.

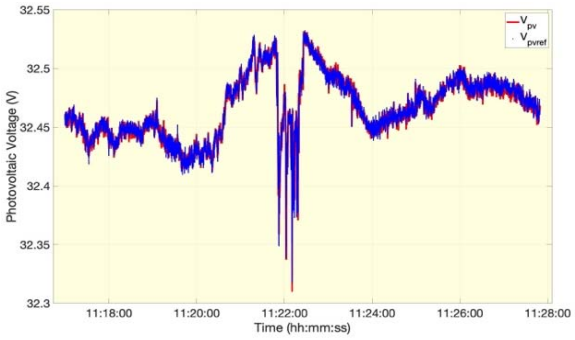


Fig. 11. Tracking of $v_{pvref}(t)$.

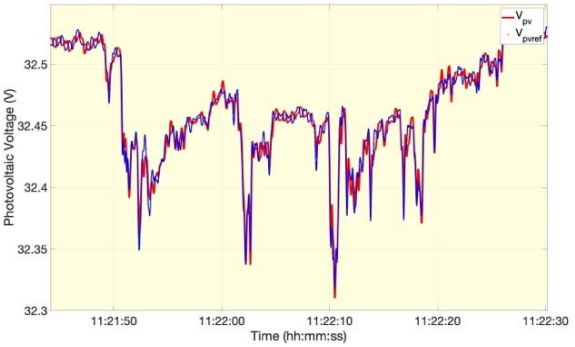


Fig. 12. Zoom of Fig. 11 during sensor fault period.

Finally, the duty cycle generated by the controller and the photovoltaic power produced by the PV panel are respectively illustrated in Fig. 13 and Fig. 14. The switching frequency of the MOSFET thyristor is 20 kHz. We can see that the value of the duty cycle is almost constant during this test despite a more significant variation around 11:22:00 when we simulated the sensor fault.

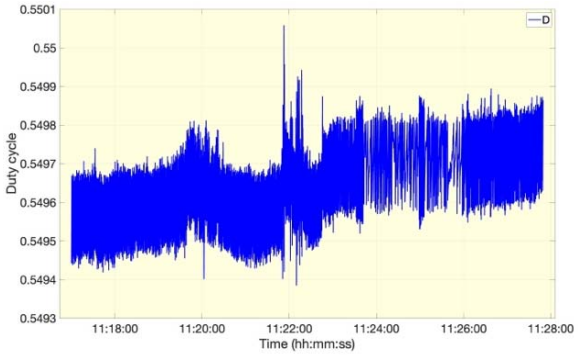


Fig. 13. Duty cycle (D).

Fig. 14 shows a slight decrease in the photovoltaic power produced by the panel during the sensor fault. This decrease is not due to a lack of performance of the controller which allows a very good tracking of $v_{pvref}(t)$ but at a bad value of this reference, computed by the MPPT algorithm and falsified by the fault.

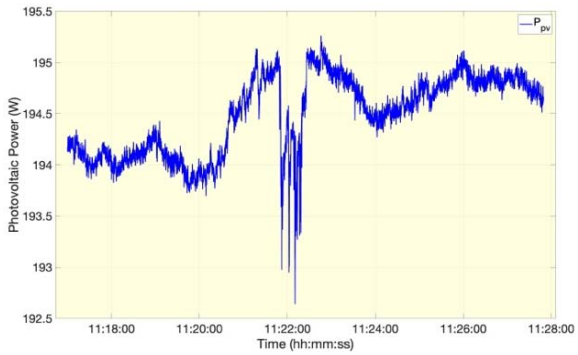


Fig. 14. Photovoltaic power (Ppv).

6. Conclusions

This paper deals with fault resilience of DC-DC boost converter sensors associated with a robustness bound generated by a state feedback control technique. The resulting problem was solved using three LMI solvers provided by different programming languages. The contribution of this study is not to the development of a new fault-tolerant control technique but rather to the robustness analysis (and therefore the fault resilience) associated with a control law,

depending on solver. The results presented in sections 4 and 5 show that the robustness of the control laws can be influenced by the solver used. However, it is not possible to conclude as to the most efficient solver because it depends on the case study. The simulation results but also the experimental tests validate the fault-tolerant control technique considered in this work. This state feedback control technique can only be effective when the fault is partial. If the fault is complete, the output feedback case should be considered and this constitutes an interesting perspective for this work.

References

[1]. C. V. Lozano and K. K. Vijayan, Literature review on Cyber Physical Systems design, *Procedia Manufacturing*, Vol. 45, 2020, pp. 295-300.

[2]. A. Baldini et al., Fault Tolerant Control for remotely operated vehicles with thruster faults using non linear disturbance observers, *IFAC PapersOnLine*, Vol. 55, Issue 31, 2022, pp. 275-280.

[3]. Y. Zhang et al., Fault Diagnosis and Fault Tolerant Control of energy maximization for wave energy converters, *IEEE Transactions on Sustainable Energy*, Vol. 13, Issue 3, 2022, pp. 1771-1778.

[4]. A. B. Masood et al., Control over blockchain for Data-Driven Fault Tolerant Control in Industry 4.0, in *Proceedings of the IEEE Mediterranean Communication and Computer Networking Conference (MedComNet)*, Pafos, Cyprus, 01-02 June 2022, pp. 131 - 139.

[5]. M. A. Ragaieg et al., A robust output feedback input constrained design for a class of LPV system, in *Proceedings of the Mediterranean Conference on Control and Automation (MED'2020)*, Saint-Raphaël, France, September 2020, pp. 284 - 291.

[6]. A. Cherifi et al., Global non-quadratic D-stabilization of Takagi-Sugeno systems with piecewise continuous membership functions, *Applied Mathematics and Computation*, Vol. 351, Issue 1, 2019, pp. 23-36.

[7]. G. Chesi, LMI conditions for time-varying uncertain systems can be non-conservative, *Automatica*, Vol. 47, Issue 3, 2011, pp. 621-624.

[8]. X. Fan et al., A fuzzy Lyapunov function method to stability analysis of fractional-order T-S fuzzy systems, *IEEE Transactions on Fuzzy Systems*,- Vol. 30, Issue 7, 2022, pp. 2769-277.

[9]. F Y. Nesterov and A. Nemirovskii, Interior-point polynomial algorithms in convex programming. *SIAM*, 1994.

[10]. J. Yuan and A. Lamperski, A random algorithm for semidefinite programming problems, in *Proceedings of the American Control Conference (ACC' 2018),* Milwaukee, USA, June 2018, pp. 1382 - 1387.

[11]. S. Sra, S. Nowozin and S. J. Wright, Optimization for machine learning, Neural Information Processing series, *The MIT Press*, September 2011.

[12]. B. O'Donoghue et al., Conic optimization via operator splitting and homogeneous self-dual embedding, *Journal of Optimization Theory and Applications*, Vol. 169, No. 3, 2016, pp. 1042-1068.

[13]. R. Nikoukhah, F. Delebecque and L. El Ghaoui, LMITOOL: a package for LMI optimization in Scilab User's guide, *Research Report RT-0170*, inria-0007000, 1995.

[14]. S. Boyd, L. El Ghaoui, E. Feron and V. Balakrishnan, Linear Matrix Inequalities in system and control theory, *SIAM*, 1994.

[15]. F. N. Lagunes et al., Impact of the programming language used to solve a LMI problem on the fault resilience of cyber-physical systems, in *Proceedings of the 3rd IFSA Winter Conference on Automation, Robotics & Communications for Industry 4.0/5.0 (ARCI' 2023),* Chamonix, France, February 2023, pp. 49-53.

Published by International Frequency Sensor Association (IFSA) Publishing, S. L., 2023 (http://www.sensorsportal.com).

Sensors & Transducers, Vol. 261, Issue 2, June 2023, pp. 55-60

www.sensorsportal.com

Sensors & Transducers

Published by IFSA Publishing, S. L., 2023
http://www.sensorsportal.com

Synergies in the Application of Industry 4.0 and Lean Manufacturing at a Product Label Manufacturer – A Discrete Event Simulation Case Study

*** Stefan HARRISON and Boppana V. CHOWDARY**
Faculty of Engineering, The University of the West Indies, St. Augustine Campus,
Trinidad, Republic of Trinidad and Tobago
E-mail: Stefan.Harrison@my.uwi.edu, Boppana.Chowdary@sta.uwi.edu

Received: 11 April 2023 Accepted: 19 May 2023 Published: 26 June 2023

Abstract: Industry 4.0 is a manufacturing philosophy and industry standard for the design of Cyber-Physical Production Systems. The aim of Industry 4.0 is the creation of a smart manufacturing system. A smart system which applies novel applications of developed and current technologies to simplify complex work and enable waste averse production. It is based on the concepts of data-driven decision support services, Horizontal and Vertical Information Technology-Operations Technology value-chain integration, decentralized control and flexible production. Lean Manufacturing is a value-to-customer-focused manufacturing philosophy which applies procedures designed to ingrain waste reduction and efficient, competency-building practices into workplace culture. The aim of this paper is to examine the synergistic benefits of these manufacturing philosophies on a local firm using Discrete Event Simulation. The key performance indicators of Flow Time, Waiting Time and Work in Process were used to determine the efficacy of the models investigated. The study results indicated a 52%, 57% and 58% improvement in the respective metrics of the best performing proposed model when com-pared to the existing system.

Keywords: Industry 4.0, Lean manufacturing, Discrete event simulation, Case study.

1. Introduction

The trend toward a modern, globalised market, has led firms from developed and developing nations to compete for increased market share. This is especially true of low-skilled industries [1] from regions such as the Caribbean. Such competition has motivated the development of innovative approaches and novel technological applications in a trend toward waste averse production with lower labour and resource costs [2]. One philosophy based on this trend of innovation is Lean Manufacturing (LM). LM focusses on a value-to-customer based approach that uses tools and techniques designed to ingrain efficiency and competency-building procedures into an organization's DNA [3, 4].

Amongst the novel technological applications developed were increasingly cost-effective CPS and ICT devices. These technologies, when combined with advances in artificial intelligence and high-volume data analytics, then made the concept of Industry 4.0 (I4.0) practicable [5]. I4.0 is the philosophy of integrating efficiency and value-creating technologies into all aspects of a product's value-chain. In essence, I4.0 uses novel applications of technology to simplify work and offer access to previously unfeasible solutions.

Current research supports the idea that LM practice can indeed augment compatible I4.0 technologies when enhancing productivity [6-8]. While mature LM practice is not a requirement for introducing basic I4.0 technological solutions, there is some evidence to

suggest a correlation between the advanced application of I4.0 technologies and a mature understanding of LM [9]. This is particularly evident when considering the stresses that enacting the digital transformation required of I4.0 places on a firm's organizational structure and workplace culture. Organisations must adopt continuous improvement and flexible thinking in order to keep pace with the new capabilities offered by I4.0. Meanwhile workers must build upon their technical skills and core competencies if they wish to take advantage of novel technologies and opportunities [10]. LM provides excellent procedural tools and approaches in both cases.

However, there exists a scarcity of academic research into the impact of the core technologies of I4.0 on LM regarding application within developing nations [6, 11]. Factors including a firm's socioeconomic environment, supply chain positioning and access to technology and training have been proposed as influences that moderate the interaction between I4.0 and LM [7, 12]. This paper therefore aims to examine the application of I4.0 and LM as improvement measures within a Trinidad manufacturing firm using a Discrete Event Simulation (DES) case study [13].

2. Case Study

2.1. System Definition

The subject of the case study was a printed label and packaging supply firm servicing the Caribbean region. The firm had identified time and quantity shortfalls in production as areas in need of improvement. A lean approach to production was sought to improve operations. Value Stream Mapping (VSM) was used to define the current state of the existing system (see Fig. 1). Based on this understanding of the existing system's current state, a DES model was formulated using Rockwell Automation's Arena® simulation software (see Fig. 2).

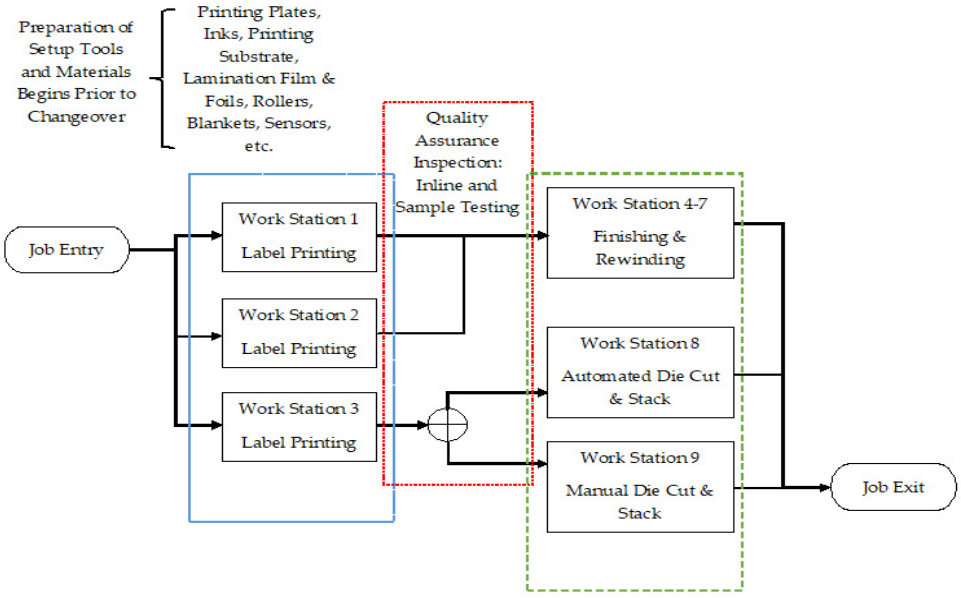


Fig. 1. Label Printing Process. A Physical Job Ticket and e-Kanban Ticket follow the Job Order from Entry to Exit.

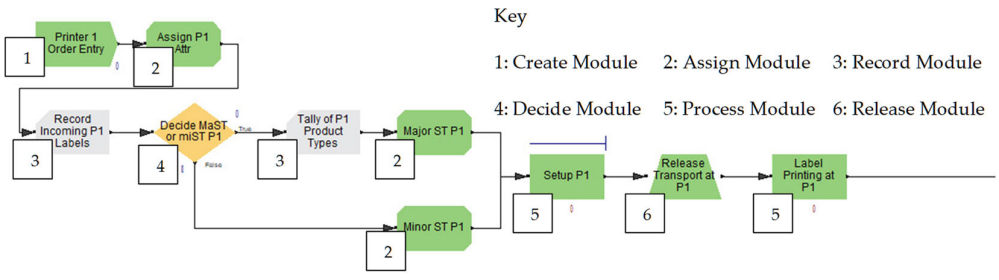


Fig. 2. Extract from Existing Model (Md0): Product Label Printing Process. Simulated Job Orders enter the system at the Create Module and are assigned user variables by the Assign Modules. Metrics are logged by the Record Modules while the job orders proceed through the system based on the logic at the Decision Module. Process Modules simulate the use of system resources while resources not used by following processes can be freed by the Release Module.

2.2. Model Formation

In addition to this model of the existing system (Md0), Arena® simulation software was also used to investigate three models (Md1, Md2, Md3) implementing proposed measures (see Table 1). The models were all configured as non-terminating simulations which reflected the current state system where, during working hours, machine tools were infrequently idle. Truncated replications were used to compensate for initiation bias. This required that a warm up period, the time needed for the operation to achieve a steady-state conditions, be determined.

Table 1. Simulation Model, Sources of Waste Addressed, LM Approach and I4.0 Approach.

Model	Source of Waste Addressed	LM Approach	I4.0 Approach
Md0	Existing Model	Existing Model	Existing Model
Md1	Over-Processing and Waiting	Simplified Processes, Reduced Required Setup Time	E-Kanban Ticket System, Automated Data Storage and Retrieval
Md2	Transport, Inventory	Increased Capacity of Material Transporters	
Md3	Over-Processing, Waiting, Transport and Inventory	Simplified Processes, Reduced Required Setup Time, Increased Capacity of Material Transporters	E-Kanban Ticket System, Automated Data Storage and Retrieval

A plot of Flow Time versus Simulation Time was generated using Arena Output Analyzer® data. Examination of this plot allowed for a conservative estimation of 30 hours as the duration of the warm up period [14]. Based on the available resources the simulation run length was set to 10 days, 16 hours a day for 150 replications. These parameters provided data output for the KPI with a precision of ± 1 hour for FT and WT, and ± 50,000 labels for WIP. The required number of replications to achieve this precision, n_e, was derived using Equation 1.

$$n_e = n_0 \frac{h_0^2}{h^2}, \quad (1)$$

where n_0, is the number of replications required to derive a precision of h_0 and h is the desired precision of the examined KPI [14]. Equations 2, 3 and 4 were random distributions used to determine the Interarrival Times (IAT) of the simulation entities representing incoming job orders at each printing work station.

$$\text{IAT \#1} = 1 + \text{LOGN}(2.72, 2.94), \quad (2)$$

$$\text{IAT \#2} = 1 + 10 * \text{BETA}(0.495, 0.636), \quad (3)$$

$$\text{IAT\# 3} = 1 + \text{EXPO}(2.31), \quad (4)$$

The Key Performance Indicators (KPI) of Flow Time (FT), Waiting Time (WT) and Work in Process (WIP) output by Md0 was compared in turn to the KPI output by the other three models, Md1, Md2, Md3, which incorporated proposed measures utilising I4.0 and LM practices. Statistical testing via SPSS was used to determine the significance of any differences observed among models at the 95 % C.I.

3. Results

The KPI for the existing and proposed models were presented in Table 2. Models Md1-3 all showed improvements to FT, WT and WIP when compared to Md0. Model Md3, when compared to Md0 improved by 52 % in FT and 57 % in WT. The models Md1 and Md3 both showed a 58 % improvement in WIP when compared to Md0.

One-way ANOVA studies were used to compare the effects of the proposed measures employed by each model (see Table 3). These studies indicated that significant differences existed at the 95% C.I. between at least two models. This result occurred with each of the examined KPI; FT, WT and WIP. The results for each KPI were, FT: ($F(3, 116) = 76.899$, $p < 0.001$); WT: ($F(3, 116) = 67.417$, $p < 0.001$); and WIP: ($F(3, 116) = 22.741$, $p < 0.001$).

Tukey HSD for multiple comparisons as presented in Table 4 outlined the mean differences among the model KPI which were significant at the 95 % C.I. For FT and WT; differences between Md1-3 and Md0, supported the finding that the proposed measures were an improvement over the existing system. In the case of WIP, models Md1 and Md3 also showed differences from Md0 that indicated a performance improvement. Among the proposed models depicted in Table 4, Md3 yielded the largest mean difference when compared to Md0 for FT, WT and WIP.

Table 2. Summary of Key Performance Indicators of Existing and Proposed Arena® Models: Flow Time (FT), Waiting Time (WT) and Work in Process (WIP).

KPI	Existing Model	Proposed Models			Precision
	Md0	**Md1**	**Md2**	**Md3**	
FT (hour)	50	27	47	24	± 1 hour
WT (hour)	42	21	39	18	± 1 hour
WIP (label)	1,200,000	500,000	1,100,000	500,000	± 50,000 labels

Table 3. One Way ANOVA studies to determine differences among the KPI of models Md0-3 ($\alpha = 0.05$). KPI: Flow Time (FT), Waiting Time (WT) and Work in Process (WIP).

KPI	Score	Sum of Squares	Degrees of Freedom	Mean Square	F-value	p-value
FT (hour)	Between Groups	6728	3	2243	76.899	< 0.001
	Within Groups	3383	116	29.17		
	Total	10112	119			
WT (hour)	Between Groups	5379	3	1793	67.417	< 0.001
	Within Groups	3085	116	26.60		
	Total	8465	119			
WIP (label)	Between Groups	1.099×10^{13}	3	3.663×10^{12}	22.741	< 0.001
	Within Groups	1.868×10^{13}	116	1.611×10^{11}		
	Total	2.967×10^{13}	119			

Table 4. Tukey Post-hoc Multiple Comparison Table. Significant Mean Differences between Models at ($\alpha = 0.05$). Key Performance Indicators (KPI): Flow Time (FT), Waiting Time (WT), Work in Process (WIP).

KPI	Model		Mean Difference	Standard Error	p-value
FT (hour)	Md0	Md1	15.92	1.39	<0.001
		Md2	3.71	1.39	0.044
		Md3	17.22	1.39	<0.001
	Md1	Md2	-12.21	1.39	<0.001
	Md2	Md3	13.51	1.39	<0.001
WT (hours)	Md0	Md1	14.25	1.33	<0.001
		Md2	3.64	1.33	0.036
		Md3	15.60	1.33	<0.001
	Md1	Md2	-10.61	1.33	<0.001
	Md2	Md3	11.96	1.33	<0.001
WIP (labels)	Md0	Md1	596,801	103,622	<0.001
		Md3	624,545	103,622	<0.001
	Md1	Md2	-585,108	103,622	<0.001
	Md2	Md3	612,852	103,622	<0.001

5. Discussion

Findings from literature have indicated that I4.0, when applied in isolation, leads to suboptimal results on productivity [7][15][16]. In contrast, a beneficial, synergistic effect has been noted when I4.0 is employed alongside other manufacturing philosophies such as LM practice [17][18][19]. In the case of LM

practice this is perhaps due the technology focused, value-creation approach of I4.0 complementing the value-to-customer focused, worker competency-building approach of LM. In essence, I4.0 offers novel technological solutions that improve productivity by simplifying complex work; while LM provides simple procedures that encourage workers to internalise and put into practice new tools and techniques with efficiency [16].

Considering these findings, the proposed measures examined were a combination of LM practices and I4.0 technologies to address the wastes observed during the VSM exercise. First, in the existing system, job orders entered as both a physical work order and a matching e-Kanban ticket provided to the workstation. As part of their work setup opera-tors were then required to compare the two sets of instructions for anomalies. This procedure added unneeded complexity to the process. In notable instances, long delays were observed when the physical job order did not match the information provided by the e-Kanban ticket.

Veteran operators often opted to overlook such discrepancies instead of pausing work to request clarification. When questioned, they noted that it was common for the physical document to fail to keep pace with changes to the production plan. As a result, when instructions were in doubt, the more dynamic e-Kanban ticket was preferentially referenced. Removing the requirement of a physical job order simplified the process which decreased the time spent on setup activities.

Second, the processes for retrieving the storage location of printing plates and logging completed job orders were automated. This addressed commonly indicated sources of wasted time during setup activities [20]. These changes were represented in Md1 and Md3 by utilizing the firm's best practice standard for setup times in the relevant processes as determined by prior time and motion studies. Finally, it was noted that time was wasted when waiting for material transporters. As a result, the capacity of the transporters within the model was increased in Md2 and Md3.

The models employing proposed measures Md1-3 were each able to improve upon the KPI of Md0 through addressing a source of waste. Model Md3 showed that the greatest KPI improvements resulted from a holistic application of I4.0 tools and LM practice [21][22]. The potential synergies between I4.0 and LM practice were also inferable from Table 1. Table 1 showed that the I4.0 applications could each be reframed in terms of a suitably compatible LM practice.

6. Conclusions

The study revealed that the greatest performance improvements resulted from a beneficial synergistic application of I4.0 and LM practice. Some of the proposed changes ap-plied existing but previously underutilised capabilities of the firm's ERP system with con-sideration for the principles of LM practice. I4.0 techniques, such as automating the process of data storage and retrieval, simplified setup requirements while causing closer integration of the firm's Printing and Production Scheduling Departments. Further process improvements were noted when these I4.0 techniques were used alongside other, simpler LM approaches. For example, reducing the waiting time for material transport by ad-dressing the need for more transporters. As a result, Md3 indicated that the KPI of FT, WT and WIP could be improved by 52%, 57% and 58% respectively. This result supports the idea that the productivity-improving I4.0 technologies are compatible with the competency-building procedures of LM practice.

References

[1]. D. Donno, and N. Rudra, David and Goliath? Small Developing Countries, Large Emerging Markets, and South-South Preferential Trade Agreements, *International Studies Quarterly*, Vol. 63, Issue 3, 2019, pp. 574-588.

[2]. J. Qin, Y. Liu, and R. Grosvenor, A Categorical Framework of Manufacturing for Industry 4.0 and Beyond, *Procedia CIRP*, Vol. 52, 2016, pp. 173-178.

[3]. K. Hozak, and E. O. Olsen, Lean habits, *International Journal of Business Excellence*, Vol. 19, Issue 3, 2019, pp. 305-322.

[4]. B. V. Chowdary, K. Ojha, and A. Alexander, Improvement of refinery maintenance and mechanical services: application of lean manufacturing principles, *International Journal of Collaborative Enterprise*, Vol. 6, Issue 1, 2018, pp. 20-36.

[5]. M. García-Garza, H. Ahuett-Garza, M. Lopez, P. Orta-Castañón, T. Kurfess, P. Urbina Coronado, D. Güemes-Castorena, S. Villa, and S. Salinas, A Case about the Upgrade of Manufacturing Equipment for Insertion into an Industry 4.0 Environment, *Sensors (Basel, Switzerland)*, Vol. 19, Issue 15, 2019, pp. 1-18.

[6]. M. Pagliosa, G. Tortorella, and J.C. Espindola Ferreira, Industry 4.0 and Lean Manufacturing: A systematic literature review and future research directions, *Journal of Manufacturing Technology Management*, Vol. 32, Issue 3, 2021, pp. 543-569.

[7]. G. L. Tortorella, R. Giglio, and D. H. van Dun, Industry 4.0 adoption as a moderator of the impact of lean production practices on operational performance improvement, *International Journal of Operations & Production Management*, Vol. 39, Issue 6/7/8, 2019, pp. 860-886.

[8]. A. Sanders, C. Elangeswaran, and J. Wulfsberg, Industry 4.0 implies lean manufacturing: Research activities in industry 4.0 function as enablers for lean manufacturing, *Journal of Industrial Engineering and Management*, Vol. 9, Issue 3, 2016, pp. 811-833.

[9]. L. R. Moura, and H. Kohl, Maturity Assessment in Industry 4.0 – A Comparative Analysis of Brazilian and German Companies, *Emerging Science Journal*, Vol. 4, Issue 5, 2020, pp. 365-375.

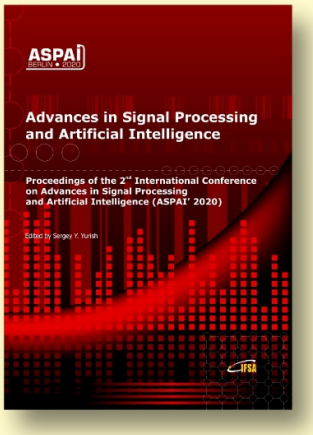
[10]. R. C. Santos, and J. L. Martinho, An Industry 4.0 maturity model proposal, *Journal of Manufacturing Technology Management*, Vol. 31, Issue 5, 2019, pp. 1023-1043.

[11]. D. Aboal, and E. Tacsir, Innovation and productivity in services and manufacturing: the role of ICT, *Industrial and Corporate Change*, Vol. 27, Issue 2, 2018, pp. 221-241.
[12]. M. Shahin, F. F. Chen, H. Bouzary, and K. Krishnaiyer, Integration of Lean practices and Industry 4.0 technologies: smart manufacturing for next-generation enterprises, *The International Journal of Advanced Manufacturing Technology*, Vol. 107, Issue 5-6, 2020, pp. 2927-2936.
[13]. S. Harrison, and B. V. Chowdary, Exploring Applications of Industry 4.0 and Lean Manufacturing Techniques within a Product Label Manufacturer: A Simulation Case Study, in *Proceedings of 3rd IFSA Winter Conference on Automation, Robotics & Communications for Industry 4.0 / 5.0 (ARCI' 2023)*, Chamonix-Mont-Blanc, France, 22-24 February 2023, pp. 88-91.
[14]. W. D. Kelton, R. P. Sadowski, and N. B. Zupick, Simulation with Arena, 6th ed., *McGraw Hill*, 2015
[15]. H. Saabye, T. B. Kristensen, B. V. Wæhrens, Real-Time Data Utilization Barriers to Improving Production Performance: An In-depth Case Study Linking Lean Management and Industry 4.0 from a Learning Organization Perspective, *Sustainability*, Vol. 12, Issue 21, 2020, pp. 1-21.
[16]. Y. Vereycken, M. Ramioul, S. Desiere, and M. Bal, Human resource practices accompanying industry 4.0 in European manufacturing industry, *Journal of Manufacturing Technology Management*, Vol. 32, Issue 5, 2021, pp. 1016-1036.
[17]. S. Buer, J. O. Strandhagen, and F. T. S. Chan, The link between Industry 4.0 and lean manufacturing: mapping current research and establishing a research agenda, *International Journal of Production Research*, Vol. 58, Issue 8, 2018, pp. 2924-2940.
[18]. S. Abdulnour, C. Baril, G. Abdulnour, and S. Gamache, Implementation of Industry 4.0 Principles and Tools: Simulation and Case Study in a Manufacturing SME, *Sustainability*, Vol. 14, Issue 10, 2022, pp. 1-20.
[19]. C. Pereira, and H. K. Sachidananda, Impact of industry 4.0 technologies on lean manufacturing and organizational performance in an organization, *International Journal on Interactive Design and Manufacturing*, Vol 16, Issue 1, 2022, pp. 25-36.
[20]. S. Harrison, J. Bansee, and B. V. Chowdary, Optimisation of Maintenance Operations Involving Three Integrated Departments at a Local Oil Company in Trinidad, *The West Indian Journal of Engineering*, Vol. 45, Issue 1, 2022, pp. 4-12.
[21]. L. Valamede, and A. Akkari, Lean 4.0: A New Holistic Approach for the Integration of Lean Manufacturing Tools and Digital Technologies, *International Journal of Mathematical, Engineering and Management Sciences*, Vol. 5, Issue 5, 2020, pp. 851-868.
[22]. D. Schmidt, J. Villalba Diez, J. Ordieres-Meré, R. Gevers, J. Schwiep, and M. Molina, Industry 4.0 Lean Shopfloor Management Characterization Using EEG Sensors and Deep Learning, *Sensors (Basel, Switzerland)*, Vol. 20, Issue 10, 2020, pp. 1-25.

Published by International Frequency Sensor Association (IFSA) Publishing, S. L., 2023 (http://www.sensorsportal.com).

Advances in Signal Processing and Artificial Intelligence

Proceedings of the 2nd ASPAI' 2020 Conference



The proceedings contains all accepted and presented papers of both: oral and poster presentations at ASPAI' 2020 conference of authors from 23 countries. The coverage includes artificial neural networks, emerging trends in machine and deep learnings, knowledge-based soft measuring systems, artificial intelligence, signal, video and image processing.

Formats: hardcover (print book) and PDF (e-book), 264 pages
ISBN: 978-84-09-21931-5, e-ISBN: 978-84-09-21930-8
IFSA Publishing, 2020

https://www.sensorsportal.com/HTML/BOOKSTORE/ASPAI_2020_Proceedings.htm

Sensors & Transducers, Vol. 261, Issue 2, June 2023, pp. 61-66

www.sensorsportal.com

Sensors & Transducers

Published by IFSA Publishing, S. L., 2023
http://www.sensorsportal.com

Digitalization of Aeronautic Painting Shop Floors for Improved Commissioning Activities

[1, *] J. H. Lugo, [2,*] A. Abassi, R. Balderas and N. Lassabe
Capgemini Engineering, Research and Innovation Department, Toulouse, France
E-mail: jesus-hiram.lugo-calles@capgemini.com, ahlam.abassi@capgemini.com

Received: 24 April 2023 Accepted: 23 June 2023 Published: 26 June 2023

Abstract: Industrial commissioning plays a critical role in ensuring the safe and efficient operation of facilities and minimizes downtime and maintenance costs over their lifetime. To extend and adjust commissioning capabilities, Virtual Commissioning uses digital models of devices and processes to verify, validate, and optimize code programming, and component selection. To perform the validation process, a simulation involving control devices and process digital twins is required, leading to inherent computational complexity. Distributed simulation approach allows for simulation of complex systems by breaking down a large simulation into smaller, manageable parts that can be run simultaneously on separate processors, while still preserving the overall behavior and interactions of the system being simulated. This paper presents a distributed Virtual Commissioning solution for a spray paint process presented in UAV painting shop floor. The methodology for developing the implementation is described in detail: greenfield scenario generation, automation process, software toolchain development, selection of communication protocols, re-use of digital twins for extended applications, and complexity analysis. A set of 3d scenarios is used to demonstrate the result's performance.

Keywords: Virtual Commissioning, Automation, Toolchain, Distributed simulation.

1. Introduction

Virtual commissioning (VC) is a method that allows the user to propose a commissioning solution using digital models of industrial systems and devices to accelerate and improve traditional processes. [1-5] The main benefits obtained from VC are:

- Early simulation, and verification and validation (V&V) of machine code by using different simulation approaches Hardware-in-the-Loop, Software-in-the-Loop, and Model-in-the-Loop (HiL, SiL, MiL) without impacting production, see Fig. 1.
- Higher quality SW with optimized controls architecture and programming;
- Faster changes implementation while maintaining quality and reducing risks;
- Shortened overall commissioning time;
- Decrease manufacturing system lead time.

VC solution methodologies have been widely studied, and standardization efforts regarding the complexity of the involved digital twin specification and V&V process used during the VC activities have been developed. [6] It is worth noting that the more specifications and realistic details are considered for developing the solution, the more accurate the representation of the system to be commissioned would be. However, the simulation of highly complex scenarios could lead to poor computer performance, hindering and sometimes, inhibiting a reliable validation process. To improve this, the VC developer could evaluate simulation complexity [7] to identify elevated consuming processes and objects in the scenario.

The aeronautic industry is characterized by its highest quality manufacturing and safety standards, leading to a constant demand of precise and accurate automated systems. This situation opens the door to

the proposal of multiple Industry 4.0 green-field scenarios where robots can collaborate with humans to improve manufacturing processes.

This article is an extension of [1] as it details the use case development and the approach used to model the system and design the architecture for the virtual environment.

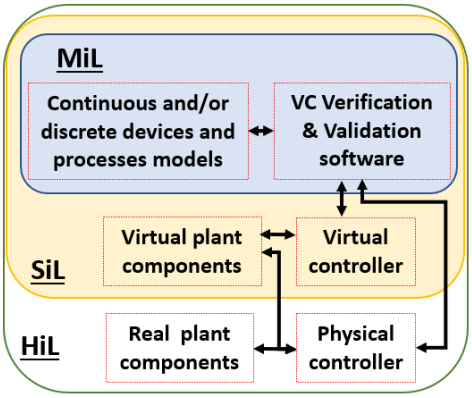


Fig. 1. Simulation approaches used for V&V purposes and their interactions. This graph demonstrates how MiL can be extended to more complex approaches like SiL and HiL.

2. Distributed Simulation Approach

Distributed simulation architectures provide better performance of industrial system representations. Several projects have successfully implemented this simulation scheme in the robotics field with different goals in mind: robot specific behaviors, either individually, as a swarm or within an organism [8]; distributed simulation system to validate the control of the real robot through the connection of GUI and digital twins [9]. It is worth noting that this approach implies issues related to the hardware specifications of each computer in terms of available memory (RAM and ROM) as well as execution time, affecting data synchronization [10], and the additional costs of using extra hardware and the energy to power it. According to the results obtained from the previous studies, the following outcomes are expected:

- Improvement of current toolchain simulation parameters (i.e., time slices, cycle times, mathematical solvers, etc.).
- Selection of alternative SW/HW tools.
- Division of complex simulation into simpler ones.
- Communication protocol parameters selection and adjustment.

3. Use case Description and Development

The use case, which is an aeronautic painting shopfloor taken from our previous work presented in [11], targets to spray paint a fairing a fairing used as a motor and propeller support of a UAV taxi, see Fig. 2. The industrial cell consists of four painting robots (equipped with smart painting nozzles), one or two smart conveyors (depends on the implementation as we will show later), and a safety system (composed of beam laser sensors), as shown in Fig. 3, and Table 1. With the development of this scenario, we try to address the need of hybrid automated environments, where robots can coexist and human workers in a safe manner; and robotize legacy industrial processes. The painting process is described as follows:

1. A fairing is placed on conveyor C1
2. C1 moves the fairing until it reaches the position sensor P1, stopping C1 and activating the spray-painting process for robots RL1 and RR1.
3. After the painting activity of RL1 and RR1 is completed, C1 moves the fairing to conveyor C2 (or remains on C1 if the cell only uses one conveyor).
4. C2 moves the fairing until it reaches the position sensor P2, stopping C2 and activating the spray-painting p After the painting activity of RL2 and RR2 is completed, C2 moves the fairing to its farthest end.
5. The safety system is always running in a parallel thread, allowing it to be activated at any time and provide an emergency stop reaction for a single device or the whole cell.

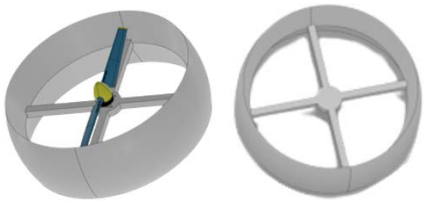


Fig. 2. Faring 3D model developed in DS CATIA. Left: propeller assembly composed of fairing, electric motor, and propeller. Right: propeller fairing before being machined.

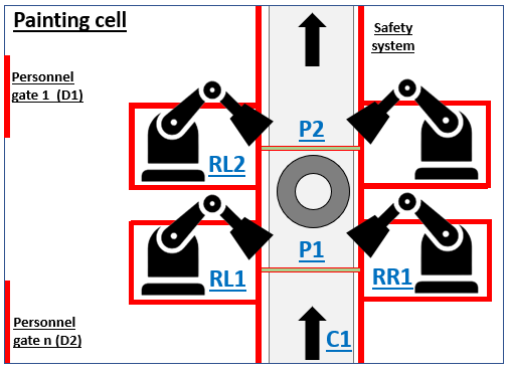


Fig. 3. Painting process schematic diagram.

To ease the modeling of the cell, we follow a Model-Based Systems Engineering approach in which, we analyze the systems from a top-down perspective, refer to Fig. 4. This method provides a practical view of the systems [12], their composing subsystems, and the communication between them, targeting reusability of the models for later projects.

Table 1. BOM for each simulation scenario.

Component	Description	DELMIA	CoppeliaSim
Industrial robotic manipulator	6 DoF spray paint robotic arm	ABB IRB 6400R/2.5-150 Quantity: 4	UR10 : Universal Robotics Arms, Quantity: 4
Paint nozzle	Customized simulated spray paint nozzle	Quantity: 4	Quantity:4
Conveyor	Customized simulated conveyor	(11m x 0.3m) Quantity: 1	(4m x 3m) Quantity: 2
Position sensors	Simulated laser beam position sensor	Quantity:2 Diameter:10 mm	Quantity:2 Diameter:10 mm
Safety sensors	Simulated laser beam safety sensor	Quantity:18	Quantity:15
Worker mannikin	Programmable dummy to represent	Quantity:1	Quantity:1
Gates	Entry levels to the cell	Quantity:4	Quantity:1

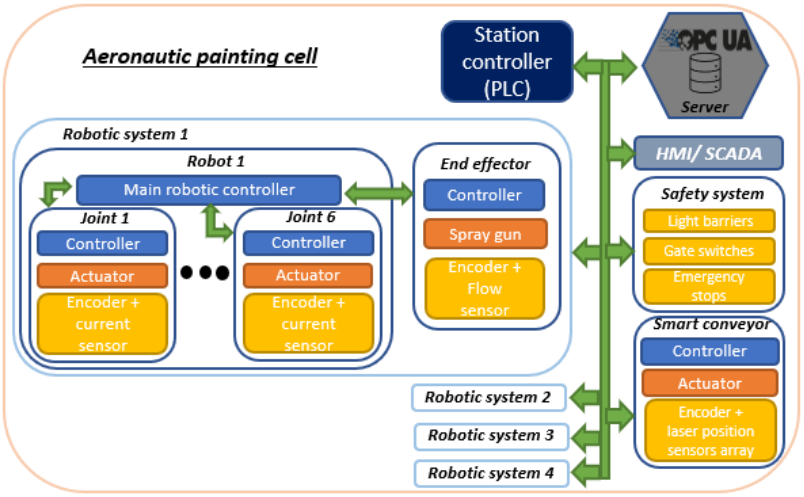


Fig. 4. Top-down view of painting cell systems. This diagram displays the elements that compose each element of the cell and how they communicate to each other.

3.1. Toolchain Design and Development

To design an efficient toolchain for VC purposes, we use the layered network shown in Fig. 5 as a template, where the different layers encompass the IT and OT according to their use and purpose. It is worth noting that the semantic layer is being represented by an OPC-UA server, which provides plenty of flexibility on the communications with the different technological levels of devices.

The scenario was developed simultaneously on two different CAM software: DELMIA and CoppeliaSim, as shown in Figs. 6 and 7. Both software are meant for similar purposes but target different applications: industrial manufacturing for the first one, and robotics programming for the second. To cope with the interoperability between our modules, we implemented an OPC-UA network, consisting of a server running on SIMIT SP, and using the client capabilities of the rest of the software to attach to it. OPC-UA supports soft real-time data exchange, event handling, and historical data access, making it a suitable choice for industrial automation, control systems, and other applications that require reliable data exchange and contain self-controlled and internal safety parameters reactions and behaviors. A PLC is used to synchronize the tasks of all smart devices and control the safety system. The PLC can share data using OPC-UA, allowing a simple data mapping between control and semantic layers.

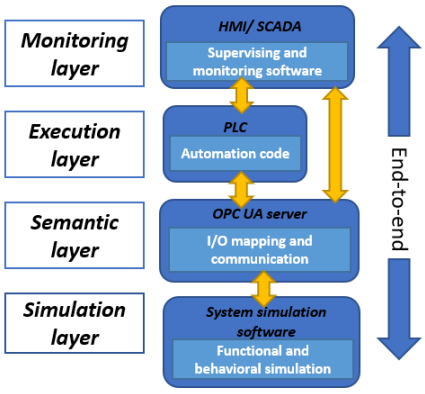


Fig. 5. Mapping and network connection between SiL layers.

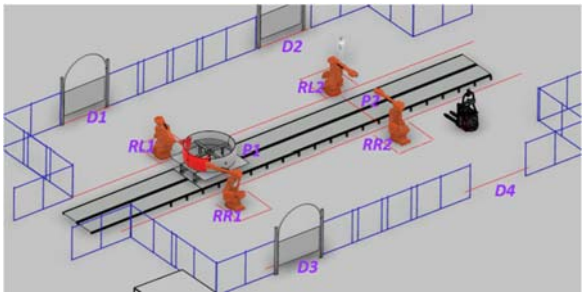


Fig. 6. Aeronautic painting cell 1 developed with Dassault Systemes tools: DELMIA 3Dexperience and ControlBuild. This cell is characterized using a single conveyor and four doors used by the shopfloor workers and forklifts.

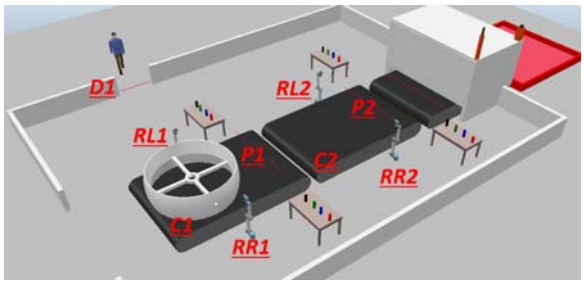


Fig. 7. Aeronautic painting cell 2 developed with CoppeliaSim EDU version and Python code. This scenario has a third conveyor that takes the painted fairing to an electric oven (white box) to accelerate the drying process.

The safety system was equally implemented on both scenarios, simple detection of position sensors (laser beams) around the robots and at the entry gates of each scenario in addition to the emergency stop button. It is worth noting that safety behaviors are programmed in every smart device to provide a fast response to events locally and send the alarm and safety signals to the cell controller for synchronization and manufacturing cell reaction.

The painting process is defined in different manner according to the CAM used: surface modification using the robot surface simulation application in the first scenario and particles projection using a simple LUA code for the second one.

Both scenarios were designed and tested individually using the toolchain shown in Fig. 8, where the digital twin of the process is connected via Control Build as a client to an OPC-UA server for the first scenario and via python in the second digital twin, working as a database, that receives and distributes information to other clients: a S7-1500 PLC (running on Siemens TIA Portal V17 and PLCSim Advanced 4.0) and a supervisory system consisting of a HMI system (Siemens WinCC) and SCADA platform (Fernhill).

To obtain better performance, we decided to divide the main system into subsystems. Thanks to OPC-UA technology, we could implement a stable industrial network between different computers allowing the interconnection of multiple simulations, see Fig. 9. The proposed toolchain consists of two workstations for the heavy computing processes and a remote PC to display system variables.

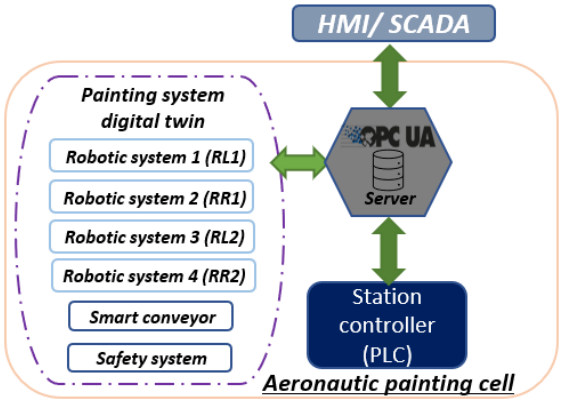


Fig. 8. Single scenario toolchain. Components of the painting system are surrounded by the purple dotted line.

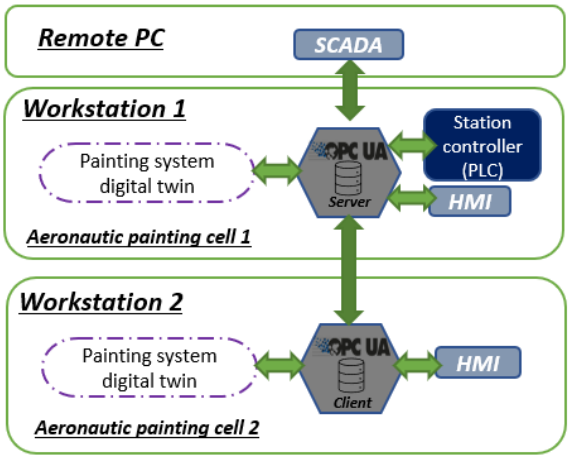


Fig. 9. Extended toolchain implemented for distributed simulation in multiple PC platforms.

3.2. Complexity Analysis

The proposed distributed approach, based on the one shown in [7], considers the modelled objects as sets of attributes and a total of 11 measures that needs to be determined for each system or toolchain. The proposed model takes several inputs into account (3D model, Programming parameters, time …). The proposed measured parameters are listed next.

- M1: the number of the modelled objects.
- M2: the number of the connections among the modelled objects.
- M3: number of attributes of all the objects (Mass, volume, gravity).
- M4: Number of manually changed attributes (more complex), like detectability.
- M5: Number of attributes that are not inherited from parent object.

- M6: Summarizing the cyclomatic complexity of all the program blocks.
- M7: Total number of lines in a program.
- M8: Required time duration
- M9: Number of running software in the toolchain
- M10: Real time estimation (create a weight parameter that effect the complexity)
    - 0: if system is not real-time
    - 1: if system soft real-time
    - 2: if system is hard real-time
- M11: Number of cycles needed to complete the simulation.

We applied this scheme to each software used in the toolchain to have a better vision of the complexity of the desired system, see Table 2.

Table 2. Complexity analysis of the extended toolchain.

ET	M1	M2	M3	M4	M5	M6	M7	M8
DELMIA	112	203	100	88	188	19	175	450
CB	0	0	0	0	0	0	33	450
CoppeliaS	135	81	236	127	363	24	1569	470
Python	0	0	0	0	0	2	192	470
SIMIT SP	98	49	0	0	0	2	0	470
PLCSim Adv	0	0	0	0	0	0	0	470
TIA PORTAL	55	13	0	0	0	2	0	470
WINCC	52	50	0	0	0	0	0	470
TOTAL	400	346	336	215	551	47	1969	470

It is noticeable that Delmia toolchain is faster than CoppeliaSim toolchain since the physics engines and the digital models programming are different, even if they share the same solution architecture. A comparison between each individual toolchain complexity is shown in Fig. 10, while Fig. 11 displays the complexity of each software used for the extended toolchain. It is worth noting that PLCSIM Advanced and SIMIT SP are the only software considered as soft real time. The simulation only requires one cycle to complete the painting tasks, taking 470 seconds in M11.

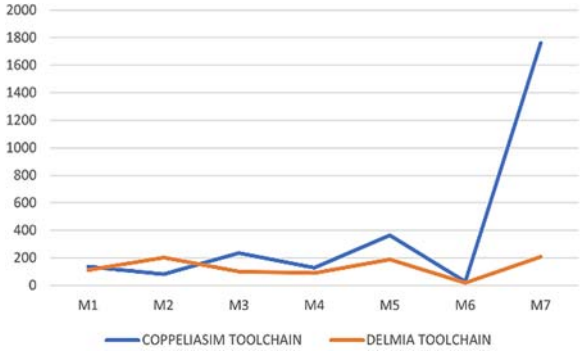


Fig. 10. Complexity comparison of individual toolchains.

4. Simulation Analysis and Results

To test the efficiency of the safety system, an operator dummy was added to both scenarios: it was programmed to behave as a human worker to verify the reduction of smart components' speed. The results were acceptable since the signals are correctly sent along all the modules: Delmia to Control Build (OPC-UA Client) directly connected to the OPC-UA server, while on the other hand, a second toolchain going from CoppeliaSim scenario to the python OPC-UA client, then, connecting to OPC-UA server, which shares the information to the PLC OPC-UA client, containing a simulated HMI for control and monitoring.

Data can also be sent in the other way, i.e., the user can send an emergency stop signal for one of the robots from the virtual HMI and see that the system in the 3d scenario fully stops. To improve simulation performance, the software toolchain was divided into three different workstations connected to a local network: one for simulation layer and OPC-UA server, another one for execution layer and HMI, and the last one for SCADA client configurator and operator interface.

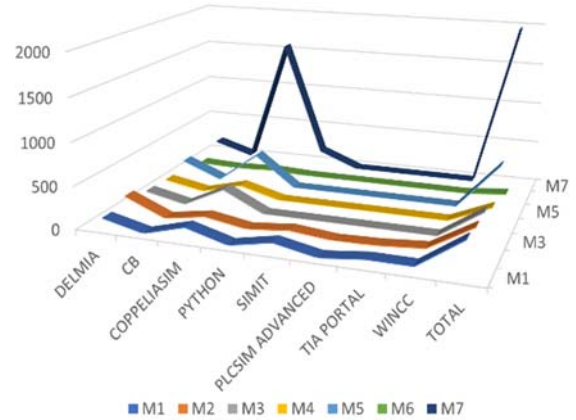


Fig. 11. Complexity analysis of the extended toolchain using the indicators from M1 to M7.

5. Conclusion

A distributed simulation approach can be applied whenever a system or process is highly complex and high computer resource consumer. For VC

applications, the distribution of scenarios on multiple computers allows the developer to achieve high performance during validation and verification of simulations, and even physically test communication protocols. Some of the advantages obtained from this approach are listed below:

1. Resource utilization. By distributing the simulation load among multiple entities, each entity only needs to focus on simulating a smaller portion of the overall system, allowing for more efficient use of available computing resources.
2. Realism. By modeling the interactions between different parts of a system in parallel.
3. Scalability and flexibility: dynamic addition or removal of simulation entities, making it possible to adapt to changing simulation requirements in real-time.
4. Improved accuracy: By breaking down the simulation into smaller parts that can be run in parallel, the overall simulation can be run faster and with greater accuracy, since the errors in each part are independent.

It is worth noting that the use of several computers increases the cost of VC solutions due to the use of extra hardware.

Another method to improve the distributed simulation approach is the use of hard real-time SW and HW, creating a fully realistic representation of the scenarios and validating HiL simulations.

Acknowledgements

This work was conducted and funded with the support of the Research Tax Credit (CIR in French). A special thanks to all the R&I Virtual Commissioning non-permanent collaborators that help us to develop the necessary tools, libraries, and models, allowing us to turn ideas into projects.

References

[1]. A. Abassi, J. Lugo-Calles, R. Balderas-Hill, and N. Lassabe, Distributed Virtual Commissioning implementation of an aeronautic shopfloor. in *Proceedings of the 3rd IFSA Winter Conference on Automation, Robotics & Communications for Industry 4.0 / 5.0 (ARCI' 2023)*, 2023, pp. 145-149.

[2]. R. Balderas Hill, J. Lugo Calles, J. Tsague, T. Master and N. Lassabe, Improving interoperability of Virtual Commissioning toolchains by using OPC-UA-based technologies, in *Proceedings of the 26th IEEE International Conference on Emerging Technologies and Factory Automation*, September 2021, pp. 1-7.

[3]. R. Balderas Hill, J. Lugo Calles, J. Tsague, T. Master and N. Lassabe, Virtual Commissioning Implementation of Side Panel Assembly Process for Automotive Shop Floor, *Sensors & Transducers Journal*, Vol. 257, Issue 3, May 2022, pp. 12-19.

[4]. J. Lugo Calles, A. Abassi, R. Balderas Hill, and N. Lassabe, Zero to hero: a generalized virtual commissioning implementation method, in *Proceedings of the Meeting for the Dissemination of Research in the Study of Complex Systems and their Applications (EDIESCA2022)*, September 2022, pp. 1-13.

[5]. J. Lugo Calles, A. Abassi, R. Balderas Hill, and N. Lassabe, Virtual Commissioning Implementation of Industrial Aeronautic Assembly Process, in *Proceedings of the Meeting for the Dissemination of Research in the Study of Complex Systems and their Applications (EDIESCA2022)*, September 2022, pp. 1-16.

[6]. Albo, Anton & Falkman, Petter, A standardization approach to Virtual Commissioning strategies in complex production environments, *Procedia Manufacturing*, 51, 2020, pp. 1251-1258.

[7]. Gergely Popovics, László Monostori, An approach to determine simulation model complexity, *Procedia CIRP*, 52, December 2016, pp. 257-261.

[8]. Lutz Winkler, Heinz Wörn, Symbricator3D – A Distributed Simulation Environment for Modular Robots, in *Proceedings of the Second International Conference on Intelligent Robotics and Applications (ICIRA 2009)*, Singapore, December 16-18, 2009, pp. 1266–1277.

[9]. Chen Peihua, Cao Qixin, Yang Bixin, Leng Chuntao, An RTM based Distributed Simulation System for Guide Robot, in *Proceedings of the 4th International Conference on Digital Manufacturing and Automation (ICDMA)*, 2013, pp. 185 – 189.

[10]. Paul Breugnot, Bénédicte Herrmann, Christophe Lang, Laurent Philippe, Data Synchronization in Distributed Simulation of Multi-Agent Systems, Advances in Practical Applications of Agents, Multi-Agent Systems, and Complex Systems Simulation, in *Proceedings of the 20th International Conference PAAMS 2022*, L'Aquila, Italy, July 13–15, 2022, pp. 50–62.

[11]. A. Abassi, J. Lugo-Calles, R. Balderas-Hill, and N. Lassabe, Virtual Commissioning Implementation of Industrial Painting Process, in *Proceedings of the 2nd International Conference on Computers and Automation (CompAuto' 2022)*, France, August 18-20, 2022, pp. 65-68.

[12]. Vitolo, F., Rega, A., Di Marino, C., Pasquariello, A., Zanella, A., Patalano, S., Mobile Robots and Cobots Integration: A Preliminary Design of a Mechatronic Interface by Using MBSE Approach, *Appl. Sci.*, 2022, 12, 419.

Published by International Frequency Sensor Association (IFSA) Publishing, S. L., 2023 (http://www.sensorsportal.com).

Sensors & Transducers, Vol. 261, Issue 2, June 2023, pp. 67-76

Sensors & Transducers

Published by IFSA Publishing, S. L., 2023
http://www.sensorsportal.com

The use of Industry 4.0 in Managing the Covid-19 Pandemic: Literature Review

*** Mephtaha GUENNOUN and Fatima BENNOUNA**
National School of Applied Sciences, Engineering, Systems and Applications Laboratory,
Fez, Morocco
Tel.: +212 660 64 44 62
E-mail: guennounmephtaha@gmail.com

Received:29 March 2023 Accepted: 5 May 2023 Published:26 June 2023

Abstract: Nowadays, most countries are going through a rapid technological change and need to think of new ideas to keep up with this pace. With the industrial sector being one of the cornerstones of any country, companies need to find ways to adapt and accelerate the digitization process "Industry 4.0". This is to continue production in the future in the face of pandemics like Covid-19. The latter has plunged the industrial sector into a serious crisis, as many factories have indeed been closed for weeks to protect the health of their employees.

This paper examines in detail, on the one hand, the results of existing research carried out on the impact of the Covid-19 crisis on industrial enterprises at the national and international levels. On the other hand, it presents the evolution of Industry 4.0, its advantages and disadvantages, and the relevant technologies of this industry. Finally, it shows the use of Industry 4.0 in the management of this crisis.

Keywords: Covid-19, Industry 4.0, Industrial revolution, Digitalization, Impact.

1. Introduction

The world is witnessing a rapid progression of digitization and networking, leading to an increase in competition among companies at both domestic and international levels. As a result, customer-specific production has become more diverse and complex, emphasizing the need for an innovative and efficient approach to production management. In response to this, the integration of the fourth industrial revolution, known as Industry 4.0, has become more prevalent in information management and production.

Industry 4.0 is based on the application of new advanced technologies such as Artificial Intelligence, Internet of Things (IoT), and additive manufacturing. These technologies have revolutionized the manufacturing sector, enabling companies to improve their operational efficiency, reduce production costs, and increase their competitive edge. Artificial Intelligence and IoT, for instance, can enhance decision-making processes, optimize supply chains, and automate production processes, while additive manufacturing allows companies to create complex and customized products quickly and efficiently.

However, the emergence of the Covid-19 pandemic in early 2020 has created a major disruption in the global economy, causing many companies to close or scale back their operations. Some businesses have sought alternative solutions to cope with the pandemic's impact, investing heavily in technology such as Industry 4.0. Moroccan businesses are among those adopting these solutions, recognizing the potential benefits of integrating advanced technologies into their operations.

The integration of Industry 4.0 technologies has become crucial for businesses to remain competitive in today's fast-paced and ever-changing business environment. The Covid-19 pandemic has further

emphasized the importance of these technologies, as companies seek to adapt to the new normal and overcome the challenges posed by the pandemic. Moroccan businesses are taking steps towards integrating Industry 4.0 technologies to improve their operational efficiency, reduce costs, and enhance their competitiveness in the global market.

2. Impact of the Covid-19 Crisis on Industrial Moroccan Companies

2.1. Globally

The Covid-19 pandemic that hit the globe in 2020 has had a real impact on all the world's economies, halting after containment/decontamination and sanitary measures were continuously implemented. The pandemic has severely impacted the financial health of companies. Some industries are experiencing unprecedented sharp declines in sales and have had to cut back on spending and borrowing to make the payments.

Of the Covid-19 pandemic on businesses and individuals, the economic fallout from the crisis continues to be felt across various sectors. According to the World Bank, a wave of bankruptcies is expected in several industries, including travel, hospitality, and entertainment, with some experts predicting that the true extent of the damage to the economy may not be fully realized until several years down the line.

The pandemic has led to a significant drop in consumer demand, with a quarter of companies worldwide seeing their turnover fall by 50 % or more. This has resulted in widespread job losses, with 11 % of companies reporting an increase in the number of registered unemployed during 2020 and having to lay off their employees. These layoffs have had a disproportionate impact on vulnerable groups, such as low-income workers and those in precarious employment, who are often the first to be let go during times of economic uncertainty.

Moreover, the pandemic has highlighted the need for businesses to adapt to changing circumstances and invest in new technologies and ways of working. Companies that were able to pivot quickly and adopt new business models, such as online ordering and delivery services, have fared better than those that were slow to adapt. However, the cost of such investments can be high, particularly for small and medium-sized enterprises (SMEs) that may not have the financial resources to weather the storm.

Here are some of the possible impacts of the coronavirus on the global economy:

- Supply chain disruption;
- Cancellation of technical and technology meeting;
- 'The need for remote interaction is increasing;
- Telemedicine/Telework;
- Use of virtual reality (VR) in business.

2.2. Nationally

Morocco, like all countries in the world, has not been able to escape the Covid-19 crisis, which has had a very serious impact on its economy and health. Faced with this situation, the Moroccan government has made great efforts to ensure that the effects of this crisis do not become too severe. Anticipated and monitored the direct and indirect impact of the Covid-19 pandemic on the economy and identified support for the most affected sectors [1].

From the onset of the pandemic, the Moroccan government implemented a number of measures to anticipate and monitor the direct and indirect impacts of Covid-19 on the economy. The government established a special committee to manage the response to the pandemic and set up a national fund to support the health sector, provide emergency financial assistance, and mitigate the economic impact of the crisis.

The current health crisis (COVID-19) has hit Morocco's economy hard and will have a huge impact in the coming years. Entire sectors are severely affected:

- Tourism sector;
- Textile department;
- Sector of the automotive industry;
- Transportation and logistics department;
- Craft department;
- Commercial sector;
- Services department.

According to a study on the impact of Covid-19 conducted by the High Commission, as of the end of April 2020, 57 % of 4,000 Moroccan companies had temporarily or permanently closed their operations (see figure 1).

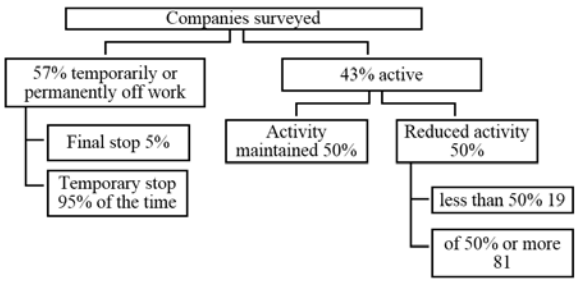


Fig. 1. Impact of covid-19: level of activity (from HCP survey).

Of the surveyed companies that were temporarily or permanently out of business, 72% were very small companies, 26% were small and medium-sized companies and 2% were large companies [2]. According to figure 2, these companies are divided into four main sectors: Services, Industry, Construction and Commerce.

The Moroccan government has also implemented a number of measures to support SMEs, including providing them with access to low-interest loans and

establishing a special fund to support the development of innovative and technology-driven SMEs.

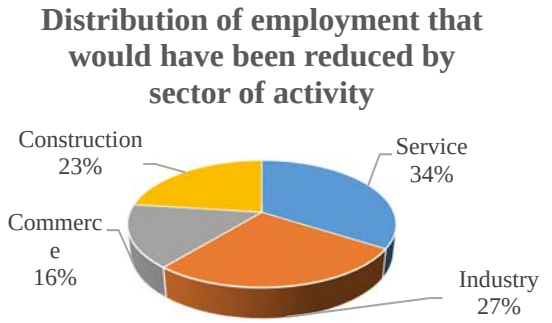


Fig. 2. Results of the High Commission's survey on the effects of covid-19 on Moroccan business activity in 2020.

In addition to the impact of Covid-19 on company operations, there are also interesting economic implications, which can be summarized in three points: [3]:

- Demand shock:
  - Partially self-imposed quarantine measures that reduced consumer spending.
  - Decline in consumer confidence as well as decline in consumption.
- Supply shock:
  - Plant closures and logical bottlenecks that reduced the supply of consumer and industrial goods.
  - Firms that reduced investment activity.
- Credit Crisis:
  - Business and consumer lending stalled.
  - Liquidity constraints that have further reduced investment and consumption (cash flow).

3. Evolution of the Industry

The industry has undergone a major revolution (see figure 3). From the original production system (Industry 1.0), which was essentially based on agriculture, we have evolved into an intelligent industrial system (Industry 4.0).

3.1. Industry 1.0 “Mechanization”

Between 1680 and 1720 there was the Agricultural Revolution and the Population Revolution which imposed the Industrial Revolution. Indeed, in 1765 James Watt harnessed coal and invented the steam engine, fundamentally changing the general organization of production. This production is agricultural in nature. This increased production capacity and forced the market to start production at various outlets [5].

This revolution allows the creation of factories that use steam engines to power equipment and increase speed for more important manufacturing. However, with the advent of these factories, society has begun to take an interest in environmental issues [6].

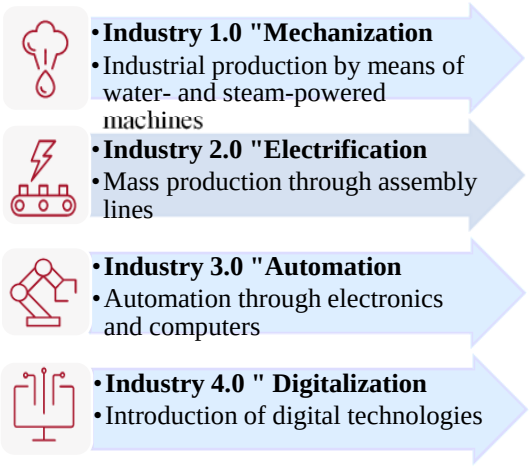


Fig. 3. The evolution of the industry over time [4].

3.2. Industry 2.0 “Electrification”

The second industrial revolution began in the early 20th century with the invention of electricity, motors and assembly lines. The main objectives of this revolution were the introduction of mass production and innovation in chemistry and related fields [7].

Henry Ford (1863-1947) conceived the idea of mass production in a Chicago slaughterhouse and invented an assembly line for the mass production of vehicles, making the machines he designed more mobile. Thanks to technology, respecting the environment becomes an obstacle as vehicles, means of transport, some devices embedded in machines and even machines consume oil.

3.3. Industry 3.0 “Automation”

Computers appeared in the late 20th century. Electronic devices have been invented and used in industrial environments since the 1970s. Vacuum tubes were replaced by transistors and electronic circuits moved to integrated circuit chips [5].

At that time, production was further advanced by the automation of mechanical machines, computers, programmable logic controllers and telecommunications.

Since the introduction of these techniques, we have been able to collect more and more data over time or retrospectively.

In the face of this revolution, the problem of environmental pollution caused by these machines and the untreated industrial waste became a very big obstacle [8].

3.4. Industry 4.0 "Digitalization"

Industry 4.0 is the final stage of the industrial development process. The term Industry 4.0 was first introduced at the 2011 Hannover Fair in Germany [9].

This latest revolution is also called the Industrial Internet of Things or Factory of the Future. This revolution aims to implement smart factories that can produce products with greener and more efficient processes.

Industry 4.0 is characterized by highly developed automation and digitalization processes and the use of electronics and information technology (IT) in manufacturing and services [10].

One of the main goals of Industry 4.0 is to connect the physical and virtual worlds through a combination of assembly lines and custom manufacturing.

The benefits of this technology include increased productivity, reduced errors and rework, and the execution of high-risk tasks [5].

4. Advantages and Disadvantages of Industry 4.0

4.1. Benefits of Industry 4.0

The benefits of Industry 4.0 can be divided into three main aspects [5]:

-Technical aspects: increased productivity and operational efficiency, simple networking and information in traditional industry, communication between machines and humans via IoT, analytics and processing.

- Logical dimensions: industry 4.0 can reduce logistics costs, optimize throughput times and deliver orders faster.

- Ecological and human aspects: The industry can reduce production waste, energy consumption, errors, and worker complaints, making it easier to perform high-risk tasks.

4.2. Obstacles to the Implementation of Industry 4.0

After analyzing the following articles: [11-14] we can synthesize a series of barriers to: High cost; Limited enterprise structure; Hacking by cyber-attacks; Mindset of the staff and adapting to new changes and Lack of skilled manpower.

5. Technologies Associated with Industry 4.0

The technologies associated with Industry 4.0 are diverse and the list continues to grow over time. According to PFEIFFER [15] and his KAHMANN [16], he has four dimensions of technology for industrial applications. However, their impact differs in terms of human-machine interaction, qualifications, work organization, and staff representation:

- Mobile and internet-based communication;
- Strengthen production network;
- New robots and production techniques;
- Wearable computing objects.

All those programs are primarily based totally on nine technological pillars (see figure 4). These improvements bridge the bodily and virtual worlds and make clever and self-sustaining structures possible.

In general, companies use most of these technologies, but the effectiveness of Industry 4.0 is only realized when they are used together.

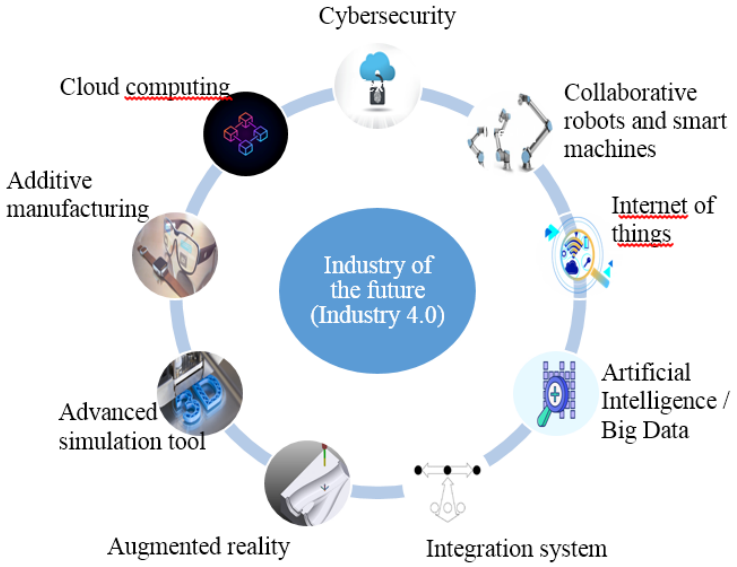


Fig. 4. The nine technological pillars of Industry 4.0 inspired by the work of the Digital Region (Auvergne-Rhône-Alpes region).

5.1. Artificial Intelligence / Big Data

Artificial intelligence is defined as the set of technologies and computer programs aimed at performing cognitive tasks traditionally and satisfactorily performed by human beings that require high-level mental processes.

In 2017 DEVILLERS defined artificial intelligence as "the set of theories of algorithms and software, which aim to simulate human cognitive abilities" [17].

Confirmed by MONNIER in 2018, artificial intelligence "refers to the simulation of human intelligence processes by machines and computer systems. These processes include learning (the acquisition of information and rules related to its use), reasoning (the use of rules to reach approximate or accurate conclusions) and self-correction." [18]

In Industry 4.0, the application of artificial intelligence resources such as neural networks, machine learning and Bayesian networks can be applied to make decisions and control production machines.

Big Data analytics applies massive data from a variety of complex sources and formats and processes it to make better decisions. Big Data helps optimize production quality, save energy, improve equipment service and accelerate the competitive advantage of companies.

The Big Data framework could be described as follows: data as a tool (solving traditional value chain problems with existing capabilities), data as an industry (new ventures and development of software systems for processing big data), and data as a strategy (building data resources by developing new innovative business models). [19]

In the context of Industry 4.0, the comprehensive collection and evaluation of data from many different sources (production equipment and systems, business and customer management, etc.) allows to support real-time decision making [20]

5.2. Internet of Things

According to ISO/IEC 30141, the Internet of Things is one of the most dynamic and exciting areas of new information and communication technologies. It involves the connection of physical entities (objects) with computer systems over large distances via networks. This interconnection is able to process information from the physical and virtual world collected by sensors, to self-configure, to make decisions independently and to influence the activities of the physical world by actuators.

One of the biggest advances in the Internet of Things is bringing the physical and information worlds together. Sensors play a very important role in bridging the gap between the physical world and the information world. Sensors collect data about their environment and generate information that provides contextual awareness. [21]

Through the use of IoT, business operations become more agile and integrated and gain a competitive advantage [19].

For IoT to work, "objects" must meet five criteria [22]:

1. They must have their own identity, e.g. through barcodes, RFID chips and serial numbers;
2. They must be able to communicate, whether by Wi-Fi, Bluetooth, or other;
3. They must have senses via sensors (thermometer, GPS, accelerometer, barometer, optical sensor, etc.);
4. They must be remotely controllable;
5. They must (or can) be self-learning.

For Industry 4.0, the Internet of Things enables the connection of a huge variety of digital and physical resources, embedded or not. The network enables decentralized decision making and real-time reaction at the system level.

5.3. Collaborative Robots and Smart Machines

In industry, robots have been used for a long time to perform complex tasks that cannot be easily solved by a human.

Lately, they are able to collaborate with each other and with humans (Collaborative Robots). These robots are autonomous, flexible and cooperative. In addition, they cost less and have a wider range of capabilities. [23]

Collaborative robots, sometimes called "cobots", are a branch of robotics, their purpose of use and use by human operators is the physical sharing of the same workspace [24]. From a technical point of view, they are designed to be isolated by grids and physical barriers in order to ensure the safety of the workers and they are equipped with sensors allowing the detection of the human presence in the shared physical environment.

Collaborative robots must not only share the same workstation as workers, but also perform tasks with them, become their assistants and remain dependent on their intentions and gestures.

In the Industry 4.0 paradigm, machines are equipped with new connected technologies to become more autonomous, flexible and collaborative. They interact with each other and can operate safely alongside humans.

5.4. Cloud Computing

According to the National Institute of Standards and Technology (NIST), "Cloud computing is a model for enabling convenient, on-demand network access to a shared pool of configurable computing resources (e.g., networks, computers, etc.) that can be rapidly provisioned and released with minimal management effort or interaction with the service provider." [25]

LeBigData.fr defines cloud computing as the storage and access of data via the Internet rather than via a local hard drive. In contrast to Big Data, cloud computing represents the infrastructure that manages and organizes the data. Big Data represents the content, that is, the data itself [22].

Cloud computing allows companies to outsource and virtualize the management and administration of their IT infrastructure and reduce their IT costs and technology investments.

Cloud software is used by companies to increase data storage capacity and facilitate communication with different stakeholders (resources, suppliers and customers) [23].

There are three models of cloud computing: software as a service (SaaS), where access depends on the customer purchasing an enterprise resource planning (ERP) system; platform as a service (PaaS), where customers are allowed to access their applications on the cloud, such as software developers; and infrastructure as a service (IPS), which provides core activities such as data storage and management. The best-known examples of cloud solutions are Google Drive, offered by Google, Microsoft's Windows Azur and IBM's BlueCloud [19].

Companies are already using cloud-based software for some enterprise and analytics applications, but with Industry 4.0, more production-related businesses will require increased data sharing across sites and corporate boundaries [20]. Even data and functionality related to production, monitoring and process control will be able to be deployed in the cloud.

5.5. Cybersecurity

Cloud computing offers many benefits to businesses, but the promise of commercial success has somewhat overshadowed the cybersecurity debate. Indeed, the exchange of industrial data and the remote control of production systems requires heightened security measures to ensure that the data that is stored and traveling over the network, is not vulnerable to cyber-attacks. Cybersecurity is the set of tools, policies, security concepts, security safeguards, guidelines, risk management approaches, actions, training, best practices, insurance, and technologies that can be used to protect the cyber environment and organizational and user assets. [26]

In the context of Industry 4.0, it is essential to create a secure and reliable communication, as well as a sophisticated management of identities and access to machines and users.

Some examples of cybersecurity solutions we can mention are: virtual private networks (VPN), antivirus and firewalls.

5.6. Additive Manufacturing

Additive Manufacturing (AM) has gained considerable momentum in recent years. The gradual shift from prototyping to direct manufacturing of functional parts is challenging traditional design and manufacturing methods based on conventional subtractive processes.

According to Afnor NF ISO/ASTM 52900 Version 2017, Additive manufacturing, also known as 3D printing, includes technologies that allow the manufacture of parts by successive layers of material from a digital model. Compared to traditional manufacturing methods for which the parts are molded to a specific format or obtained by machining or cutting a block of material, they can build parts with complex shapes.

The primary market for these technologies was the production of models and prototypes to allow better visualization of designs and to see how the designed part would interact with pre-existing parts. Because the use of these technologies reduced the time required to produce prototypes, they were often referred to as "rapid prototyping" [27]

3D printing facilitates outsourcing as well as sharing designs between designers and users. Software such as Alibre and Autodesk allow a person to design a product at home or in the office and then email the design to a client. Designs can also be shared very easily in 3D printing [28]

As part of Industry 4.0, this method allows prototypes and small batches of unique and unusually shaped custom components to be manufactured from a digital model to meet customer needs, reducing part weight, decreasing raw material costs and increasing design complexity. Additive manufacturing reduces distance, inventory and overproduction.

5.7. Advanced Simulation Tool

For years, simulation has been successfully used to solve optimization problems in the fields of production and logistics. It should be noted that a simulation is not equivalent to an optimization, because the parameters must be defined and proposed by the user and the solutions must be evaluated afterwards. [29]

Simulation is a technology that consists in simulating and testing the entire production operations, the machine settings and the flows before transposing them into the real world. It is therefore the virtual mirror of the physical world such as machines, products and humans.

In Industry 4.0, Simulations provide real-time data to replicate the physical world in a virtual model, including machines, products and humans. These simulations will help the operator make short-term adjustments by providing insight into complex systems, gathering information and knowledge without disrupting the real situation, and planning or testing, in the virtual world, the processes being run [30]. This reduces machine setup times and increases production quality.

5.8. Augmented Reality

Augmented reality (AR) is an enhanced version of reality where direct or indirect views of real-world physical environments are augmented by the overlay of computer-generated images. [31]

It is defined as the interactive technology that enables harmony between the virtual world and its users, while the virtual world is used as part of the real world. It improves human-machine interaction, remote control of maintenance tasks and visual inspection of the virtually provided human. [19]

This approach uses several techniques to achieve this fusion between the physical and computer worlds such as the integration of computing capabilities into physical objects, the projection of computer data onto physical objects, etc., using augmented reality glasses. [32]

It allows to control and avoid errors that could be observed at different stages of manufacturing, especially in product design and increases productivity.

For Industry 4.0, augmented reality can provide assembly or repair instructions based on the current situation. The implementation of selected elements from this range of alternatives can redefine, depending on the situation, how an Industry 4.0 product, process or service is monitored, controlled, optimized or even made autonomous.

5.8. Integration System

Most IT systems today are not fully integrated. Companies, suppliers and customers are rarely closely linked.

Horizontal integration is characterized by the network between individual machines, pieces of equipment and production units. In contrast to vertical integration, which allows production data to be used to make business, personnel and other decisions by enabling communication between the horizontally integrated network and other systems, such as enterprise resource planning (ERP).

Enterprise Resource Planning (ERP) systems are solutions composed of several computer modules such as: accounting, finance, manufacturing costs, engineering, human resources, invoicing, etc. They are integrated with each other and allow the management of information in a single database [22].

In Industry 4.0, horizontal integration ensures that machines and processes cooperate smoothly. Vertical integration ensures that production data is used at higher organizational levels when making marketing, personnel or other decisions. This integration creates connectivity within the supply chain, between suppliers and customers.

6. Implementation of Industry 4.0 in Moroccan Companies

The study of industrial companies in special economic zones aimed to identify the level of adoption of Industry 4.0 technologies among Moroccan companies. The study was conducted to raise awareness of the benefits of Industry 4.0 among Moroccan companies and encourage them to adopt these technologies to improve their production processes and competitiveness.

The results of SAMADI's study (see figure 5) revealed that 25% of the companies surveyed have already implemented Industry 4.0 technologies in their production processes. This indicates that some Moroccan companies have recognized the potential benefits of Industry 4.0 and have taken steps to integrate these technologies into their operations. In addition, 56.25% of the companies used a lot of less sophisticated Industry 4.0 technologies, and 12.5% of the companies used a lot of less sophisticated Industry 4.0 technologies. On the other hand, 6.25% of companies used only a little Industry 4.0 technologies.

The study also found that 75% of companies that have not yet converted their production methods to Industry 4.0 tend to approve an Industry 4.0 strategy. This is a positive sign, as it shows that the majority of companies understand the importance of Industry 4.0 and are ready to adopt it. However, 8% of companies' reject Industry 4.0, indicating a lack of understanding or resistance to change. Finally, 17% of companies surveyed are neutral.

Of the companies that have accepted an Industry 4.0 strategy, 38.89% have already started or are preparing to implement new production methods using Industry 4.0. This shows that some Moroccan companies are taking proactive steps to adopt Industry 4.0 and are making progress in implementing these technologies.

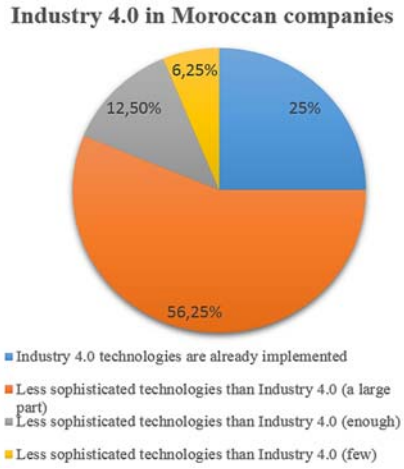


Fig. 5. Results on the implementation of Industry 4.0 in Moroccan companies [5].

7. The use of Industry 4.0 in the Management of the Covid-19 Crisis

The Covid-19 pandemic had a profound impact on businesses worldwide. With lockdowns and social distancing measures in place, many companies have had to adapt quickly to survive in this new reality. The pandemic has highlighted the importance of technology and innovation in meeting these challenges. Businesses are now looking for new and innovative ways to use technology to their advantage, and to find ways to continue operating effectively despite the constraints imposed by the pandemic.

One of the key technologies that is helping businesses to overcome these challenges is Industry 4.0. This includes a range of technologies, such as artificial intelligence, the Internet of Things, and robotics, that are transforming the way businesses operate. These technologies are helping companies to automate processes, improve efficiency, and reduce costs, even in the face of the pandemic.

Remote collaboration has also become essential for many businesses. With most employees forced to work from home due to lockdowns and social distancing, telecommuting has become an appropriate solution for businesses to continue many of their remote production methods. [4]

One of the main benefits of Industry 4.0 technologies is instant remote communication between teams. Tools such as video conferencing, instant messaging, and project management software have enabled teams to communicate effectively and work together remotely. Remote meetings have become the norm and teams can now collaborate from anywhere in the world.

Another important aspect of remote collaboration is remote management of computers and machines. With Industry 4.0 technologies, companies can remotely manage and monitor their manufacturing processes, ensuring optimal performance and reducing the need for on-site personnel. This remote management allows companies to continue their production processes while meeting social distancing guidelines.

Industry 4.0 technologies also provide organizational and project management tools. Project management software such as Trello, Asana and Jira are commonly used by remote teams to effectively manage projects. These tools allow teams to collaborate on projects, assign tasks, set deadlines and track progress in real time.

Also, managing documents that can be accessed at any time is essential for remote collaboration. Product lifecycle management (PLM) software enables companies to manage and track product development from ideation to launch. PLM software provides a single source of truth for product data, enabling teams to collaborate effectively on product development remotely.

Indeed, Industry 4.0 was able to ensure this continuity through its technology. Human-machine connectivity and connected objects based on the Internet of Things (IoT) have improved manufacturing plant automation and significantly reduced human intervention. A Gartner survey found that 47% of companies plan to increase their IoT investment due to constraints, and a McKinsey report found that IoT could boost productivity by 10% to 30%, depending on the industry. 3D printing, or additive manufacturing, has enabled companies to produce complex parts that are integral to the production chain in hours, as opposed to weeks using traditional methods (such as manufacturing respiratory organs).

Additionally, other employees are in critical positions and need to work on-site and follow World Health Organization precautions to prevent the spread of Covid-19 [4].

- Wear a mask: Wearing a mask is one of the most effective ways to prevent the spread of Covid-19 in the workplace. Masks should be worn by all employees, customers, and visitors, and should cover both the nose and mouth. Masks should be changed regularly and disposed of properly.

- Ventilate for 10 minutes and wash hands every hour: Proper ventilation is crucial in preventing the spread of Covid-19 in indoor spaces. Employers should ensure that the workplace is properly ventilated by opening windows or using air conditioning systems that circulate fresh air. Additionally, employees should wash their hands frequently with soap and water for at least 20 seconds, or use hand sanitizer if soap and water are not available.

- Observe physical distancing: Physical distancing, or maintaining at least 6 feet of distance from others, is another important way to prevent the spread of Covid-19. Employers should modify workspaces and schedules to ensure that employees can maintain physical distancing at all times.

- Test for Covid-19 if necessary: Employers should have a plan in place for testing employees who may have been exposed to Covid-19. Testing can help identify asymptomatic cases and prevent further spread of the virus in the workplace.

Certainly! Industry 4.0 refers to the fourth industrial revolution, which involves the integration of advanced technologies such as the Internet of Things (IoT), machine learning, and computer vision in manufacturing and other industries. According to studies, these technologies have been found to have a positive impact on the application of Covid-19 precautions in the workplace.

One example of how Industry 4.0 technologies can help with Covid-19 precautions is the use of IoT devices to manage personnel who are not wearing face masks or not respecting physical distancing guidelines. These devices can detect when employees are in close proximity to one another and alert them to maintain a safe distance. They can also monitor whether employees are wearing face masks and remind them to put them on if they are not.

Another example is the use of computer vision and sensors to monitor physical distancing in the workplace. Computer vision systems can detect the

presence of people in a given area and measure the distance between them. This information can be used to ensure that employees are maintaining a safe distance from one another.

Machine learning has also played a role in Covid-19 testing. For example, machine learning algorithms can be used to analyze large amounts of data from Covid-19 tests and predict which individuals are most likely to test positive. This can help to identify high-risk individuals and prioritize them for testing, which can help to prevent the spread of the virus in the workplace.

Overall, Industry 4.0 technologies have the potential to improve the effectiveness of Covid-19 precautions in the workplace. By using advanced technologies such as IoT, machine learning, and computer vision, employers can better monitor and enforce Covid-19 guidelines, and keep their employees safe and healthy.

8. Conclusion

The Covid-19 pandemic has undoubtedly had a significant impact on the global economy and has forced many companies to rethink their strategies and priorities. Before the pandemic, the goal of implementing Industry 4.0 was to enhance the competitiveness, productivity, sustainability, and innovation of companies. However, the pandemic has shifted the focus of many manufacturers towards weathering the storm and mitigating the damage caused by this unprecedented crisis.

Despite this shift in priorities, it is still crucial to consider whether Industry 4.0 is still relevant in today's world. The answer is unequivocally yes. Industry 4.0 remains as relevant as ever, and in fact, it may be even more critical now than before the pandemic. This is because Industry 4.0 technologies, such as automation, artificial intelligence, and the Internet of Things (IoT), can help companies to increase their resilience and adaptability to the rapidly changing business environment.

Moreover, Industry 4.0 technologies can also play a significant role in helping companies to overcome the pandemic's challenges. For example, automation can help companies to maintain social distancing and reduce the risk of infection in the workplace, while IoT can enable remote monitoring and control of machines and equipment. Artificial intelligence can also be used to develop predictive models for supply chain disruptions and help companies to better manage their inventory and production.

In conclusion, while the Covid-19 pandemic has undoubtedly disrupted the business world, Industry 4.0 remains as relevant as ever. In fact, it can be argued that the pandemic has highlighted the critical importance of Industry 4.0 technologies in increasing companies' resilience and adaptability to future crises.

References

[1]. S. El Amine, N. Bouayad, Moroccan companies in the area of Covid19 : Impacts, measures and recovery policies of tourism, automotive and real estate sectors, *Revue Internationale des Sciences de Gestion*, Vol. 3, 4, 2020, pp. 506-519.

[2]. S. Labrar et al., Moroccan industry in the covid-19 era: the case of the automotive sector. in Proceedings of the Congrès du réseau international de recherche sur les organisations et le développement durable: La “société entrepreneuriale” à l’épreuve de la crise sanitaire, 2021, ffhal-0340738.

[3]. I. Bakkali, et al., Etude d’impact du covid-19 sur les salariés du secteur industrie automobile au Maroc, *Revue African Scientific Journal*, Vol. 3, 11, 2022, pp. 382-392.

[4]. M. Guennoun, F. Bennouna, Industry 4.0 and the Covid-19 Pandemic: Literature Review, in *Proceedings of the 3rd IFSA winter Conference on Automation, Robotics Communications for Industrys 4.0/5.0*, 2023, pp. 175-177.

[5]. A. Samadi, H. Achelhi, Industry 4.0 in The Economic Activity Zones in Morocco: Tangier-Tetouan-Alhoceima Region Case, *International Journal of Accounting, Finance, Auditing, Management & Economics*, 2, 6-1, 2021, pp. 327-338.

[6]. W. Shin, Y. Lee, J. J. Seok, Dahlgaard, A pattern-based decision framework in the era of Industry 4.0, *Total Quality Management and Business Excellence*, 30, 3, 2019, pp. 1-24.

[7]. M. Javaid, A. Haleem, Industry 4.0 applications in medical field: A brief review, *Current Medecine Research and Practice*, 2019, pp. 102-109.

[8]. K. Tantawi, A. Sokolov, O. Tantawi, Advances in Industrial Robotics: From Industry 3.0 Automation to Industry 4.0 Collaboration, in *Proceedings of the 4th Technology Innovation Management and Engineering Science International Conference TIMES-iCON 2019*, 2019.

[9]. A. Grieco et al., An Industry 4.0 case study in fashion manufacturing, *Procedia Manufacturing*, 11, 2017, pp. 871-877.

[10]. Y. Lu, Industry 4.0: A survey on technologies, applications and open research issues, *Journal of Industrial Information Integration*, Vol. 6, June 2017, pp. 1-10.

[11]. A. Raj, G. Dwivedi, A. Sharma, A. Jabbour, & S. Rajak, Barriers to the adoption of industry 4.0 technologies in the manufacturing sector: An inter-country comparative perspective, *International Journal of Production Economics*, 2020, 224, 107546.

[12]. V. Alcacer, & V. Cruz-Machado, Scanning the industry 4.0: A literature review on technologies for manufacturing systems, *Engineering Science and Technology*, 2018, pp. 899-919.

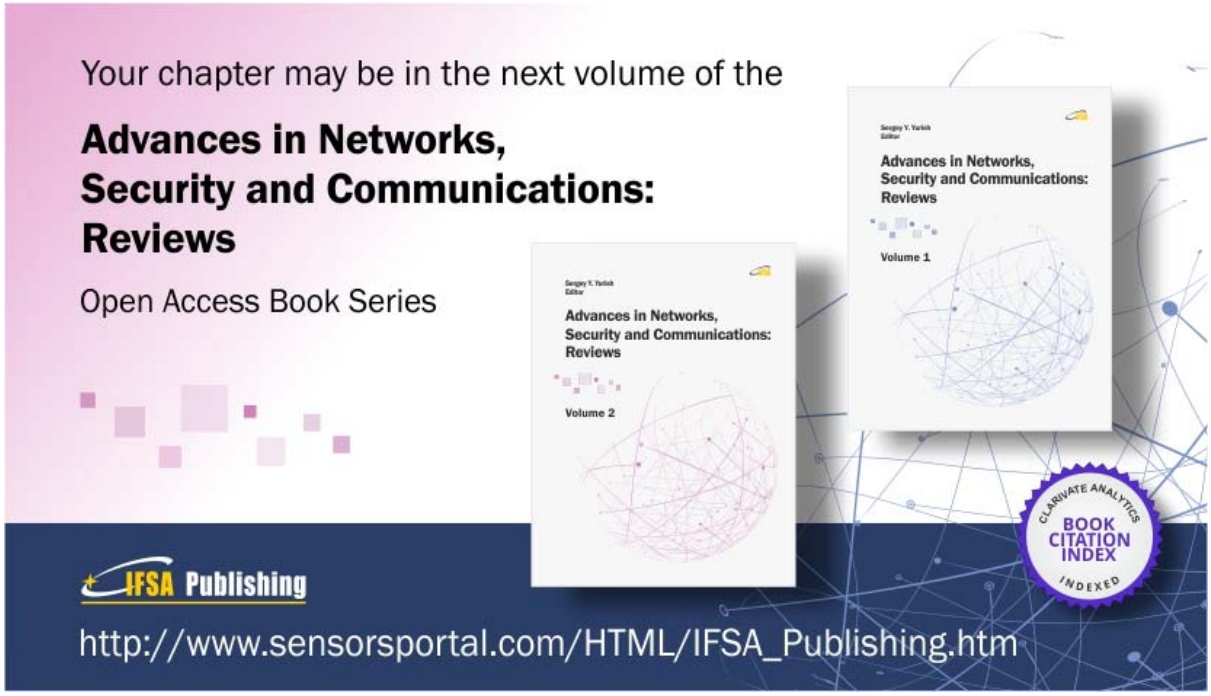
[13]. D. Kiel, C. Arnold, & K. Voigt, The infuence of the Industrial Internet of Things on business models of established manufacturing companies - A business level perspective, *Technovation*, 68, 2017, pp 4–19.

[14]. M. Mamad, Challenges and Benefits of Industry 4.0: An overview, *International Journal of Supply and Operations Management (IJSOM)*, Vol. 5, Issue 3, 2018, pp. 256-265.

[15]. S. Pfeiffer, Technisierung von Arbeit, in Böhle F., Voß G.G., Wachtler G. (eds.), Handbuch Arbeitssoziologie, 2. ed., Wiesbaden, *Springer*, 2018, pp. 321-357.

[16]. M. Kahmann, Allemagne. L'Industrie 4.0: vers la digitalisation concertée de l'industrie manufacturière ?, *Chronique Internationale de l'IRES*, Numéro 173, 2021, pp. 33-40.
[17]. L. Devillers, Of robots and men: myths, fantasies and reality, *Plon Ed*, Paris, 2017.
[18]. B. Monnier, What future for AI? *Up' magazine*, 2018.
[19]. G. Erboz. S. Istvan, How to Define Industry 4.0: The Main Pillars of Industry 4.0, *Managerial Trends in the Development of Enterprises in Globalization Era*, 2017, pp. 761-767.
[20]. M. Rubmann et al., Industry 4.0: The Future of Productivity and Growth in Manufacturing Industries, *Boston Consulting Group*, 2015.
[21]. L. Tan, N. Wang, Future Internet: The Internet of Things, in Proceedings of the 3rd International Conference on Advanced Computer Theory and Engineering, 2010, 11537787.
[22]. S. Gamache, trategies for implementing Industry 4.0 in small and medium-sized Quebec manufacturing companies, Thesis, *Université Du Québec*, 2019.
[23]. E. Asadollahi-Yazdi et al., Industry 4.0: Revolution or Evolution?, *American Journal of Operations Research*, 10, 6, 2020, pp. 241-268.
[24]. M. Bounouar et al., Ergonomics, collaborative robotics and industrial engineering: Towards a multidisciplinary design of Human-Robot systems, *55ème congrès Self*, 2021.
[25]. H. Khodkari, S. G. Maghrebi, Neccessity of the integration of Internet of Things and Clous services with quality of service assurance approach, *Bulletin de la Société Royale des Sciences de Liège*, 85, 2016, pp. 434 – 445.
[26]. R. Solms, J. Niekerk, From information security to cyber security, Computers & Security, 38, 2013, pp. 97-102.
[27]. J. Jiang, Support Structures for Additive Manufacturing: A review, *Journal of Manufacturing and Materials Processing*, 2, 4, 2018, 64.
[28]. B. Berman, 3-D printing: The new industrial revolution, *Bus. Horiz*, 2012, 55, pp. 155-162.
[29]. T. H. Uhlemann et al., The Digital Twin: Realizing the Cyber-Physical Production System for Industry 4.0. *Procedia CIRP*, 2017, 61, pp. 335-340.
[30]. S. Weyer et al., Future Modeling and Simulation of CPS-based Factories: an Example from the Automotive Industry, *IFAC-PapersOnLine*, 49, 31, 2016, pp. 97-102.
[31]. E. Oztemel, S. Gursev, Literature Review of Industry 4.0 and Related Technologies, *Journal of Intelligent Manufacturing*, 2020, 31, pp. 127-182.
[32]. M. Beaudouin-Lafon, Instrumental interaction: An interaction model for designing post-wimp user interfaces, in *Proc. CHI '00, ACM*, 2000, pp. 446-453.

Published by International Frequency Sensor Association (IFSA) Publishing, S. L., 2023 (http://www.sensorsportal.com).



Sensors & Transducers, Vol. 261, Issue 2, June 2023, pp. 77-86

Sensors & Transducers

Published by IFSA Publishing, S. L., 2023
http://www.sensorsportal.com

Multimodal Deep Learning Architecture for Hindustani Raga Classification

[1] Stella PASCHALIDOU and [2] Ioanna MILIARESI
[1] Hellenic Mediterranean University, E. Daskalaki, Rethymno, Greece
Tel.: +30 2831021918
[2] Ionian University, Plateia Tsirigoti 7, Corfu 49100, Greece
Tel.: +30 2661087860
E-mail: pashalidou@hmu.gr, imiliaresi@ionio.gr

Received: 27 May 2023 Accepted: 23 June 2023 Published: 26 June 2023

Abstract: In this paper, our key aspect is the design of a deep learning architecture for the classification of Hindustani (classical North Indian music) ragas (music modes). In an attempt to address this task, we propose a modular deep learning architecture designed to process data from two modalities, comprising audio recordings and metadata. Our bipolar classifier utilizes convolutional and feed forward neural networks and incorporates spectral information of audio data and metadata descriptors tailored to the peculiar melodic characteristics of Hindustani music. In specific, audio recordings as well as manually annotated and automatically extracted metadata were utilized for audio samples of both Hindustani improvisations and compositions available in the Saraga open dataset of Indian art music. Experiments are conducted on two Hindustani ragas, namely Yaman and Bhairavi. Results indicate that the integration of multimodal data increases the classification accuracy of the classifier in comparison to simply using audio features. Additionally, for the specific task of raga classification the use of the swaragram feature, which is customized for Hindustani music, outperforms the effectiveness of audio features that are commonly used in Eurocentric music genres.

Keywords: Hindustani raga identification, Deep learning, Convolutional neural networks, Multimodal.

1. Introduction

This work focuses on machine listening identification of ragas in Hindustani music, which is the north Indian style of classical Indian music. Tzanetakis was the one to highlight the importance in expanding data-driven research to cover non-Eurocentric music traditions too [1], aiming—among other things—at improving the current state of the art in MIR (Music Information Retrieval).

Hindustani music is a so-called oral music tradition, which means that it is based on the transmission of knowledge from teacher to student through direct imitation rather than written instructions of music notation. It relies heavily on improvisation, which is rule-based and conforms to the so-called raga system. Raga refers to a concept of melodic mode lying between scale and tune [2], and it provides a tonal framework for composition and improvisation. A mode is a collection of musical notes (the degrees of a scale) coupled with rules about how to treat them. In other words, in contrast to the way a scale is performed and perceived in Eurocentric music genres, a raga cannot be merely understood based on the set of used notes; given the same set, a different raga could be performed, the differentiation of which relies on other musical features.

For a concrete explanation of the term, following readings are suggested: [3-5]. However, defining what exactly constitutes a raga is not a straightforward task [6]. Loosely, one can say that a raga refers to a group of important features, including the scale (discrete pitches), the notes' sequence, their hierarchy, relative duration, importance, micro-tonal intonation and

ornamentation, types of melodic movement, specific phrases, mood, etc. To further perplex matters, there are other attributes that extend beyond purely musical features and contribute to the rendering of different ragas by performers—and their identification by listeners—that would ideally also need to be taken into account. These may include elements of mood and aesthetics, such as distinct mental images that adhere to specific ragas as depicted in the so-called Ragamala miniature paintings, but have not been considered in our work.

For these reasons, mode classification tasks, such as those of Hindustani ragas, fundamentally differ to those applied to scale or genre identification tasks in Eurocentric music genres. The following offers a short introduction to Hindustani music, which highlights the peculiar characteristics of the music genre and justifies the selection of extracted features in our implementation.

Hindustani music follows a movable tonic system, which means that the tonic (Do) is defined by the most comfortable pitch area of the singer; therefore, the pitches of scale-degrees (swaras) need to be computationally deduced based on the (either manually or automatically) extracted tonic frequency. The soloist is invariably accompanied by a constantly sounding drone instrument (called tanpura), which is used to create a sonic canvas as a tonal reference, from which the pitch of the tonic can be both perceived and computationally extracted. Manual annotations for the tonic frequency provided by the used corpus have been considered in this paper.

Three registers (octaves) are commonly used in performance, the low, the middle and the high. There are seven basic scale degrees, from which the first (tonic) and 5th are never altered. The 2nd, 3rd, 6th and 7th degrees can be lowered by a semitone and the 4th degree can be raised by a semitone. All degrees of a raga scale need to be computed relative to the tonic frequency. There is a great sense of pitch accuracy by Hindustani musicians. However, notes are not considered exactly fixed in pitch and—in contrast to Western styles of music—the exact position of the semitones, excluding the natural 4th, natural 5th and octave, can vary slightly according to the specific raga [3]. Another peculiar characteristic of ragas is the intricate micro-tonal embellishment (shrutis) of scale-degrees as well as the abundance of smooth melodic glides by which musicians often connect discrete notes; the space between notes is often considered more important than the discrete notes themselves [7]. It is for this reason, that pitch identification in Hindustani music is an especially challenging task [8], and a fundamental aspect that differentiates computational approaches of note extraction in Hindustani music from those used for Eurocentric music genres.

A raga can be further characterized by its overall melodic outline in terms of ascent and descent, whereby different degrees of the scale may be used or omitted in ascending versus descending order according to the raga. In most cases, the tonic and the 5th function as strong anchor points, while two notes, unique to individual ragas, gain attention and special treatment and contribute to the special mood of each raga. Pitch distribution plots of a Hindustani improvisation reflect the tonal hierarchy of a raga.

Characteristic motifs, key phrases and ornaments constitute prominent aspects of a raga, and therefore also strong cues (the 'signature') for raga identification. It is for this reason, that we take advantage of the manual annotations of raga key phrases in the used corpus, which are described as a sequence of notes. However, one needs to emphasize here that, while the problem of automatic melodic phrase detection has been attempted for Western music, Hindustani music presents additional challenges due to the conception and treatment of notes in a pitch continuum [9]. In specific, phrases and motifs cannot be simply recognized in terms of discrete note sequences, as is the case in Western styles of music, but would rather need to be considered as melodic shapes as represented by computed pitch contours [10]. For a more extensive contribution to the discussion of pertinent features and proposed computational methods of feature extraction the reader can refer to [11] and [12].

To address the complexity of raga identification, in this paper we formulate a methodology for machine listening raga classification, which is based on customized features for the specific task utilizing deep learning architectures. The current paper extends our previous work [13] by relying on an audio feature that is tailor-made for Hindustani music—called swaragram—which have been recently introduced in research literature.

Raga identification methods are expected to find application in music education, aiding the oral tradition of music training, as well as in Music Information Retrieval tasks, such as the automatic labelling of unknown audio material and hence the development of automatically annotated repositories of Hindustani music.

In this study we focus on two ragas of Hindustani music, namely Yaman and Bhairavi, with each having the tone material that is illustrated in Table 1.

Table 1. Basic information for Yaman and Bhairavi. Upper case letters denote the higher (sharper) pitch alternative, while lower case letters denote the lower pitch (flatter) alternative of the note.

Raga	Tone material	Characteristic phrases
Yaman	S R G M P D N	MDNR\DS NRGMP\RG– RGM\RMG GMDNDP
Bhairavi	S r g m P d n	Sg-mPmgmrS gmPdP mg-SrS

What follows in this paper is organized in five sections. The next section offers an overview and discussion of related work. The third section describes the data corpus where experiments were conducted, and details the proposed methodology, mostly focusing on the feature extraction stage and the network architecture. All experiments and results are reported in the fourth section, leading to the concluding part of the work.

2. Related Work

Automatic raga identification is a challenging task in music information retrieval research due to complexity and diversity of Indian music. The lack of a standardized notation system and the variability in performance by different musicians between different ragas increases the complexity of their accurate identification. However, recent studies report progress in developing architectures for automatic raga identification with the usage of machine learning and deep learning techniques. Most studies in this field focus on Carnatic (south Indian classical) music ([14-22]) and less are reported on Hindustani ([23-29]), while some papers refer to both genres ([30 -34, 8, 35-37]). There is still significant room for improvement in this field, mainly in the Hindustani genre and further research is needed to develop robust algorithms; this is where the current paper targets. Conventional classifiers have been used in Carnatic and Hindustani music for this task and have reported promising results. In [8] k-Nearest Neighborhood and Support vector machine classifiers have been used. Gaussian Mixture Model based Hidden Markov Models (HMMs), discrete HMMs and classification trees have been also utilized in [38].

Recent studies incorporate machine learning techniques and involve various neural network architectures. Convolutional neural networks are reported as well-suited architectures for raga identification tasks in ([23, 15, 24, 22]). Recurrent neural networks and Long-short-term neural networks were utilized in [14] and [26] respectively. Transfer learning aggregated methods [39] and supervised learning techniques ([40, 22]) have also reported good results.

The aforementioned architectures have been tested in conjunction with the development of effective feature extraction techniques to improve accuracy and robustness. Several features have been defined, conveying information about the identity, mood, and characteristics of a raga. Patterns of melodic phrases were utilized in [10] using vector space modeling.

Audio features conveying temporal and spectral information are considered to be the most important and provide good results. Various features extracted from audio recordings have been tested, mainly Mel-spectrogram, Mel-frequency Cepstrum Coefficients (MFCC), chromagram, modgdgram, pitch and timbre features ([32, 26, 41, 16, 34]). The specific features are aimed at Eurocentric music genres, and in a way don't successfully capture the melodic structure of Indian classical music. In a recently study [17], an alternative audio feature (swaragram) that is tailored to the distinct characteristics of Hindustani music was utilized by a residual neural network (ResNets) for raga identification tasks, and it has reported an accuracy of 79.9 % for the Carnatic and 90.4 % for the Hindustani music genre.

In this work, we define a two-class raga classification task on recordings of Hindustani music, namely Yaman and Bhairavi. The specific problem has been addressed in [25], where experiments were carried out on 341 web-extracted audio clips, 60sec-long each, for both instrumental and vocal music, 194 of which in Yaman and 147 in Bhairavi. In the proposed method conventional classifiers, K-Nearest Neighbor (KNN) and Support vector machine (SVM) classifiers were used, achieving a 92 % classification accuracy.

In our method, a deep learning architecture consisting of convolutional and fully connected networks is utilized to process data of two modalities; audio-based features and metadata. The proposed performance optimization scheme processes audio signals as an image representation of the swaragram Indian music-specific audio feature. The proposed classifier achieves a classification accuracy of 98.22%, thus outperforming the state-of-the-art score in the specific classification task.

3. Material and Method

3.1. Data Corpus

The most widely used databases of classical Indian music are the CompMusic Art Indian music dataset—and its subset, Dunya Corpora, for Music Information Research in Indian Art Music [33]—and the Saraga music research corpus of Indian Art Music [42]. Notwithstanding the mp3-quality of the Saraga music research corpus, it was preferred, as it served the scope of this paper in raising the raga classification accuracy by incorporating metadata, which was possible because it includes additional information other than audio.

A Hindustani performance involves a number of sections, which can be different according to the specific sub-genre, and may include a non-metrical melodic improvisational introduction, rhythmic improvising sections and one or more compositions. All sections of a single performance adhere to the same raga and were included in our implementation.

Hindustani music is monophonic, which means that a performance will typically entail the melodic development by a single performer or the accompaniment by another melodic instrument in unison with the soloist (e.g. by a harmonium, which will repeat or imitate phrases of the soloist's melodic line with a slight delay). It can be performed either vocally or by an instrument, and in the former case a vocalist can employ either lyrics or non-lexical

syllables. The chosen corpus includes all abovementioned cases.

In specific, the corpus comprises 107 multitrack (rarely available in Music Information Retrieval) audio recordings of 68 different ragas by 11 singers of Hindustani music. The recordings are accompanied by editorial metadata and time-aligned structural, melodic, and rhythmic (the latter not used for our purposes) annotations, which are either extracted automatically or created manually by expert listeners.

The editorial metadata includes foremost the raga name extracted from the cover-art, manual annotations by Classical Indian Music experts (such as start/end time-stamps of individual sections, section name and melodic transitions, with time-stamped melodic phrase annotations being flagged according to raga-importance as characteristic of the raga or not), and automatically extracted annotations (such as the tonic and the sequence of time-stamped pitches for the lead musician). From the multi-track recordings, the track corresponding to the lead vocalist was only used for the purposes of this work 44100 Hz sampling rate, 16 bit PCM.

For our experiments, we use a subset of the entire corpus, specifically targeting two ragas of interest, namely Yaman and Bhairavi. The subset includes all three predominant classical forms of Hindustani music, namely Dhrupad, Khayal, as well as the rather semi-classical form of Thumri. That results in an unbalanced dataset with Bhairavi being the minority class. Table 2 provides an overview of information concerning the data structure of the Saraga subset which was used for our experiments.

Table 2. Dataset description.

Saraga music research corpus of Indian Art Music 107 multitrack audio recordings of 68 different ragas by 11 singers of Hindustani vocal music	
Mp3 multi-track recordings only the track corresponding to the lead vocalist	Editorial metadata and time-aligned structural, melodic and rhythmic annotations
Training-Testing dataset Two classes	
Yaman 361 samples	Bhairavi 202 samples

3.2. Feature Extraction

At the feature extraction stage, we construct a complex input vector with audio-based features and metadata descriptors (automatically extracted as well as manually annotated in the Saraga music research corpus), which is fed into the classifier.

Given that raga identification is predominantly substantiated upon the melodic structure, as opposed to the strongly harmony-based structure of Eurocentric music genres, the information that was considered to be most relevant to the task of raga classification among all available meta-data were the c-tonic (automatic extraction), pitch values (automatic extraction) and characteristic melodic phrases (manual annotations). Metadata-drawn descriptors are part of the input vector. All numerical parameters are represented as a number and all categorical features are transformed to numerical by mapping the state "presence" to the 0 numerical value and "non presence" to 1.

To optimize our system's performance, we improve upon our previous study by exploiting the swaragram audio feature, which is tailored to the needs of classical Indian music. Mel-scale based features and swaragram have showed high robustness across datasets of various deep learning models for music genre classification tasks [35, 43] and have been favored in this paper for the raga classification task too.

In music information retrieval, the analysis of the chromagram is often selected. A chromagram is a visual representation of energies in the 12 semitones (or chromas) of the musical octave. However, chromagram lacks information about the pitch of the tonic, which is fundamental for music genres that are based on a movable tonic system. Hence, it also lacks information about the pitch class distribution (the relative pitch information of all scale-degrees in relation to the tonic), as well as the micro-tonal embellishment of scale-degrees in Hindustani music. For this reason, the swaragram (SGram), which is a shruti-based chromagram, is considered as better suited for Hindustani music and raga classification tasks [43].

To serve one of the key aspects of our research—that is the comparison on the processing of MFCC and swaragram features—we also calculate MFFC coefficients from the raw audio signal. The extraction process for Mel frequency cepstrum coefficients and the swaragram is illustrated in Fig. 1.

At the first step, all audio recordings are pre-processed. The audio file format is converted from mp3 to wav and all signals are normalized and re-sampled to 44100 Hz. The initial recordings are segmented into clips of 3 seconds. Recordings for both classes (Yaman and Bhairavi) vary heavily in duration, ranging between 1081.678 sec and 718.915 sec and as a result, 361 and 202 audio clips are produced for each class respectively.

To calculate MFCC features, all audio clips are parsed with a 40 ms long moving window with a hop size of 20 ms. A standard zero padding procedure is applied. At each frame, the Discrete Fourier Transform (DFT) is computed and it is given as input to a mel-filter-bank, with each mel-filter performing a weighted sum of the magnitude of the DFT coefficients that lie inside its frequency range. The logarithm of each filterbank output and the discrete cosine transform of the logarithms is calculated. From the set of Mel frequency cepstrum coefficients

(MFCCs), the first coefficient is discarded (as recommended in bibliography), while the following 12 MFCCs are included and the rest are discarded too.

In order to extract the swaragram, the pitch of the tonic—for each specific audio clip from the corpus—is first computed, from which all remaining scale-degree pitches are also extracted. Then, a logarithmic pooling is performed followed by a 12 note (swara) binning. In parallel, a Short-Term Fourier Transform (STFT) and the log-scale frequency Spectrogram are also calculated.

To calculate the swaragram, we follow the algorithmic implementation that is described in [44], with reference pitch set to 69, reference frequency value set to 440 Hz, sample rate set to 22050 Hz and with the number of fft points set to 2048. This results in a 2-D one channel image representation of the audio sample with dimensions [198, 130, 1]. Two representative images of swaragrams for Yaman (a,b) and Bhairavi (c,d) respectively are displayed in contrast in the following images of Fig. 2.

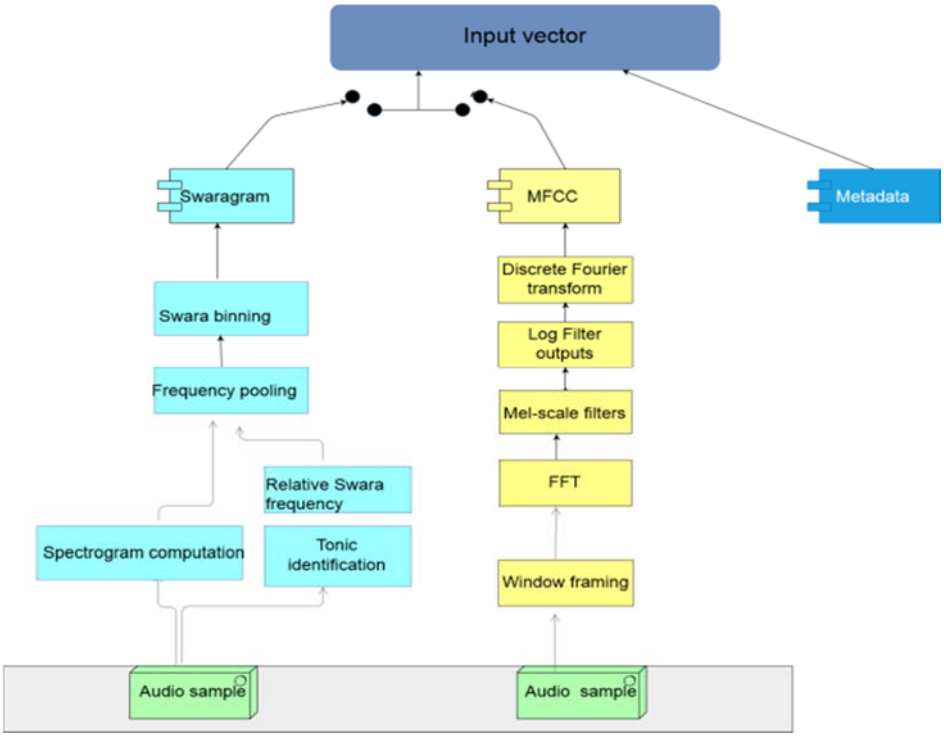


Fig.1. Illustration of the input feature vector composition with swaragram or MFCC feature extraction process.

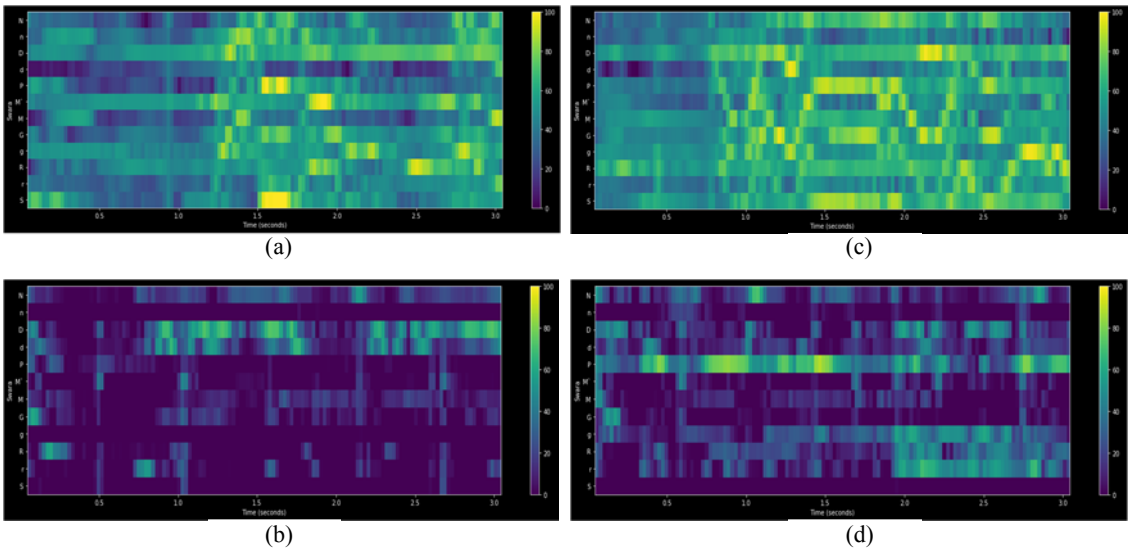


Fig. 2. Illustration of swaragram images for melodic movements in raga Yaman and Bhairavi.

3.3. Network Architecture

The proposed classifier is a deep neural network architecture designed to address the problem of raga identification. The architecture is based on the idea of multimodal learning, which allows the network to learn with reference to two modalities, rather than processing audio signal only. This is achieved by adding two separate branches that process audio and metadata.

As displayed in Fig. 3, the overall system architecture consists of three modules. The basic building blocks are convolutional and fully connected sub-networks. A convolutional (CNN) neural sub-network processes swaragrams, a fully connected (FCN) neural sub-network processes metadata, and a final fully connected sub-network merges information and yields the final classification decision.

The structure of the CNN sub-network involves a series of convolutional layers with different filter sizes and numbers of filters, followed by batch normalization and activation functions. At the end, a max pooling layer is added to reduce the spatial dimension of the feature maps of the last four subsequently convolutional layers, where rectified linear unit is used as an activation function. The initial convolutional layer consists of 64 filters of size 3x3 and stride 2, followed by a batch normalization layer. Subsequently, three convolutional layers follow with 64, 32 and 32 filters of size 3x3, 5x5, 5x5 respectively and stride size 2. Each convolutional layer is followed by a batch normalization layer, which is used to normalize the contributions to each convolutional layer for every mini-batch. At the end, a max-pooling layer with a pool shape of 2x2 is used to average the size of the feature maps. The output of the final layer is flattened into a 1D vector and passed through the final fully connected layer to produce the final prediction.

The second sub-network processes information from metadata utilizing two sequentially fully connected layers with 16 and 12 nodes each.

The embeddings produced by the modules are fed to a final fully connected layer of 1024 nodes and are followed by a two output softmax layer in order for the classification decision to be drawn. Table 3 summarizes the dimensions of the architecture and displays the output of each layer when swaragram is processed.

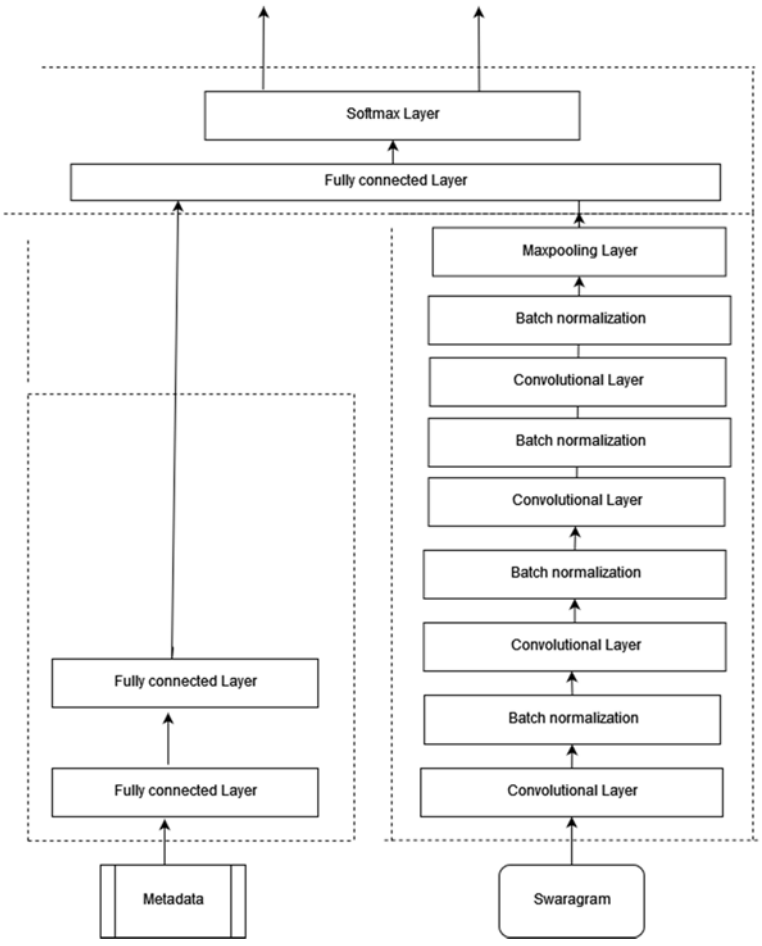


Fig. 3. Block diagram of the overall network architecture consisting of three sub-networks. A convolutional branch that processes audio features, a feed forward branch for metadata descriptors and a final feed forward stage that yields the classification decision.

Table 3. Network dimensionality.

Layer	Number of Filters	Kernel size	Stride	Output
Input	-	-	-	[198, 130, 1]
Conv2D	64	3×3	1×1	[198, 130, 64]
Batch_normalization	-	-	-	[198, 130, 64]
Conv2D	64	3×3	1×1	[198, 130, 64]
Batch_normalization	-	-	-	[198, 130, 64]
Conv2D	32	5×5	1×1	[198, 130, 32]
Batch_normalization	-	-	-	[198, 130, 32]
Conv2D	32	5×5	1×1	[198, 130, 32]
Batch_normalization	-	-	-	[198, 130, 32]
MaxPooling2D	-	-	-	[99, 65, 32]
Dense1	-	-		16
Dense2	-	-		12
Dense3	-	-	-	1024

4. Experiments and Results

4.1. Ablation Study

The ablation study of the proposed architecture involved several key components on model architecture and training procedure, with systematic experimentations on the role of sub-networks, the number of layers, the trade-off between depth and performance and any other design choices. In addition, ablation experiments were conducted on the effect of the dimensionality of the feature maps, the stride and zero padding values.

To support the training and testing of the network, backpropagation method was applied. To fine tune the model and define the model hyperparameters, training was performed for 300 epochs with the Adam gradient descent algorithm and a learning rate of 0.0001. Categorical cross entropy loss was optimized towards validation accuracy. To prevent network overfitting, we applied an early-stopping criterion of 10 epochs and dropout regularization, with a dropout value set to 0.2 for the fully connected layers and 0.4 for the convolutional layers. The network was evaluated using a 5-fold cross-validation scheme. The training-testing subsets of the entire dataset are defined by 90 % -10 % splitting percentages.

Training is performed on the subset of the Saraga dataset described in subsection 3.1, which is an unbalanced dataset. Training with an unbalanced dataset is challenging, as it can lead to poor performance of the model on the minority class. To address the class imbalance problem, the minority class was oversampled by replicating its audio samples with the usage of the random oversampling algorithm.

Experiments were designed to thoroughly evaluate the performance of the architecture and compare it with the state-of-the-art model. We conducted extensive experiments with different variations of the architecture, for three alternative system setups. The experimental setups were designed to serve the main directions of our study; in specific, the comparison of MFCC coefficients versus the swaragram audio feature, as well as the comparison between the combined used of audio features and metadata versus using only audio-extracted features. To evaluate the contribution of each modality on the classification task, we experimented with bimodal and unimodal models. A unimodal classifier, where the CNN sub-network processes image representations of the audio signal, compares the performance of MFCC and swaragrams. The overall model configuration, where all sub-networks are present, evaluates whether the integration of metadata descriptors can improve the classification accuracy and generalization capability.

Our previous work [13] reported that information obtained from Mel frequency Cepstrum coefficients analysis effectively serves Hindustani raga discrimination tasks. Their performance is now compared with swaragram audio representations, and we rely on the single CNN network configuration to figure out which feature set is more effective for raga identification. The bimodal configurations experiment on the relative emphases to be placed on the two modalities.

4.2. Experimental Results

Overall, the experimental results of all model variations demonstrate that the bipolar architecture is highly effective for raga identification tasks and achieves state-of-the-art performance on the specific task.

To gain insight on the modalities and features impact we study the results presented in Table 4. All results, reported in the table, are expressed in terms of testing accuracy, in order to compare with the best reported result in the specified task. When a unimodal classifier, where MFCCs feature vectors are processed is used, classification accuracy for all five folds in terms of % scores [94.44, 96.29, 88.88, 96.29, 95.37], with an average value of 94.25. The unimodal classifier, where swaragrams are processed, reports a higher classification accuracy of 96.24, [96.45, 96.27, 95.72, 96.41, 96.36], which is a significant improvement over the previous performance.

Table 4. Experimental results in terms of accuracy for all folds.

Classifier	Input vector	Accuracy (%)	Average (%)
Unimodal	MFCC	[94.44, 96.29, 88.88, 96.29, 95.37]	994.25
Unimodal	Swaragram	[96.45, 96.27, 95.72, 96.41, 96.36]	996.24
Bimodal	MFCC + metadata	[97.14, 98.07, 99.19, 97.31, 95.37]	997.41
Bimodal	Swaragram + metadata	[97.74, 98.27, 99.38, 97.36, 98.48]	998.22

The classification accuracy values (%) for the bimodal classifier when MFCC coefficients are processed raises at [97.14, 98.07, 99.19, 97.31, 95.37] with an average score of 97.41. A combination of the swaragram feature and metadata, further increases the performance up to 98.22 (%), [97.74, 98.27, 99.38, 97.36, 98.48].

Experimental evaluation shows that fusion of audio features and metadata achieve the best classification performance. The classification accuracy results clarify the statement that representing Indian music with swaragrams, offers more information to a deep learning architecture for raga identification. The proposed method consistently outperforms the existing method of the reference paper [25], by 6.22% units, even though results are reported on a smaller dataset.

Hence, we further investigation should be made to the limitations that poor network interpretability imply, since it hinders the robustness evaluation of each network layer, as well as the models adaptability and transferability to alternative tasks on different data collections.

5. Conclusions

This work challenges machine driven raga identification with the application of a deep learning architectures. Our architecture utilizes convolutional and fully connected neural networks, for the classification task of two Hindustani ragas, namely Yaman and Bhairavi. The research focuses on more sophisticated audio features that are better suited to Hinstuani music rather than generic audio features typically used in Eurocentric types of music. Our experimental results reported that the swaragram audio feature can serve as a 2-D image representation of the audio signal, which—processed by a convolutional network—achieves high classification accuracy for Hindustani ragas. The classification capability of such an architecture increases with the integration of metadata, providing evidence that fusion of data from multiple modalities into deep learning architectures increases the accuracy of machine listening techniques in raga identification tasks. It has been shown, that integration of swaragram representations of the audio signals and metadata has increased the ability of discriminating between Yaman and Bairavi ragas of Hindustani music, achieving a classification accuracy of 98.22%.

The classification capability of the proposed methodology should be further tested on several Indian datasets, with collections of various artists and types of instruments. We plan to expand the classifiers' performance on extended multiclass classification tasks, with the inclusion of different raga classes, on both Carnatic and Hindustani genres. Integration of more modalities, where face expressions, motion or emotional situation of the musician can be assessed, expresses the main direction of our future research, where the final scope is the formulation of a robust, multiclass classifier for raga identification.

References

[1]. G. Tzanetakis, Computational ethnomusicology: a music information retrieval perspective, in *Proceedings of the Joint International Computer Music Conference / Sound and Music Computing Conference (ICMC/SMC)*, Athens, Greece, 14-20 September 2014, pp. 112–117.

[2]. R. Powers and S. India, The New Grove Dicitionary of Music and Musicians, *Macmillan*, London, 2001.

[3]. J. Bor, S. Rao, W. Van Der Meer, and J. Harvey, The raga guide: a survey of 74 hindustani ragas, *Nimbus Records with Rotterdam Conservatory of Music*, 1999.

[4]. R. Widdess, The rāgas of early Indian music: Modes, melodies, and musical notations from the Gupta period to c. 1250, *Clarendon Press*, Oxford, 1995.

[5]. Melody, *Music in Motion*, 17-May-2013. [Online]. Available [Accessed: 23-Feb-2023]: https://autrimncpa.wordpress.com/melodic-concepts/.

[6]. W. Kaufmann, The Ragas of North India. Bloomington: Asian Studies Research Institute, International Affairs Center, 1968.

[7]. W. Van Der Meer and S. Rao, What you hear isn't what you see: The representation and cognition of fast movements in Hindustani music, in *Proceedings of the International Symposium Frontiers of Research on Speech and Music*, Baripada, India, 11-12 November 2006, pp. 12–20.

[8]. A. Bhat, K. G. Krishnan, V. Mahesh, and V. K. Ananthapadmanabha, Deep learning approach to joint identification of instrument pitch and raga for Indian classical music, in Advances in Speech and Music Technology, *Springer International Publishing*, Cham, 2023, pp. 159–174.

[9]. J. C. Ross and P. Rao, Detection of raga-characteristic phrases from Hindustani classical music audio, in *Proceedings of the 2nd CompMusic Workshop*, Istanbul, Turkey, 12-13 July 2012, pp. 133–138.

[10]. S. Gulati, J. Serrà, V. Ishwar, S. Sentürk, and X. Serra, Phrase-based r¯Aga recognition using vector space modeling, in *Proceedings of the IEEE International Conference on Acoustics, Speech and Signal*

Processing (ICASSP), Shanghai, China, 20-25 March 2016, pp. 66–70.

[11]. Y. Singh and A. Biswas, Computational approaches for Indian classical music: A comprehensive review, in Advances in Speech and Music Technology, *Springer International Publishing*, Cham, 2023, pp. 91–118.

[12]. A. K. Datta, S. S. Solanki, R. Sengupta, S. Chakraborty, K. Mahto, and A. Patranabis, *Signal analysis of Hindustani classical music*. Singapore: Springer, 2017.

[13]. I. Miliaresi and S. Paschalidou, A deep learning architecture for automatic raga identification, in *Proceedings of the 4rd International Conference on Advances in Signal Processing and Artificial Intelligence (ASPAI' 2022)*, Corfu, Greece, 19-21 October 2022, pp. 39-42.

[14]. S. Madhusudhan and G. Chowdhary, Deepsrgm - sequence classification and ranking in Indian classical music via deep learning, in *Proceedings of Music Information Retrieval Conference (ISMIR)*, Delft, Netherlands, 4-8 November 2019, pp. 533-540.

[15]. A. Anand, Raga identification using convolutional neural network, in *Proceedings of the Second International Conference on Advanced Computational and Communication Paradigms (ICACCP' 2019)*, Majitar, India, 25-28 February 2019, pp. 1-6.

[16]. P. Kavitha, J. Charles, and L. S. Lekamge, A deep learning based approach for Janya raga classification in carnatic music, in *Proceedings of the 6th SLAAI International Conference on Artificial Intelligence (SLAAI-ICAI' 2022)*, Kelaniya, Colombo, Sri Lanka, 1-2 December 2022, pp. 1-6.

[17]. R. Sridhar and T. Geetha, Raga Identification of Carnatic music for Music Information Retrieval, *International Journal of Recent Trends in Engineering*, Vol. 1, Issue 1, 2009, pp. 571–574.

[18]. S. Samsekai Manjabhat, S. G. Koolagudi, K. S. Rao, and P. B. Ramteke, Raga and tonic identification in carnatic music, *J. New Music Res.*, Vol. 46, Issue 3, 2017, pp. 229–245.

[19]. A. Bhat, A. V. Krishna, and S. Acharya, Analytical comparison of classification models for raga identification in carnatic classical instrumental polyphonic audio, *SN Computer Science*, Vol. 1, 6, 2020, pp. 1-9.

[20]. B. T. Rao, S. Chinnam, P. L. Kanth, and M. Gargi, Automatic Melakarta Raaga Identification Syste: Carnatic Music, *International Journal of Advanced Research in Artificial Intelligence*, Vol. 1, Issue 4, 2012, pp. 43–48.

[21]. S. John, M. S. Sinith, R. S. Sudheesh, and P. P. Lalu, Classification of Indian classical carnatic music based on raga using deep learning, in *Proceedings of the IEEE Recent Advances in Intelligent Computational Systems (RAICS' 2020)*, Thiruvananthapuram, India, 3-5 December 2020, pp. 110-113.

[22]. R. Rajan and S. Sivan, Multi-channel CNN-Based Rāga Recognition in Carnatic Music Using Sequential Aggregation Strategy, *Circuits, Systems, and Signal Processing*, 2023, pp. 1–24.

[23]. M. S. Siji John, R. S. Sudheesh, and P. P. Lalu, Classification of indian classical hindustani music based on raga using deep learning, in *Proceedings of the IEEE Recent Advances in Intelligent Computational Systems (RAICS' 2020)*, Thiruvananthapuram, India, 3-5 December 2020, pp. 110–113.

[24]. A. Vasudevan and H. Ramasangu, A hybrid cluster-classifier model for hindustani raga classification, in *Proceedings of the IEEE International Conference on Electronics, Computing and Communication Technologies (CONECCT' 2021)*, Bangalore, India, 9-11 July 2021, pp. 1–6.

[25]. D. Joshi, J. Pareek, and P. Ambatkar, Indian classical raga identification using machine learning, in *Proceedings of the International Semantic Intelligence Conference (ISIC)*, New Delhi, India, February 2021, pp. 259–263.

[26]. S. Chowdhuri, Phononet: multi-stage deep neural networks for raga identification in hindustani classical music, in *Proceedings of the International Conference on Multimedia Retrieval*, 2019, pp. 197–201.

[27]. D. P. Shah, N. M. Jagtap, P. T. Talekar, and K. Gawande, Raga Recognition in Indian Classical Music Using Deep Learning, in *Artificial Intelligence in Music, Sound, Art and Design, Proceedings of the 11th International Conference (EvoMUSART' 2022)*, Madrid, Spain, April 20–22, 2021, pp. 248–263.

[28]. V. S. Pendyala, N. Yadav, C. Kulkarni, and L. Vadlamudi, Towards building a Deep Learning based Automated Indian Classical Music Tutor for the Masses, *Systems and Soft Computing*, Vol. 4, Issue 200042, 2022, pp. 1-8.

[29]. S. Banerjee, G. Hota, R. Sanyal, and M. K. Rath, Two step recognition of raags in Hindustani classical music using supervised deep learning, in *Proceedings of the 1st IEEE International Conference on Data, Decision and Systems (ICDDS' 2022)*, Bangalora, India, 2-3 December 2022, pp. 1-5.

[30]. C. Alyani and A. Balwant, Raga identification techniques for classifying indian classical music: A survey, *International Journal of Signal Processing Systems*, Vol. 5, Issue 4, 2017, pp. 1-6.

[31]. R. Shastry and A. Bai, Signal processing and machine learning approaches and evaluation for Indian Classical music, in *Proceedings of the IOP Conference Series: Materials Science and Engineering*, Vol. 1116, No. 1, Jeju Island, Korea, 12-14 March 2021, pp. 012188.

[32]. C. Kalyani and A. Balwant, Analyzing acoustics of indian music audio signal using timbre and pitch features for raga identification, in *Proceedings of the 3rd International Conference on Imaging, Signal Processing and Communication (ICISPC' 2019)*, 2019, pp. 42–46.

[33]. A. Srinivasamurthy, K. Gopala, S. Koduri, V. Gulati, and X. Ishwar, Corpora for music information research in indian art music, in *Proceedings of the Joint International Computer Music Conference / Sound and Music Computing Conference (ICMC/SMC)*, Athens, Greece, 14-20 September 2014, pp. 1029-1036.

[34]. P. Dighe, P. Agarwal, and H. Karnick, Siddartha Thota, and Bhiksha Raj, Scale independent raga identification using chromagram patterns and swara based features, in *Proceedings of the IEEE International Conference on Multimedia and Expo Workshops (ICMEW)*, San Jose, US, 15-19 July 2013, pp. 1–4.

[35]. Y. Singh and A. Biswas, Swaragram based residual neural architecture for raag identification in Indian classical music, in *Proceedings of the 12th International Conference on Computing Communication and Networking Technologies (ICCCNT' 2021)*, Khargpur, India, July 6-8, 2021, pp. 1-6.

[36]. S. Patil, R. P. Bhavsar, and B. V. Pawar, A survey on computational approaches for raga identification, in *Proceedings of the IEEE World Conference on Applied Intelligence and Computing (AIC' 2022)*, Sonbhadra, India, 17-19 June 2022, pp. 85-92.
[37]. P. Sutar, M. Saitwal, and S. Wakchaure, Rohit Shinde, and Poonam Sawdekar, A survey on raga identification using machine learning techniques, *International Journal of Innovative Research in Technology (IJIRT)*, Vol. 6, Issue 11, 2020, pp. 691-694.
[38]. S. Alekh, Automatic Raga Recognition in Hindustani Classical Music, *arXiv:1708.02322*, 2017.
[39]. S. Sreejith and R. Rajan, R¯aga recognition in indian carnatic music using transfer learning, in *Proceedings of the Fourth International Conference on Microelectronics, Signals & Systems (ICMSS)*, Kollam, India, 18-19 November 2021, pp. 1–5.
[40]. V. Kaimal and S. Barde, Implementation of a supervised learning model for raga identification in carnatic music, in *Proceedings of the Asian Conference on Innovation in Technology (ASIANCON' 2021)*, Pune, India, 27-29 August 2021, pp. 1-6.
[41]. M. Hemali Dodia and P. N. P. Pandey, Identification of raga by machine learning with chromagram, *International Research Journal of Engineering and Technology (IRJET)*, Vol. 7, Issue 5, 2020, pp. 3220-3225.
[42]. A. Srinivasamurthy, S. Gulati, R. Caro Repetto, and X. Serra, Saraga: Open datasets for research on Indian Art Music, *Empir. Musicol. Rev.*, Vol. 16, No. 1, 2021, pp. 85–98.
[43]. Y. Singh and A. Biswas, Robustness of musical features on deep learning models for music genre classification, *Expert Systems with Applications*, Vol. 199, Issue 116879, 2022, pp. 1-14.
[44]. Singh, Yeshwant and Kumar, Ranjeet and Biswas, Anupam, Swaragram: Shruti-Based Chromagram for Indian Classical Music, Advances in Speech and Music Technology, *Springer*, Singapore, 2021, pp. 109—118.

Published by International Frequency Sensor Association (IFSA) Publishing, S. L., 2023 (http://www.sensorsportal.com).



Automation, Robotics & Communications for Industry 4.0/5.0 (ARCI' 2024): 4th IFSA Winter Conference

7-9 February 2024
Innsbruck, Austria

CALL FOR PAPERS

Deadlines:

Submission
(2-page abstract):
20 November 2023

Notification of acceptance:
5 December 2023

Registration:
22 November 2023

Camera ready
(4-6 pages paper):
15 January 2024

The series of annual ARCI Winter IFSA conferences have been launched to provide a forum for open discussion of state-of-the-art technologies related to control, automation, robotics, communication and data analysis - main components of Industry 4.0, and new, coming technologies for Industry 5.0.

The ARCI' 2024 conference will incorporate four symposiums covering research and development in a broaden range in automation, robotics, communication and data analysis, and united by the Industry 4.0/5.0 challenges.

The ARCI' 2024 conference is organized by the IFSA - one of the major professional, non-profit association serving for sensor industry and academy since 1999.

Main Topics:

- Industry 4.0/5.0
- Automation
- Robotics
- Communications



Contribution Types:

- Keynote presentations
- Invited presentations
- Special sessions
- Regular sessions
- Poster sessions
- Industrial presentations
- Panel discussions and Round tables
- Exhibition

Special Sessions:

Authors are welcome to propose and manage special sessions during the ARCI' 2024 conference. Each special session will contain 4-6 papers in a related field as specified above. Session organizers will get:

- Certificate of Appreciation
- Free Registration
- Special Publishing Theme within Conference Proceedings

arci@sensorsportal.com
https://arci-conference.com/



Venue:

The ARCI' 2024 Conference will take place in the modern 4-star Austria Trend Hotel Congress Innsbruck, conference rooms Tyrol. The hotel is located on the banks of the Inn River, close to the Congress and Exhibition Centre of Innsbruck, opposite the new Hungerburgbahn (cable car), and just a few steps away from the historic city centre. Parking in a garage is possible upon a surcharge. The hotel is situated in 5 km from the Airport and 3 km from the Railway Station, and provides a shuttle service to nearby skiing areas. Address: Rennweg 12a, 6020 Innsbruck, Austria.

Organizing Committee

Chairman:
Prof., Dr. Sergey Y. Yurish (IFSA, Spain)

Advisory Chairman:
Prof., Dr. Vijayakumar Varadarajan (The University of New South Wales, Australia)

Conference and Publication Manager:
Mrs. Tetyana Zakharchenko
(IFSA Publishing, S. L., Spain)

Organizing Committee:
Mr. Javier Cañete (Universitat Politecnica de Catalynya (UPC), Barcelona, Spain)
Mr. Luis Morey (Universitat Politecnica de Catalynya (UPC), Barcelona, Spain)
Mr. Sergey Garmash (IFSA Publishing, S. L., Spain)

One event - three publications !

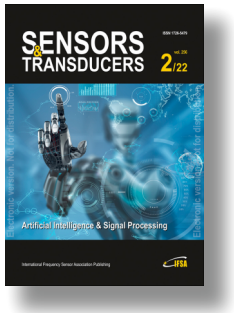
All abstracts will be published in the conference proceedings (USB flash drive edition of published Proceedings with the ISBN), distributed during the conference.

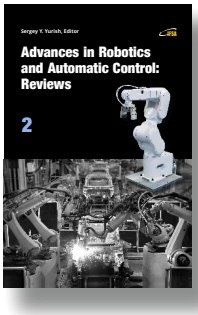
Authors will be invited to submit full-page extended papers to the special issues of Sensors & Transducers, MDPI Processes or MDPI Machines open access journals.

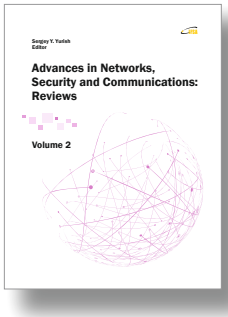
The limited number of full-page papers published in the journals will be selected by the Editorial Board to extend for book chapters for the open access Book Series on 'Advances in Robotics and Automatic Control: Reviews', Vol. 3, 'Advances in Networks, Security and Communications: Reviews', Vol. 3 or 'Advances in Intelligent Systems: Reviews', Vol. 3. All books will published in 2024 and submitted to the Book Citation Index by Clarivate Analytics

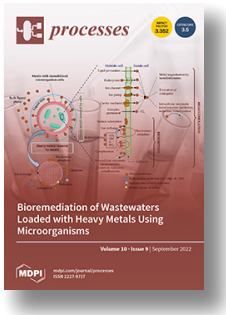
processes
an Open Access Journal by MDPI

machines
an Open Access Journal by MDPI













Call for Chapters

IFSA Publishing

Your Chapter may be in the next Volume of the popular Book Series

ADVANCES IN SENSORS: REVIEWS 8

Open Access Book Series

Sinse 2012



- Physical, chemical and biosensors
- Sensor uncertainty, accuracy, calibration
- Smart sensors and systems
- Intelligent sensors and systems
- Artificial Intelligence enabled sensors
- Virtual and soft sensors
- Sensor instrumentation
- Sensor buses and networks
- Signal processing, sensor fusion
- Nanosensors
- Photonic sensors
- Sensor interfacing and signal conditioning
- Materials for sensors
- MEMS, BioMEMS and NEMS
- Remote Sensors and Telemetry
- Sensor packages and reliability

https://www.sensorsportal.com/HTML/IFSA_Publishing.htm

IFSA

International Frequency Sensor Association Publishing

www.sensorsportal.com

ISSN 1726- 5479